Deformation and Exhumation at Convergent Margins: The Franciscan Subduction Complex

Uwe Ring

THE GEOLOGICAL SOCIETY OF AMERICA®

Special Paper 445

Deformation and Exhumation at Convergent Margins: The Franciscan Subduction Complex • Uwe Ring • Special Paper 445

Published by The Geological Society of America, Inc.
3300 Penrose Place, P.O. Box 9140, Boulder, Colorado 80301-9140, USA
www.geosociety.org

Printed in U.S.A.

GSA Books Science Editors: Marion E. Bickford and Donald I. Siegel

Library of Congress Cataloging-in-Publication Data

Ring, Uwe.
Deformation and exhumation at convergent margins : the Franciscan subduction complex / Uwe Ring.
p. cm. — (Special paper ; 445)
Includes bibliographical references.
ISBN 978-0-8137-2445-4 (pbk.)
1. Geology, Structural—California, Northern. 2. Franciscan Complex (Calif.) 3. Plate tectonics—California, Northern. 4. Subduction zones—California, Northern. 5. Convergent margins—California, Northern. I. Title.
QE627.5.C2R56 2008
551.809794—dc22

2008023272

Cover: Golden Gate Bridge with San Francisco in the background. The rocks in the lower left are chert and graywacke of the Marin Headland terrane.

10 9 8 7 6 5 4 3 2 1

Preface

Our work in the Franciscan subduction complex began in 1993 when I was a postdoc with Mark Brandon at Yale University. Over the years I frequently visited the Franciscan complex and had a number of graduate students mapping various parts of the Franciscan margin. During those years John Wakabayashi was involved in our work in various ways. He was a constant source of detailed knowledge, was always interested in our strange ideas about the Franciscan complex, and forever and a day had a beer from his chilly bin handy when things got too complicated.

Although Mark Brandon is not an author of this Special Paper, a number of ideas expressed here are Mark's, and he also has done part of the writing. However, I take full responsibility for what is being published in this contribution. We started to put this paper together in the late 1990s and first submitted it in 2001. Finally, with Editor Pat Bickford's help and support, it is published.

I am fully aware that our ideas on how the Franciscan subduction complex may have evolved tectonically are not accepted by some of our colleagues. Well, I guess every now and then there has to be someone who does not want to go with the flow, and sometimes even peculiar ideas are not necessarily wrong. I realize, however, that they are not always right.

The Geological Society of America
Special Paper 445
2008

Deformation and Exhumation at Convergent Margins: The Franciscan Subduction Complex

Uwe Ring
Department of Geological Sciences, Canterbury University, Christchurch 8140, New Zealand

ABSTRACT

The Franciscan subduction complex formed a long-lived accretionary wedge of Late Jurassic through Oligocene age that fringed the western edge of the North American Cordillera. It is an archetypal subduction complex, and therefore its tectonic evolution is important for understanding convergent plate margins. This complex is widely regarded as an example of a convergent orogenic wedge that underwent a phase of subhorizontal extension. Extension is thought to have been mainly accommodated by normal slip at the Coast Range fault zone, which directly overlies the Franciscan subduction complex and separates the latter from the Great Valley forearc basin. Subhorizontal extension, caused by sustained collapse of a supercritical wedge, is envisioned to be responsible for the exhumation of the high-pressure metamorphic interior of this subduction complex.

Brittle kinematic data from the Coast Range fault zone and intra–Franciscan subduction complex faults (including the Coastal Belt thrust) indicate top-W reverse faulting. We regard these faults as out-of-sequence thrusts. Absolute ductile finite-strain data from 142 samples from the Franciscan subduction complex indicate that the stretches (L_f/L_i) of individual samples in the X direction of the finite strain ellipsoid (S_X) range between 1.00 and 1.59; S_Y varies between 0.60 and 1.26, and shortening in the Z direction (S_Z) is 0.33–0.91. The principal stretches of the tensor average are S_X: S_Y: S_Z = 0.91: 0.90: 0.80. A rather surprising discovery is that there is no bulk extension associated with solution-mass-transfer (SMT) deformation at the regional scale. Instead, shortening is accommodated by pervasive mass loss, with an average mass loss of 34%. The geometry of fiber overgrowths on grains indicates that the deformation was close to coaxial. Measured internal rotation values range from 0° to 15°, with an average of 0.7°, which corresponds to an average kinematic vorticity number of ~0.1.

A simple model, which integrates velocity gradients along a vertical flow path with a steady-state wedge, shows that the estimated average contribution of ductile flattening to exhumation is ~12%. Given that the high-pressure rocks resided within the wedge for 30–40 m.y., this model indicates vertically averaged strain rates of –0.2% to –0.4% m.y.$^{-1}$ for across-strike horizontal deformation. Given an across-strike dimension of ~100–200 km for that portion of the Franciscan subduction complex affected by SMT deformation, the estimated rate of horizontal shortening is <~1% of the total convergence across the Franciscan margin. This result suggests

Ring, U., 2008, Deformation and Exhumation at Convergent Margins: The Franciscan Subduction Complex: Geological Society of America Special Paper 445, 61 p., doi: 10.1130/2008.2445. For permission to copy, contact editing@geosociety.org.

that SMT deformation within the subduction wedge represents a background deformation process that accounts for only a small fraction of the entire orogenic convergence. It is concluded that almost all of the orogenic convergence has been accommodated by slip at the base of the wedge.

We conclude that the brittle and ductile strain data are incompatible with models, which argue for top-E normal faulting at the Coast Range fault zone. However, we do acknowledge recent published evidence for Paleocene normal faults in the Mount Diablo area of the westernmost Great Valley basin. The ductile finite-strain data and the results of the exhumation model indicate that ductile thinning of the overburden did not significantly contribute to the exhumation of the high-pressure metamorphic rocks. The negligible extensional strains and the large mass loss suggest that ductile deformation mechanisms are not responsible for the development of an unstable, supercritical Franciscan wedge, which would have triggered normal faulting in its upper rear part. We propose that erosion was the dominant process that exhumed the high-pressure rocks of the Franciscan subduction complex during the Late Cretaceous and earliest Tertiary. Differential exhumation across the east side of the Coast Ranges has juxtaposed high-pressure rocks of the Eastern Franciscan Belt against very low grade rocks of the Great Valley Group to the east. Differential exhumation may have been in part resolved by the high-angle normal faults in the westernmost Great Valley basin. We argue that exhumation was due to deep erosion of a mountainous forearc high, perhaps analogous to the Olympic Mountains of the modern Cascadian margin of the North American Cordillera. Differential exhumation is attributed to higher rates of erosion on the seaward side of the forearc high. We infer that eroded sediments were transported mainly to the west into the trench, which would explain why sedimentologic evidence for erosion of the Franciscan subduction complex is difficult to find in the Great Valley forearc basin.

INTRODUCTION—STATEMENT OF THE PROBLEM

The widely recognized occurrence of regionally coherent high-pressure metamorphic belts in many orogens represents a fundamental tectonic problem. In the last two decades the role of extensional faulting in the exhumation of high-pressure rocks has received favorable attention because it provides an elegant and apparently widely pertinent mechanism for unroofing the interior of mountain belts (Platt, 1986, 1987, 1993, 2007). Platt (1986) based his “extension model” on the concept of wedge taper as originally proposed by Chapple (1978) and Davis et al. (1983). Platt (1986) argues that the dominant ductile deformation mechanism within the wedge is solution mass transfer (SMT), a linear viscous mechanism, which operates by selective dissolution and precipitation along grain boundaries. In Platt’s model, deep accretion and within-wedge ductile deformation promote upward flow within the rear part of the wedge, which causes the wedge to become unstable, resulting in brittle extensional faulting and horizontal stretching near the surface (Platt, 1987) (Fig. 1). A key assumption in the model is that rates of within-wedge ductile flow are great enough to contribute to the overall stability of the wedge. Platt’s model does not provide specific quantitative predictions of strain rate, but he envisions ductile strain rates of ~10^{-14} s^{-1} (31% m.y.$^{-1}$) or more (Platt, 1986, p. 1040). Platt’s model highlights the importance of within-wedge deformation for understanding wedge stability. In other words, ductile flow controls the geometry of the wedge, which in turn controls the development of reverse or normal faults in the upper brittle parts of the wedge. Platt’s two-dimensional model implicitly assumes that deformation within the wedge conserves volume. Despite the importance of ductile deformation and volume strains for understanding subduction complexes, there have been surprisingly few quantitative studies of the magnitude, pattern, rate, and nature of ductile strain in accretionary wedges above subduction zones (Norris and Bishop, 1990; Fisher and Byrne, 1992; Wallis

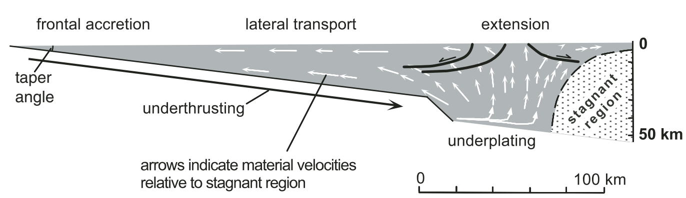

Figure 1. Idealized pattern of material flow in isochorically deforming accretionary wedge in which underplating is dominant mode of accretion and little to no erosion occurs at top; upward flow in rear of wedge causes diverging velocity pattern in upper rear part of wedge, which in turn drives brittle normal faulting in that part of wedge; note that geometry of stagnant region influences velocity distribution within wedge (modified from Platt, 1987). Supercritical or overcritical tapering describes unstable wedge geometry in which angle of taper becomes too great, and wedge is forced to regain stable taper by horizontal lengthening; note that within-wedge volume loss and erosion at top of rear wedge would tend to suppress supercritical tapering.

et al., 1993; Feehan and Brandon, 1999; Kassem and Ring, 2004; Richter et al., 2007; Ring et al., 1988, 1989; Ring and Kassem, 2007), and therefore little is known about deformation and exhumation processes in this setting.

The Franciscan subduction complex of coastal California (Figs. 2, 3) is widely regarded as an example of a convergent wedge that underwent a phase of subhorizontal extension (Fig. 4; Platt, 1986; Jayko et al., 1987; Harms et al., 1992). Platt (1986) was the first to propose that normal slip on the Coast Range fault zone, attributed to sustained collapse of a supercritical Franciscan wedge, was responsible for the exhumation of its high-pressure metamorphic interior. Platt (1986), however, did acknowledge contractional deformation on the Coast Range fault zone during its initial development. The principal evidence cited for normal slip is as follows:

1. A major hiatus in metamorphic grade across the Coast Range fault zone, which places very low grade rocks of the Great Valley forearc basin on high-pressure rocks of the Franciscan subduction complex.

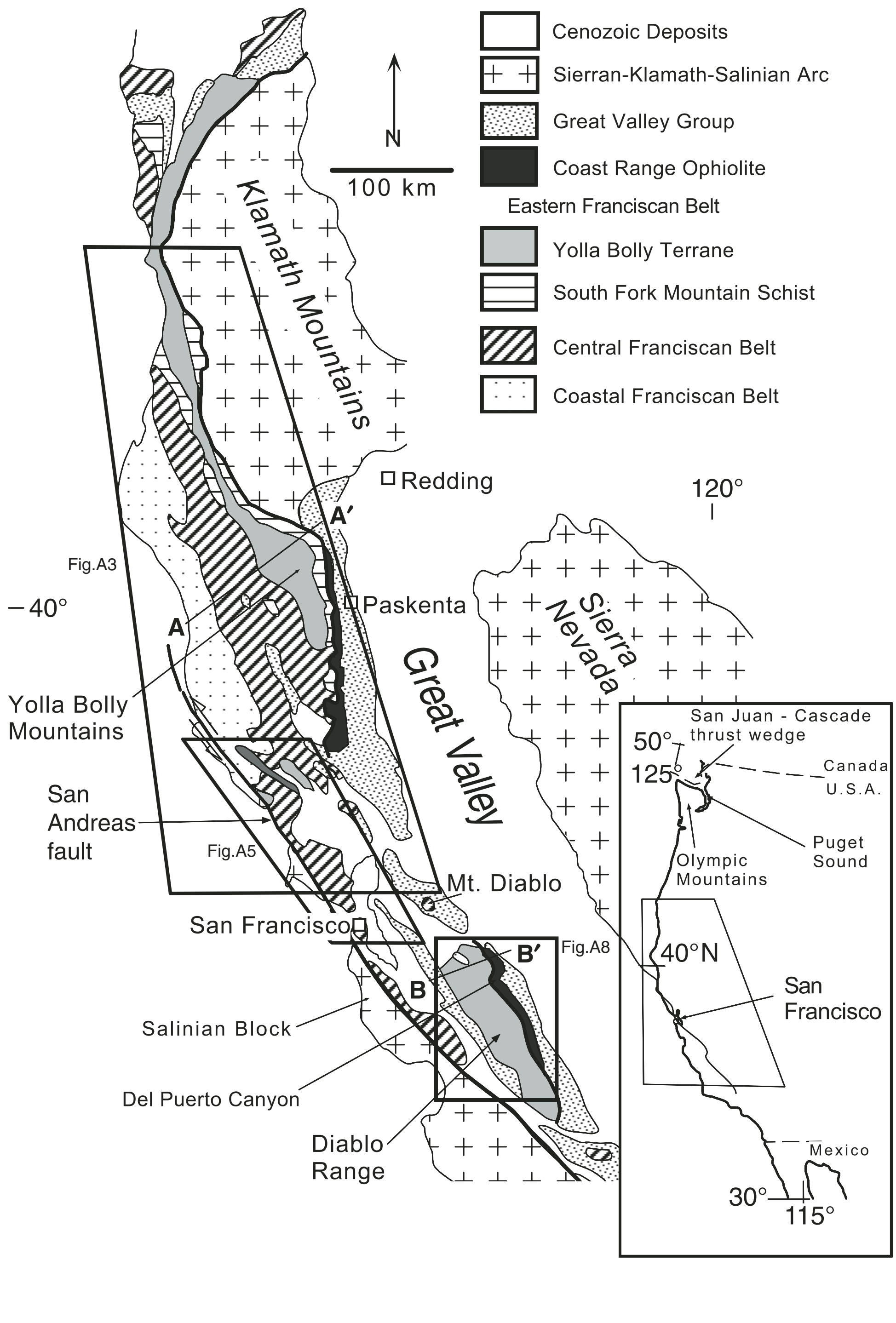

Figure 2. Map showing main Mesozoic and Cenozoic tectonic elements of western California; study areas along Coast Range fault zone are near Paskenta in northern Coast Ranges and at Mount Diablo and Del Puerto Canyon in central Coast Ranges; locations of cross sections A–A′ and B–B′ in Figure 3 and maps in Figures A3, A5, and A8 in Appendix are indicated. Inset shows general geography at North American west coast, location of main map, and Olympic Mountains and its forearc basin (Puget Sound) and San Juan–Cascades thrust wedge.

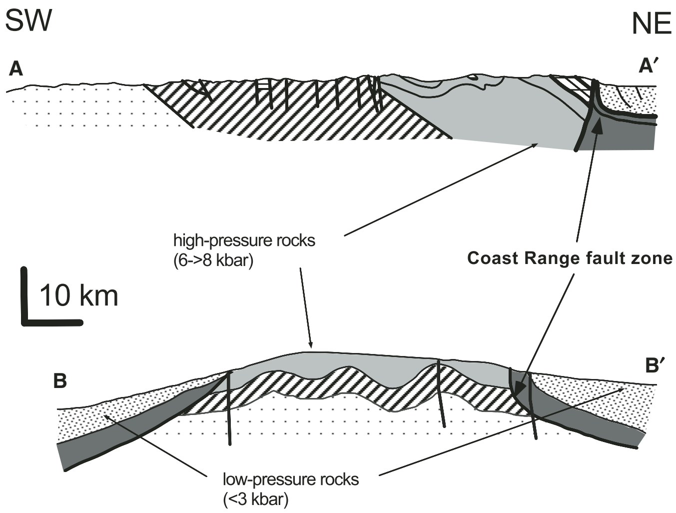

Figure 3. Generalized cross sections (locations shown in Fig. 2) through Yolla Bolly Mountains (A–A′, modified from Cowan and Bruhn, 1992) and northern Diablo Range (B–B′, modified from Bauder and Liou, 1979); sections illustrate present steep attitude of Coast Range fault zone and pronounced break in metamorphic grade at that contact; note disruption of entire structure by younger crosscutting strike-slip faults.

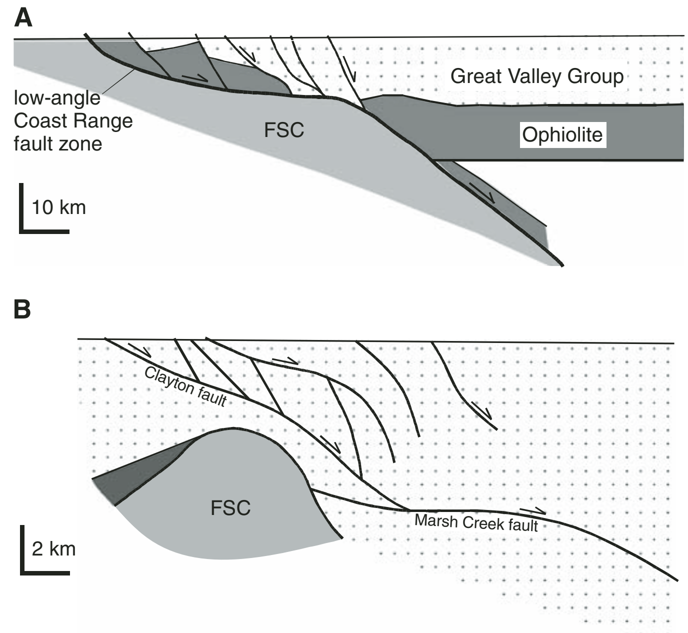

Figure 4. (A) Extensional model explaining contact of Franciscan subduction complex (FSC) and Great Valley Group by Late Cretaceous to early Tertiary top-E, low-angle normal faulting at Franciscan subduction complex–ophiolite contact (modified from Harms et al., 1992). (B) Alternative model of Unruh et al. (2007), showing early Tertiary high-angle normal faults in western Great Valley basin.

2. The Coast Range ophiolite, which lies above and within the Coast Range fault zone, appears to have been vertically thinned at the same time (Platt, 1986; Jayko et al., 1987).
3. The presence of younger-over-older rocks along some segments of the Coast Range fault zone (Jayko et al., 1987).
4. Kinematic evidence from Del Puerto Canyon (Fig. 2) by Harms et al. (1992) that has been interpreted to support top-E low-angle normal slip across the Coast Range fault zone.

We maintain that the first three arguments are inconclusive because out-of-sequence or backstepping thrust faults—defined as faults that step back and cut through the rearward or more internal part of a contractional wedge—can also result in younger-over-older relationships and can put rocks of lower metamorphic grade above ones of higher grade if the section dips more steeply than the faults (Wheeler and Butler, 1994; Ring and Brandon, 1994; Ring, 1995a). Furthermore, available kinematic data from the Coast Range fault zone (Ring and Brandon, 1994, 1997) indicate E-up motion on the fault, which is inconsistent with the top-down-E normal-slip interpretation. These data have been interpreted by Ring and Brandon (1994, 1997) to indicate that the Coast Range fault zone formed as a postmetamorphic, out-of-sequence thrust with a general top-W sense of motion. The Yolla Bolly and Pickett Peak terranes of the Eastern Franciscan Belt below the Coast Range fault zone are imbricated by a series of widely spaced E-dipping faults, all of which are postmetamorphic. In contrast to the Coast Range fault zone, these intra–Franciscan subduction complex faults generally place higher-grade metamorphic rocks above lower-grade rocks and therefore duplicated the original metamorphic section. Glen (1990) showed that the Great Valley Group west of the Yolla Bolly Mountain area was shortened by a series of top-W thrust faults. We envision that all of these faults are related to young (Tertiary) shortening across the Coast Ranges. The tectonic wedge models of Wentworth et al. (1984) and Unruh et al. (1995) have called attention to this young deformation, but they do not address in any detail the possibility of young slip on the intra-Franciscan postmetamorphic faults. The point to be stressed, however, is that the Coast Range fault zone does not appear to have any structures that would correspond to the Late Cretaceous normal faults proposed in Platt's (1986) model. The Franciscan subduction complex might still have been exhumed by normal faulting, but one would have to concede that there is no longer any direct evidence for such structures.

One major remaining piece of evidence is the kinematic study of Harms et al. (1992). These authors interpreted "mylonitic stretching lineations" from a small area in the Del Puerto Canyon of the Diablo Range to reflect top-E simple-shear low-angle extensional movement at the Coast Range fault zone (Fig. 4A). The "mylonitic stretching lineations," as reported by Harms et al. (1992), show highly variable orientations. Apparent asymmetries of an anastomosing SMT cleavage have been compared with S-C fabrics, as defined for crystal-plastically deformed mylonites by Berthé et al. (1979). The so obtained shear-sense indicators are also variable (13 out of 22 data are top-E, 7 are top-W, and 2 are top-N). Harms et al. (1992) neither report quantitative finite strain nor quantitative internal rotation data to support their interpretation that the "mylonitic stretching lineations" represent true displacement trajectories—i.e., that they result from simple-shear deformation. Therefore, and because of the highly variable pattern of the lineations, Harms et al.'s interpretation of a uniform top-E displacement during ductile deformation in the direct footwall of the Coast Range fault zone remains questionable. Our deformation measurements reported here are important because they provide further information about the kinematics of the structures studied by Harms et al. (1992).

However, the recent study of Unruh et al. (2007) supplies strong evidence for a phase of early Tertiary high-angle normal faulting in the Great Valley basin of the northern Diablo Range. This event aided the exhumation the Franciscan high-pressure rocks from ~9 to ~3 km (Fig. 4B), and the rocks were close to the surface by ca. 60 Ma. Unruh et al. (2007) argued that normal faulting occurred beneath the forearc basin and thus well inboard of the trench and the Franciscan subduction complex, and that therefore orogenic wedge models as proposed by Platt (1986) are probably not applicable to explain the normal faults.

The high-angle normal faults of Unruh et al. (2007) would have caused ~4 km of extension (assuming a dip angle of 60°) for achieving the 6 km of exhumation envisioned by these authors. The low-angle normal fault of Harms et al. (1992) would have caused 18–40 km of extension (assuming a dip angle of 30°) for fully exhuming the Franciscan blueschists. Both extensional models differ in geometry, the amount of extension (by a factor of ~5–10), and the envisioned trigger for normal faulting.

In general, three major processes allow for deep exhumation of an orogenic wedge (Ring et al., 1999): (1) normal faulting (e.g., Platt, 1986), (2) vertical thinning owing to within-wedge ductile flow (e.g., Selverstone, 1985, 2005), and (3) erosion (e.g., England and Richardson, 1977; Rubie, 1984), as follows:

(1) There is abundant evidence that normal faulting aids the exhumation of metamorphic rocks. The Basin and Range province (Armstrong, 1972; Davis, 1988; Foster and John, 1999), the Aegean (Lister et al., 1984; Buick, 1991; Thomson et al., 1999; Ring et al., 2003), the Betic Cordillera (Platt and Vissers, 1980), and the Alps (Mancktelow, 1985; Ring, 1992; Ring and Merle, 1992; Reddy et al., 1999) are well-documented examples for which normal faulting contributed to exhumation.

A variant of normal faulting would be the development of a lateral extrusion wedge, as first proposed for the Franciscan by Maruyama et al. (1996). Such an extrusion wedge is defined by a basal thrust, coupled with a coeval normal fault at the top of the extruding wedge, and typical forms in subduction settings (Wintsch et al., 1999, for the Sanbagawa Belt; Thomson et al., 1999, for Crete; Ring et al., 2007, for the Cycladic Blueschist Unit in the Aegean; Glodny et al., 2008, for the Eclogite Zone in the Tauern Window of the Alps). The basal thrust indicates that an extrusion wedge forms in a contractional environment.

(2) Vertical ductile thinning refers to exhumation by ductile flow, i.e., vertical thinning (shortening) of the ductile crust associated with a subhorizontal foliation. Feehan and Brandon (1999) outlined potential problems of using vertical strains to quantify exhumation. In the simplest case, in which exhumation is entirely controlled by ductile thinning, exhumation by the latter is given by the average stretch (final length/initial length) in the vertical, because this tells how much the vertical has changed in thickness (Wallis, 1992; Wallis et al., 1993). In the general case of exhumation by the interaction of various processes, it is more difficult to quantify the contribution of ductile thinning to exhumation. In this case the vertical rate at which a rock moves through its overburden, and the rate of thinning of the remaining overburden at each step along the exhumation path, have to be considered (Feehan and Brandon, 1999).

(3) The large volumes of detrital deposits found adjacent to almost all convergent continental orogens provide ample evidence that erosion is a significant exhumation process. In most orogens, dispersal of eroded material occurs over distances of thousands of kilometers, with some eroded material reaching distant ocean basins and subduction zones. The reason for wide dispersal is that foreland basins usually never hold more than about half of the sediment produced by erosional lowering of the orogen (England, 1981). Wide dispersal makes it difficult to make a useful comparison between the volume of eroded sediment and the depth of exhumation. Another factor that has to be taken into account in subduction settings is the recycling of eroded material back into the trench (Ring and Brandon, 2008).

Herein we present a detailed analysis of kinematic data from two serpentinite-rich segments of the Coast Range fault zone in the northern and central Coast Ranges (Fig. 2). We apply the internal rotation axis (IRA) method (Cowan and Brandon, 1994) to resolve the sense of slip across the Coast Range fault zone. This comprehensive analysis allows one to better resolve the role the Coast Range fault zone had in the tectonic evolution of the Franciscan subduction complex and in the exhumation of its high-pressure interior. Since the tilting of the Coast Range fault zone postdated its formation (Ernst, 1971), kinematic data from the fault zone have to be restored (Fig. 5). We also present fault-slip data from intra–Franciscan subduction complex faults. For northern California, the vertical orientation of the extension axes from the Coast Range fault zone, the Grogan fault, the Redwood Mountain fault, the Bald Mountain fault, and the minor faults at and south of Humboldt Lagoons and at Titlow Hill indicates reverse faulting. At the Coastal belt thrust the shortening axes cluster in a NE-SW direction, which, in conjunction with the small-scale kinematic indicators, reflect top-SW tectonic transport. Overall, all brittle strain data from the Coast Range fault zone and the intra–Franciscan subduction complex faults show postmetamorphic NE-SW contraction.

Metaclastic high-pressure metamorphic rocks of the Franciscan subduction complex show evidence of SMT deformation. The clockwise pressure-temperature (P-T) loop of these rocks indicates a general displacement path involving subduction, accretion at the base of the wedge, exhumation, and exposure at Earth's surface. Therefore, the finite strain recorded

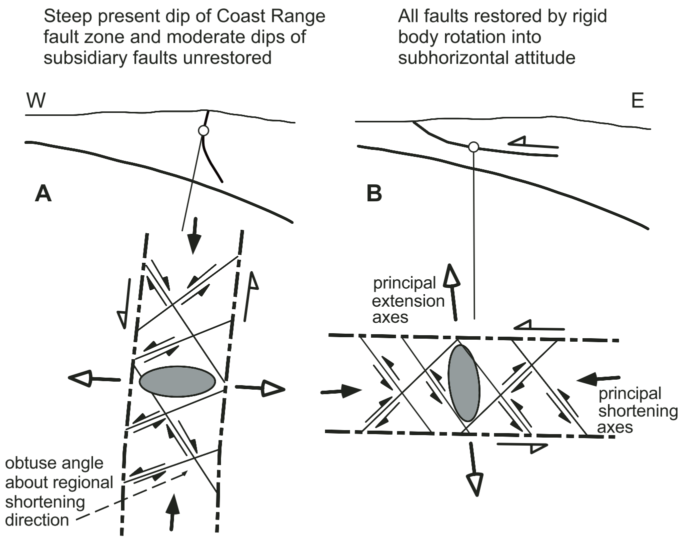

Figure 5. Sketch illustrating (A) present and (B) original configuration of Coast Range fault zone. When viewed in present configuration, faults within fault zone appear as W- and E-dipping normal faults; when viewed in original configuration, same faults would be interpreted as W- and E-dipping reverse faults. Coast Range fault zone is considered to have originated in subhorizontal orientation and was rotated into present steep attitude at same time Great Valley homocline formed.

in the exhumed Franciscan high-pressure rocks represents the integrated strain history along that displacement path, and the samples can be viewed as flight recorders that tell about the tectonic history of the wedge they traveled through. We utilize methods developed by Brandon et al. (1994), which provide a full determination of absolute finite strains produced by the SMT mechanism, including volume strain and internal rotation. We also use a simple numerical model devised by Feehan and Brandon (1999) (Fig. 6) to estimate the contribution of ductile strain mechanisms (i.e., vertical ductile thinning) to the overall deformation and exhumation of high-pressure metamorphic rocks of the Franciscan subduction complex. In closing, we consider the implications of the results of the deformation and exhumation history of this complex.

THE FRANCISCAN TRIAD—AN OVERVIEW

The Franciscan triad comprises the Franciscan subduction complex, which underlies the Coast Ranges of western California; the Great Valley forearc basin; and the Sierran magmatic arc (e.g., Cowan and Bruhn, 1992) (Fig. 2).

Franciscan Subduction Complex

This complex is dominated by clastic sedimentary rocks interpreted as accreted trench sediments and superimposed trench-slope basins but also includes subordinate amounts of mafic and keratophyric volcanic rocks and thick chert sequences. The latter represent, at least in part, accreted fragments of seamounts and oceanic plateaus as well as imbricated slices from the overlying forearc basin (e.g., Blake, 1984; Blake et al., 1985). In the northern Coast Ranges the complex is commonly subdivided into three NW-striking belts (Fig. 2), which are, from west to east, the Coastal, Central, and Eastern belts (Bailey et al., 1964; Berkland et al., 1972; Blake et al., 1988). South of San Francisco, this subdivision has been obscured by the system of faults that make up the modern San Andreas transform. Stratigraphic age, as well as the degree and age of metamorphism and deformation, generally increase in an eastward direction across these belts.

The Coastal Belt is the westernmost and structurally lowest belt and was metamorphosed under zeolite-facies conditions (Blake et al., 1988). Except for pelagic rocks, fossils suggest a Paleocene to Miocene age for the Coastal Belt (Blake and Jones, 1981; Blake et al., 1988).

The Central Belt lies inboard and east of the Coastal Belt. The two belts are separated by the Coastal Belt thrust. The Central Belt contains coherent graywacke, but also a shale-matrix

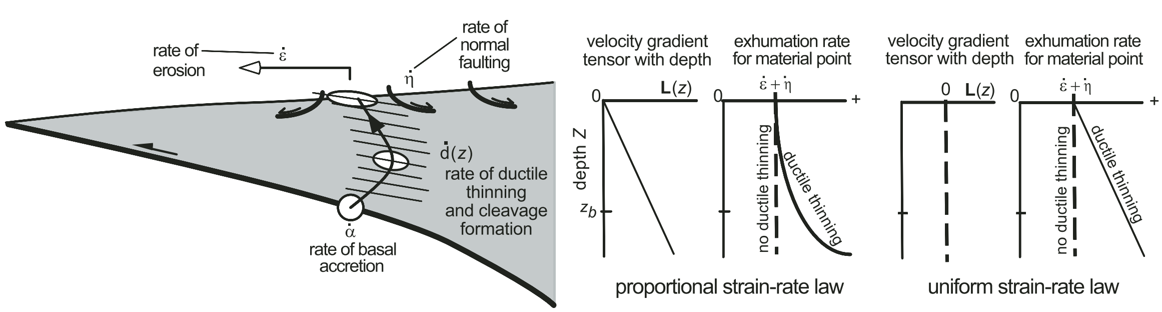

Figure 6. Schematic cross section through accretionary wedge, illustrating major processes causing vertical thinning or thickening and how they effect exhumation of particle moving through wedge. For this study, these processes are represented as accretion at base of wedge, ductile flow within wedge, and denudation; denudation is expressed as normal faulting and/or erosion, causing thinning near top of wedge. Particle enters base of wedge at z_b unstrained and acquires its finite ductile strain as it rises through wedge; vertical velocity divided into two components: first includes erosion rate and rate of brittle normal faulting, and second is rate of thinning owing to ductile flow. Upward-moving particle follows exhumation path while it acquires ductile strain. Graphs to right schematically illustrate proportional and uniform strain-rate law; because strain rate for proportional strain-rate law changes in linear fashion with depth, exhumation velocity accumulates exponentially; model assumes steady-state wedge, where accretion, ductile flow, erosion, and normal faulting remain constant (Feehan and Brandon, 1999).

mélange that includes blocks of metagraywacke, greenstone, and chert, as well as exotic blocks (the so-called knockers) of higher-grade blueschist, amphibolite, and eclogite (Bailey et al., 1964; Blake et al., 1988; Wakabayashi, 1990). Rare fossils from the mélange matrix indicate Tithonian to Valanginian (uppermost Jurassic and Early Cretaceous) ages for the eastern part of the Central Belt, whereas Albian to Coniacian (Late Cretaceous) fossils are present in graywacke slabs and accreted limestones in the west (Blake and Jones, 1981; Maxwell, 1974; McDowell et al., 1984).

The Eastern Belt comprises the two uppermost units of the Franciscan subduction complex (Figs. 2, 3) and is made up of several thick, gently dipping, fault-bounded units, each of which contains a relatively coherent internal stratigraphy (e.g., Suppe, 1973; Worrall, 1981; Constenius et al., 2000). The two main units within this structural succession are the Yolla Bolly terrane and the structurally higher Pickett Peak terrane (Blake et al., 1988; Figs. 2, 3). The Pickett Peak terrane is further subdivided into the South Fork Mountain Schist and the underlying Valentine Springs Formation (Worrall, 1981) and crops out only in the northern Coast Ranges.

Isotopic ages from the Eastern Belt indicate a protracted history of high-pressure metamorphism, followed by cooling in the Late Cretaceous and early Cenozoic (Suppe and Armstrong, 1972; Lanphere et al., 1978; McDowell et al., 1984; Mattinson, 1988; Dumitru, 1989; Wakabayashi and Dumitru, 2007). The oldest metamorphic ages (ca. 169–160 Ma) are from high-grade blocks in the mélanges (Ross and Sharp, 1986, 1988; Anczkiewicz et al., 2004). The Pickett Peak terrane yielded ages of 152–125 Ma. Regional metamorphism of the Yolla Bolly terrane probably occurred at ca. 90 Ma (Mattinson and Echeverria, 1980; Mattinson, 1988; Cowan and Bruhn, 1992). It is important to note that pronounced differences in metamorphic grade between adjacent units indicate that the present pattern of thrust imbrication postdates high-pressure metamorphism of the Yolla Bolly and Pickett Peak terranes (Suppe, 1973; Cowan, 1974; Platt, 1975; Worrall, 1981).

The age of scarce fossils in the Yolla Bolly Formation is generally Berriasian to Valanginian, but Cenomanian (i.e., 91–98 Ma) *Inoceramus* in lawsonite- and aragonite-bearing shale and metagraywacke, and Santonian-Campanian (ca. 85–80 Ma) fossils occur as well (Blake et al., 1988; Elder and Miller, 1993). Depositional ages in the Diablo Range are in the same range, i.e., 98–85 Ma (Joesten et al., 2004; Tripathy et al., 2005). The fossil evidence and the depositional ages indicate that metamorphism in parts of the Yolla Bolly terrane is <90 Ma and probably occurred slightly later in the structurally lowest parts of the terrane. Paired zircon and apatite fission-track ages show that the exhumation of the Eastern Belt occurred during the Late Cretaceous and Early Tertiary at 100–60 Ma (Tagami and Dumitru, 1996; Unruh et al., 2007). These observations suggest that the rocks have been subducted rapidly and that the high-pressure rocks of the Yolla Bolly terrane reached upper crustal levels, i.e., depths of ~5 km, which is the approximate closure depth for fission tracks in apatite, by 60 Ma. In other words, the rocks of the Yolla Bolly terrane needed ~10–40 m.y. to become juxtaposed against the Great Valley Group.

Coast Range Fault Zone

The Coast Range fault zone has long been recognized as a fundamental structural element of the Mesozoic–Cenozoic convergent margin of western North America (Fig. 2) (see review in Cowan and Bruhn, 1992). Over most of California the Coast Range fault zone has been steeply tilted to the east with the formation of the Great Valley homocline, which flanks the east side of the Coast Range uplift (Fig. 3). Locally, the fault zone is overturned and dips steeply to the west.

Traditionally, the Coast Range fault zone has been interpreted as a major crustal to lithospheric-scale thrust that juxtaposes the Great Valley forearc basin, comprising the Coast Range ophiolite and the overlying Great Valley Group, against the Franciscan subduction complex (e.g., Bailey et al., 1970; Ernst, 1970; Ingersoll, 1978; Dickinson and Seely, 1979) (Fig. 3). The occurrence of a major metamorphic hiatus across the fault has led Platt (1986) to propose that the most recent movement on the Coast Range fault zone is normal slip (Fig. 4A).

Throughout most of California, the Coast Range fault zone juxtaposes the Franciscan subduction complex in the footwall against the Great Valley forearc basin in the hanging wall. In southwest Oregon the Coast Range fault zone places older terranes of the Klamath Mountains directly over this subduction complex. The fault zone itself is commonly decorated by brittle serpentinite-rich shear zones, presumably derived from ultramafic rocks of the overlying Coast Range ophiolite. Major motion on the Coast Range fault zone is considered to have been Late Cretaceous and early Tertiary in age (Suppe, 1978; Cowan and Bruhn, 1992).

Most of the differential exhumation across the Coast Ranges occurred in latest Cretaceous to earliest Tertiary times, as indicated by the following three major lines of evidence:

(1) Erosional reworking of the Franciscan subduction complex in Late Cretaceous pumpellyite-bearing trench-slope sediments (Cowan and Page, 1975; Cowan, 1978; Dickinson et al., 1982). Reworked material includes blocky clasts of greenstone, chert, ultramafic rocks, glaucophane-lawsonite schist, metagraywacke, and large amounts of non-high-pressure metamorphic rocks. According to Cowan and Page (1975), a scenario is envisioned in which submarine debris flows of Franciscan mélange were shed from the emerging Franciscan wedge into the trench, arc-trench gap, or smaller intervening basins.

(2) The fission-track studies of Dumitru (1988, 1989) and Unruh et al. (2007) on apatite, as well as Tagami and Dumitru (1996) on zircon, indicate that the Eastern Franciscan Belt cooled from temperatures >~240 °C (zircon fission-track closure temperature), and the lower part of the Great Valley Group from temperatures >~110 °C (apatite fission-track closure temperature) at ca. 65–60 Ma. On the basis of an angular

unconformity detected in well correlations in the southern part of the Great Valley, Almgren (1984) also proposed strong exhumation at this time. The apatite fission-track data indicate that the present exhumation gradient from the Great Valley to the Eastern Franciscan Belt was developed at that time and that there has been little exhumation after the Paleocene. Temperatures must remain below ~40–50 °C to avoid significant resetting of apatite (based on 10% annealing for a stepwise thermal event of ~1–25 m.y.; Brandon et al., 1998). The modern thermal gradient is 28–35 °C km^{-1} (Dumitru, 1989), which is a reasonable approximation of the paleogradient since the initiation of the San Andreas fault in the late Oligocene. Thus, the amount of post-Oligocene erosion along the east flank of the Coast Ranges must be <~1.5 km. This argument can be extended back to the Eocene, although the paleothermal gradients are more poorly known but were probably somewhat lower at that time.

(3) The backstripping analysis of 30 sections of Moxon and Graham (1987) in the Great Valley basin. These authors reported a complicated history of subsidence and exhumation, which was partitioned in time and space. In the western part of the basin, exhumation migrated from north to south and from west to east. The analysis of Moxon and Graham (1987) provides a record of tectonically driven shoaling in the forearc basin, starting at 84 Ma and becoming more pronounced at ca. 60 Ma. The ages given by Moxon and Graham (1987) are similar to those obtained by the fission-track studies.

This pattern of exhumation was modified in the late Oligocene by dextral motion on the San Andreas (e.g., Atwater, 1970) and related faults. The most recent stages of the Coast Range uplift are due to E-directed reverse faulting (Wentworth and Zoback, 1989; Unruh and Moores, 1992), which is, at least in the Diablo Range, accompanied by dextral strike-slip faulting (Tesla-Ortigalita fault; Anderson et al., 1982). This modern deformation has been attributed to a change in plate motion at 8–6 Ma that resulted in a component of convergence normal to the San Andreas fault (Argus and Gordon, 2001).

Great Valley Forearc Basin

The hanging wall of the Coast Range fault zone is the Jurassic Coast Range ophiolite and the Great Valley Group (Dickinson, 1970, 1971; Ingersoll, 1978, 1979; Ingersoll and Dickinson, 1981), which collectively represent the forearc basin that formed above and inboard of the Franciscan subduction complex.

The Coast Range ophiolite contains harzburgite (which is commonly highly serpentinized), serpentinitic mélange, basalt, and dolerite. The Great Valley Group is one of the best known forearc basin-fill deposits in the sedimentary record (Dickinson et al., 1969; Ingersoll, 1978; Suchecki, 1984; DeGraaff-Surpless et al., 2002; Vermeesch et al., 2006). New detrital zircon work by Surpless et al. (2006) suggests that Great Valley Group deposition was largely Cretaceous in age and probably does not include Jurassic components. If so, the basin fill would be distinctly younger than its ophiolitic substrate and younger than the high-pressure metamorphism in the upper parts of the Eastern Belt.

Structurally the Great Valley Group occupies an asymmetrical synclinorium, some 650 km long by 90 km wide, characterized by a gently W-dipping eastern limb and a steeply E-dipping western limb (Fig. 7). The eastern limb is mainly concealed beneath Cenozoic cover of the Sacramento and San Joaquin Valleys (Fig. 2) and lies on continental basement.

It has been inferred that the eastern limb has a maximum thickness of ~4–5 km (Dickinson, 1970; Constenius et al., 2000). The western limb is well exposed in the foothills of the Coast Ranges and overlies remnants of oceanic crust of the Coast Range ophiolite. The thickness of Great Valley strata in the western limb is 13–15 km (Brown and Rich, 1967; Ingersoll, 1978; Constenius et al., 2000). Since the work of Brown and Rich (1967) it has been generally assumed that the greater thickness in the western synclinorial limb is due to greater sediment accumulation in the deeper, oceanward flank of the forearc basin. The recognition of down-to-basin synsedimentary normal faults in the westernmost Great Valley Group by Constenius et al. (2000) and Unruh

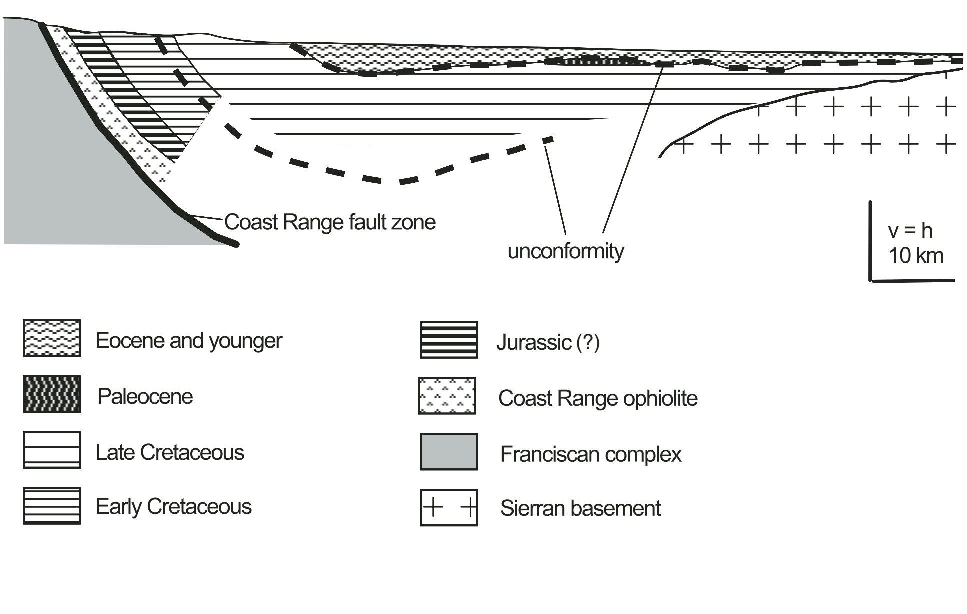

Figure 7. Composite cross section of relations in Great Valley forearc basin; subsurface relations based on seismic profile of Jacobson (1981); relations in exposed part of basin based on Kirby (1943), Rich (1971), and Ingersoll et al. (1977) (modified from Dumitru, 1988); note that new data by Surpless et al. (2006) suggest that most or all of Jurassic strata is Early Cretaceous in age. Campanian–Maastrichtian Late Cretaceous strata are regressive sequence associated with uplift or shoaling of forearc basin; base of this regressive sequence is Sacramento shale.

et al. (2007) is in line with this view. In the western part of the basin, subsidence was tectonically controlled and rapid during the period from 100 to 84 Ma, which resulted in a thick accumulation of turbidites deposited in deep water (Moxon and Graham, 1987). In the eastern basin, subsidence curves match thermal subsidence curves and thermal contraction related to cooling. Eastward migration of the Sierran magmatic arc is supposed to have been the major mechanism driving subsidence in the eastern part of the basin (Moxon and Graham, 1987), but downward flexing of the Sierran basement from sediment loading might have played an important role as well. This indicates that subsidence of the forearc basin was driven by different mechanisms on the two sides of the basin. Therefore, original thickness changes across the forearc basin are indeed verified. However, Wentworth et al. (1984) postulated from reflection and refraction seismic profiles the presence of tectonic wedges in the Great Valley Group, thereby implying that not all of the disparity is original. Glen (1990) presented detailed structural evidence for tectonic thickening in the western part of the Great Valley Group. Therefore, the original burial depth of the Great Valley Group was less than the present maximum thickness of 13–15 km. From the metamorphic study of Dickinson et al. (1969), and the fission-track work of Dumitru (1988), Vermeesch et al. (2006), and Unruh et al. (2007), it can be inferred that the original thickness in the western part did not exceed 12 km.

A first unconformity in the Great Valley basin occurred prior to the Cenomanian. This sub-Cenomanian unconformity only occurs in the eastern part of the basin (Dumitru, 1988) and is apparently due to widening of the arc-trench gap, which caused transpression toward the east and sedimentary progradation toward the west (Ingersoll, 1978). A second, much more pronounced, basinwide unconformity occurs in the Eocene strata. The Eocene Capay Formation, which contains ample evidence of Franciscan detritus (Dickinson, 1976; Swe and Dickinson, 1970; Berkland et al., 1972), rests on top of Late Cretaceous rocks. A third unconformity occurs at the base of the Pliocene–Pleistocene strata. Locally the Pliocene to Pleistocene Tehama Formation lies unconformably on top of Campanian rocks (Unruh et al., 1995).

Burial, Accretion, and Average Rates of Exhumation

In summarizing timing information from above, we estimate that the time between initial accretion and final exhumation was 60–70 m.y. for the Valentine Springs Formation and 10–40 m.y. for the Yolla Bolly terrane of northern California. Because Coniacian fossils occur in the Central Belt, the rocks were high-pressure metamorphosed not before 80–70 Ma. They probably also spent ~30–35 m.y. on their path through the wedge. These estimates are considered accurate to within ±20%–30%. Despite the low resolution, the residence time estimates show a significant and consistent westward decrease across the Franciscan subduction complex.

Much of the time the rocks spent in the subduction setting occurred after initial accretion. To illustrate, consider the average geometry of an accretionary wedge with a surface slope of ~2° and basal décollement of ~8° (Davis et al., 1983). Six kilometers of subduction are needed to get 1 km of structural burial. Convergence rates at the Franciscan margin are estimated to have been >100 km $m.y.^{-1}$ in the Late Cretaceous (Engebretson et al., 1985). Subduction to a depth of ~25–30 km would have taken <1.5 m.y. Thus, the time for subduction and initial accretion can be safely ignored in estimating residence time in the wedge. Based on these metamorphic depths and residence times, we estimate that the average exhumation rate was 0.5–1.0 km $m.y.^{-1}$, which is comparable to modern rates determined for the Cascadia margin (Brandon et al., 1998).

Current Tectonic Models for the Franciscan Subduction Complex

Early plate-tectonic models consider the Franciscan subduction complex to have formed within a huge, long-lived accretionary wedge (Hamilton, 1969; Ernst, 1970; Dickinson, 1970) (Fig. 8A) composed mainly of material scraped off an eastward-subducting oceanic plate. The Franciscan subduction complex and the Great Valley Group owe their contrasting lithologies and style of deformation, but essentially common provenance, to the fact that they were laid down on the eastern Pacific and North American plates, respectively. These models envision that the entire Franciscan triad was assembled in its present setting adjacent to coastal California. In Ernst's model, the Coast Range fault zone is considered the crustal expression of a late Mesozoic Benioff shear zone. Other workers (e.g., Ingersoll, 1978; Dickinson and Seely, 1979) proposed rather similar models but considered the Coast Range fault zone as a crustal-scale feature (Fig. 8B). In all of these "in situ" models, accretion, deformation, and metamorphism are considered to have advanced seaward as the wedge grew. These models only consider in-sequence thrusts. In contrast, Suppe (1979) and Wentworth et al. (1984) proposed out-of-sequence thrust models (Fig. 8C, D), which have the advantage that they can account for the major metamorphic break across the Coast Range fault zone. Godfrey et al. (1997) interpreted reflection-refraction seismic data in combination with density and magnetic models to argue for an ophiolite with its mantle section underlying the Great Valley basin, which in turn is underlain by a westward continuation of Sierran crust (Fig. 8E). The ophiolitic lithosphere is thought to have been obducted onto the North American margin during the Jurassic Nevadan orogeny (Godfrey et al., 1997) and thus before sediments accumulated in the Great Valley forearc basin. Based largely on gravity modeling, Constenius et al. (2000) interpreted shingled seismic reflectivity beneath the west and central Great Valley Group as interlayered mafic volcanic flows, volcaniclastic rocks, and intrusives of the Coast Range ophiolite. Dip divergences related to the subsurface feature led Constenius et al. (2000) to propose a fork structure, reflecting a combination of syndepositional normal faults and stratal onlap along the flank of the evolving Great Valley basin (Fig. 8F), an interpretation that is in contrast to the thrust-wedge hypothesis (see also Dickinson, 2002).

Figure 8. Six models for tectonic evolution of Franciscan subduction complex; symbols and patterns as in Figure 2, except for Franciscan subduction complex, which is shown in gray and undivided. (A) Benioff-zone model of Ernst (1970); Franciscan subduction complex features are related to period of active plate consumption; Coast Range fault zone controlled by Benioff master shear zone. (B) Traditional model showing original configuration of Cretaceous convergent margin; forearc basin is thrust onto Franciscan subduction complex; middle Cretaceous uplift and eastward migration of Sierran basement beneath east side of Great Valley basin accounted for truncation of older Great Valley Group (after Ingersoll, 1978; Dickinson and Seely, 1979). (C) Coast Range ophiolite as part of Cretaceous tectonic indenter that wedged eastward between overlying Great Valley basin and Sierran arc; from reflection seismic data and magnetic data it has been suggested that Sierran basement extends westward beneath homocline; Coast Range fault is interpreted as top-W out-of-sequence thrust fault that postdated and obscured original subduction-related structure of margin; Coast Range fault bounds west side of "triangle zone" (modified from Wentworth et al., 1984). Note that present geometry may not preclude original late Mesozoic situation similar to that depicted in western half of traditional model; hence, a preserved Coast Range thrust at depth. (D) Model of Cenozoic top-W out-of-sequence thrust faults (Suppe, 1979); note multiple (from imbrication), locally steepened (from folding) Coast Range thrusts; slab of Coast Range ophiolite, obducted onto Sierran basement, is inferred from central magnetic high extending near length of Great Valley. (E) Model showing Great Valley basin underlain by ophiolite with ophiolite mantle section, which in turn is underlain by westward continuation of Sierran crust; ophiolite mantle section dips west into present-day mantle (Godfrey et al., 1997). (F) West and central Great Valley Group underlain by mafic volcanic flows, volcaniclastic rocks, and intrusives of Coast Range ophiolite; dip divergences related to subsurface features create fork structure, reflecting combination of syndepositional normal faults and stratal onlap along flank of evolving Great Valley basin (Constenius et al., 2000).

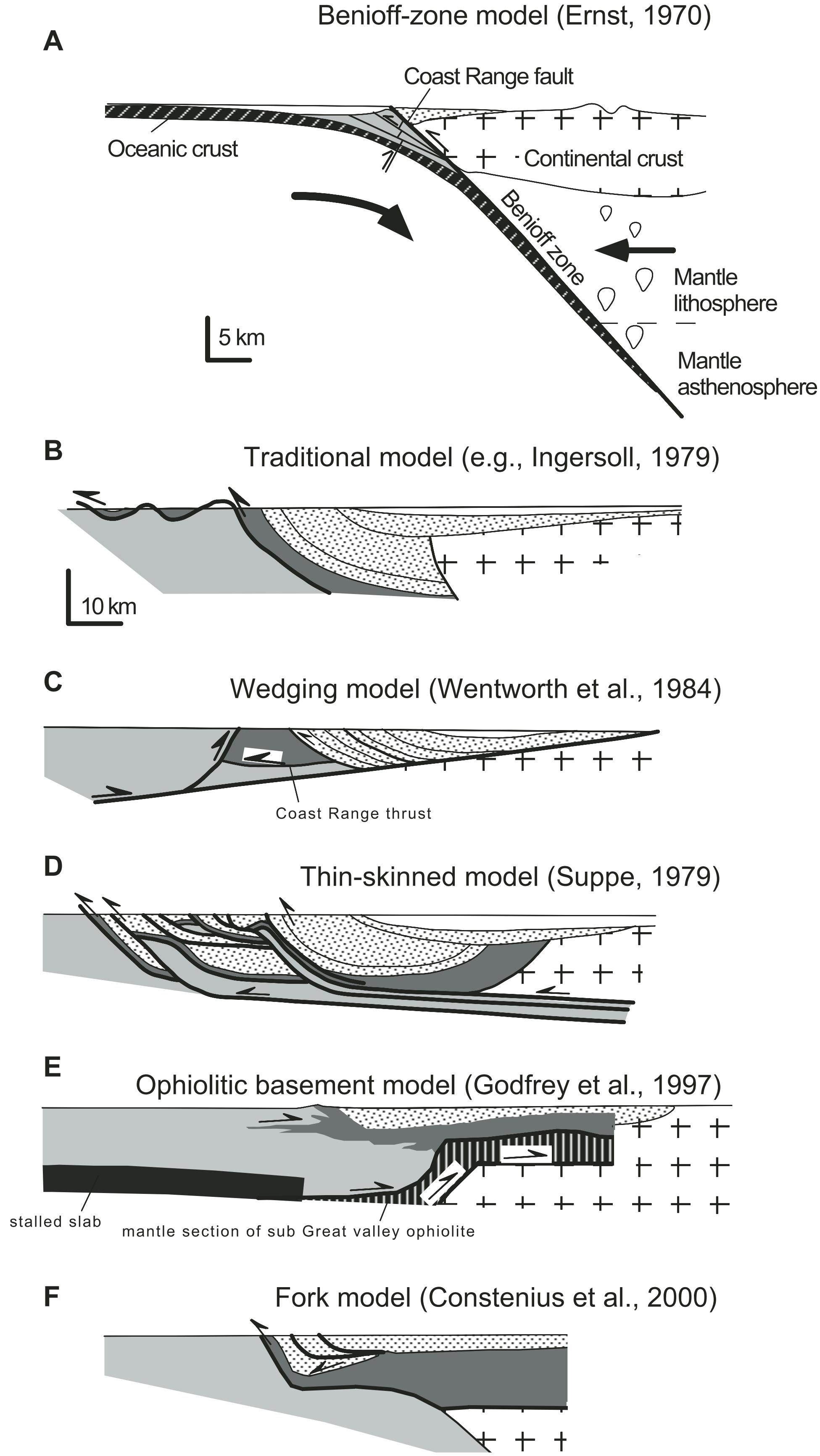

A second class of models (Page, 1981; Blake, 1984) anticipates the possibility that convergence at the Franciscan subduction zone was oblique at some time. These models attempt to account for paleomagnetic and paleontologic evidence that pelagic limestones, like the Laytonville and Calera limestones, and thick chert sequences, like the Marin Headland terrane immediately north of San Francisco, originated much farther south (Alvarez et al., 1980; Murchey, 1984). Analyses of relative plate motions also indicate that the Pacific family of plates converged obliquely with North America during the late Mesozoic (Engebretson et al., 1985). Although this second class of models recognizes that certain components of the Franciscan subduction complex are far traveled, the models basically accept that the great bulk of the terrigenous sediment in this complex was deposited in trench and trench-slope basins adjacent to the Californian margin.

A third class of more mobilistic models proposes that large parts of the Franciscan subduction complex's terrigenous sediments were transported northward before accretion (e.g., Blake and Jones, 1981). In this sense the complex would be an assemblage of displaced fragments of accretionary prism and volcanic arcs that originated hundreds or thousands of kilometers farther south.

Open Questions and Aims of Study

One of the most critical structures within the Franciscan triad is the Coast Range fault zone. Although this fault zone is currently regarded as a normal fault, we argued above that most of the evidence for such an interpretation is equivocal. It follows that there is a need for reliable kinematic indicators to unravel the role the Coast Range fault zone actually had in the development of the Franciscan subduction complex. Such kinematic data can serve to test the hypothesis that the Franciscan high-pressure rocks have been exhumed by top-E normal faulting on this structure.

Currently a major question is how much of the Franciscan subduction complex was accreted in situ, and how much of it has been transported northward. A virtual prediction of the aforementioned oblique slip models is that there should be a component of pre–San Andreas orogen-parallel strike-slip, resulting in extension parallel to the belt. In the second class of models reviewed above, belt-parallel translation might have been accomplished by major strike-slip faults that bound the displaced terranes. The last category of models is testable by a regional strain study, because the studied Franciscan metaclastic rocks should be parts of displaced fragments of accretionary prisms and thus should show pronounced along-strike extension.

The theoretical assumptions and predictions of the orogenic wedge models (e.g., Davis et al., 1983; Platt, 1986) far outstrip our field observations. Concerning the popular model of Platt (1986), one can ask two fundamental questions:

1. Is the bulk deformation within the wedge volume constant, i.e., isochoric?
2. Is the dominant deformation mechanism within an orogenic wedge in fact the SMT mechanism?

If the overall deformation within the wedge did not conserve volume, it would have had a strong impact on considerations about the development of a supercritical wedge. In general, volume gain within the wedge would tend to increase the possibility of supercritical tapering of an orogenic wedge. If, however, volume was lost during wedge deformation, supercritical tapering would be suppressed, and normal faulting would be an unfavored process.

A comprehensive study of ductile strain in the Franciscan high-pressure interior seems worthwhile to unravel the role that the SMT mechanism had in the deformation of the Franciscan subduction complex. Furthermore, such a study may shed light on the pattern and magnitude of finite strain in the Franciscan wedge. This may help to further our knowledge about the evolution of subduction complexes and whether supercritical tapering develops and leads to large-scale normal faulting that then strongly aids the exhumation of their high-pressure interior. In the particular example of the Franciscan subduction complex, a regional strain study may help to explain why the pattern of stretching lineations as reported by Harms et al. (1992) depicts such a high variability, and to test the hypothesis that this complex is an assemblage of displaced fragments of accretionary prisms. We maintain that ductile deformation in subduction complexes controls the tectonic evolution of those complexes and the development of normal faults and ductile horizontal extension. Therefore, an analysis of ductile deformation has implications for the exhumation of the high-pressure rocks from the base of subduction complexes.

Note that the paper does not attempt to explain the mélange fabrics in the Franciscan subduction complex. We believe that the mélange fabrics are largely a result of soft-sediment deformation and as such occurred before the solid-state deformation we are dealing with herein.

PRESSURE-TEMPERATURE EVOLUTION AND EVIDENCE FOR SOLUTION-MASS-TRANSFER DEFORMATION

P-T Evolution of the Eastern Franciscan Belt

Northern California

The rocks of the Yolla Bolly Mountains show a progressive W-to-E increase in metamorphic grade (Suppe, 1973; Worrall, 1981). Blue amphibole in the Pickett Peak terrane typically constitutes 30%–60% of the mafic igneous rock, whereas in the Yolla Bolly terrane blue amphibole, if present, commonly constitutes only ~1% or less of the metaigneous rocks, even in rocks of comparable bulk composition (Jayko, 1984). Lawsonite occurs throughout the Eastern Belt in metasedimentary rocks, but its grain size and abundance increase considerably toward the east.

In the South Fork Mountain Schist of the Pickett Peak terrane, clastic metasedimentary rocks contain lawsonite, phengite, blue amphibole, aragonite, and stilpnomelane. Metacherts contain crossite and spessartine-rich garnet (Blake, 1965). In metavolcanic rocks, blue amphibole is widespread and is accompanied either by lawsonite (in the west) or epidote (in the east) (Jayko et al., 1986) and acmitic-omphacitic pyroxene (Brown and Ghent, 1983). Jayko et al. (1986) concluded that P-T conditions in the South Fork Mountain Schist were 330–380 °C and 7–9 kbar.

Temperatures in the Valentine Springs Formation did not exceed 250 °C (Jayko et al., 1986). The jadeite content of pyroxene is similar to that of the South Fork Mountain Schist (Blake et al., 1988). Because temperatures in the Valentine Springs Formation were lower than in the South Fork Mountain Schist, maximum pressures were probably ~2 kbar lower than in the South Fork Mountain Schist.

Metamorphic temperatures in the Yolla Bolly terrane were 125–150 °C (Jayko et al., 1986). The jadeite content in pyroxene is 30%–40% (Jayko et al., 1986). Our microprobe reconnaissance work shows that the Si content of phengite is 3.43–3.54 per formula unit (p.f.u.) (Table 1). Collectively, the data suggest a metamorphic pressure of ~7–8 kbar.

Diablo Range

In a long series of meticulous studies, Ernst (1965, 1970, 1971, 1972, 1987, 1993), and also Seki et al. (1969), Maruyama et al. (1985), Patrick and Day (1989), and Ernst and Banno (1991), described the metamorphic evolution of the Franciscan metaclastic rocks of the Diablo Range. High-pressure metamorphism there is characterized by the widespread assemblage of jadeite, quartz, and aragonite. As was shown by McKee (1962) and Essene and Fyfe (1967), the pyroxene in the metaclastic rocks is not pure jadeite but contains significant amounts of acmite and diopside components. The inferred physical conditions of prograde metamorphism were 150 ± 50 °C at ~8 kbar or slightly more (Patrick and Day, 1989; Ernst, 1993).

P-T Evolution of the Central Franciscan Belt

In the Central Belt, metaclastic rocks typically contain pumpellyite, quartz, chlorite, and white mica (Blake et al., 1988). Fine-grained jadeite-rich pyroxene, lawsonite, and aragonite are also widespread in both graywacke and shale-matrix mélange (Blake et al., 1988; Underwood et al., 1988). Metamorphic temperatures have been estimated at 150–250 °C with pressures of 6–8 kbar (Terabayashi and Maruyama, 1998) and indicate deep burial (~25 km).

P-T Evolution of the Forearc Basin

The Great Valley Group is generally unmetamorphosed, but its lower parts show incipient burial (zeolite facies) metamorphism, as indicated by the occurrence of laumonite (Dickinson et al., 1969). Backstripping analysis revealed that the strata from the lower parts were buried >6.5 km in the Late Cretaceous without undergoing temperatures >110 °C (Dumitru, 1988). A geothermal gradient of ~15 °C km^{-1} at 90 Ma, decreasing to no greater than ~9 °C km^{-1} at 65 Ma, was reported by Dumitru (1988). This indicates a maximum burial depth of <12 km.

From the metamorphic data of the Eastern Franciscan Belt and the Great Valley forearc basin, it can be concluded that the metamorphic discontinuity across the Coast Range fault zone is on the order of 2.5–5.5 kbar, indicating that ~9–20 km of the metamorphic section is missing at the fault zone.

Evidence for SMT Deformation in the Eastern and Central Belts

To justify the use of the Projected Dimension Strain (PDS), Mode, and SMT fiber methods for strain analysis, it has to be established that solid-state ductile deformation in the analyzed rocks was solely by the SMT mechanism. In thin sections, quartz and feldspar grains are sutured and interpenetrated. Detrital grains of quartz, and to a lesser degree feldspar, are truncated by thin, dark, discontinuous selvages composed of insoluble or almost insoluble minerals (Fig. 9). Microprobe reconnaissance work reveals that these selvages contain high amounts of iron oxidic material, rutile, sphene, phengite (Table 1), and chlorite. These selvages typically have a spacing of 100–300 µm and define a non- to semipenetrative anastomosing cleavage in the rock. The detrital grains commonly show overgrowths of dominantly straight fibers oriented subparallel to the cleavage. Petrographic

TABLE 1. TYPICAL MICROPROBE ANALYSES FOR FIBROUS PHENGITE FROM VALENTINE SPRINGS FORMATION OF PICKETT PEAK TERRANE AND YOLLA BOLLY TERRANE

Sample	VSF 93-9	YBT 93-17	YBT 93-19	YBT 93-26	YBT 93-29
SiO_2	53.70	51.75	52.65	52.02	52.89
TiO_2	0.16	0.23	0.28	0.29	0.34
Al_2O_3	25.43	27.04	26.14	27.53	26.69
FeO	2.70	4.53	4.57	4.37	3.99
MnO	0.07	0.04	0.07	0.09	0.19
MgO	4.00	2.95	2.88	3.09	2.85
CaO	0.10	0.00	0.00	0.04	0.02
Na_2O	0.00	0.03	0.00	0.04	0.11
K_2O	6.39	8.31	8.44	8.12	8.12
Total	92.55	94.88	95.03	95.59	95.20

Note: VSF—Valentine Springs Formation; YBT—Yolla Bolly terrane.

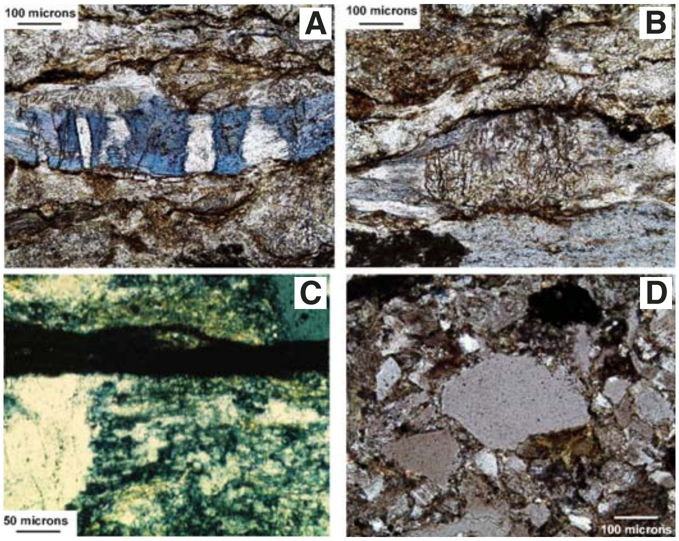

Figure 9. Photomicrographs, XZ sections, crossed nicols: (A) Extended and pulled-apart blue amphibole; shortening in Z direction caused dissolution of grains at surfaces at high angle to Z and relatively high grain aspect ratios; dark anastomosing and discontinuous selvages made up by insoluble material; sample 96-16. (B) Fiber bundles around jadeite, showing tapering "bow tie" geometry; sample 96-16. (C) Parallelism between fibrous overgrowths and selvage, indicating that incremental strain directions coincide with finite strain directions, implying coaxial deformation; sample 93-17. (D) No fibrous overgrowths around quartz, indicating very little strain; sample 97-102.

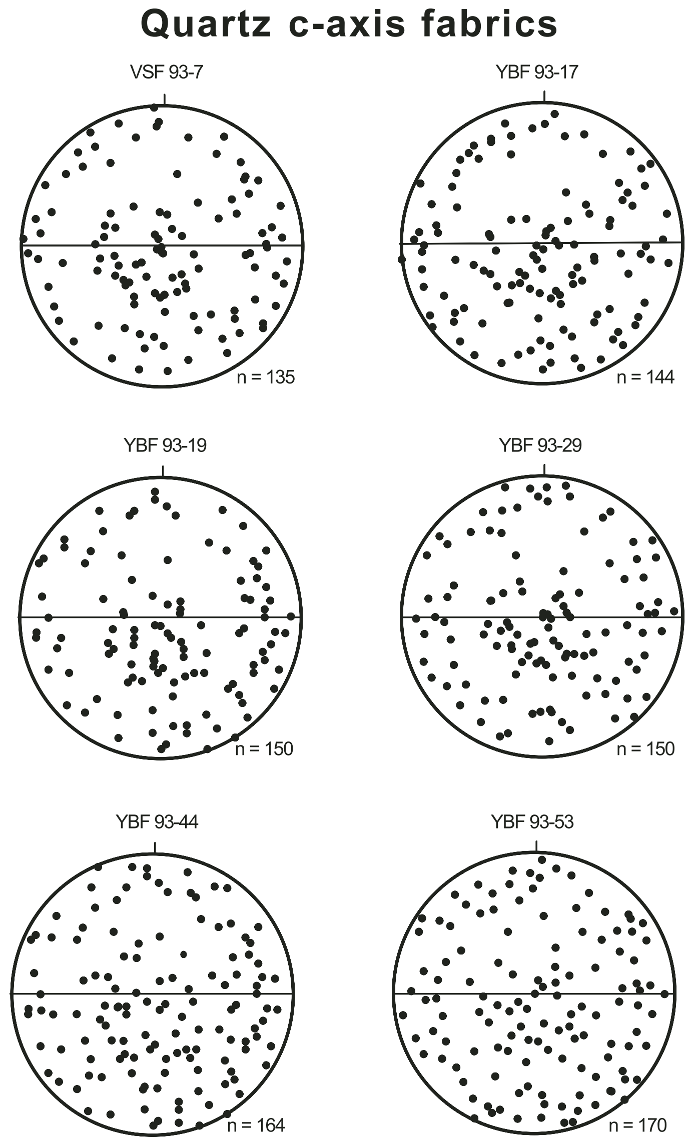

Figure 10. Quartz c-axis fabrics from six samples of Yolla Bolly terrane; note absence of any preferred crystallographic orientation in all samples.

evidence indicates that the fibers were actively accreted at the grain boundary (e.g., pyrite type of Ramsay and Huber, 1983).

The detrital grains of quartz and feldspar show no signs of internal deformation except for rare grain breakage and undulose extinction. Undulose extinction occurs only in grains that apparently have had a long history before deposition in Franciscan graywacke. Relatively fresh, first-cycle grains of volcanic quartz and feldspar grains show no evidence of undulose extinction or subgrain formation. Therefore, it is assumed that undulose extinction in some quartz and feldspar grains is an inherited feature.

The use of the gypsum plate suggests that quartz grains have no preferred crystal orientation. To verify this finding, quartz c-axis fabrics from six of the most deformed samples were measured. The c-axis plots (Fig. 10) demonstrate that the quartz grains in the metaclastic rocks of the Eastern Belt have no preferred lattice orientation. Furthermore, the metamorphic temperatures for the Yolla Bolly terrane and the Valentine Springs Formation of the Pickett Peak terrane (see above) are below the threshold of ~280 °C for activation of dislocation-glide deformation mechanisms in quartz (e.g., White et al., 1980).

These textural observations indicate that SMT was the dominant deformation mechanism, with grains shortened by grain-boundary dissolution and extended by precipitation of directed fiber overgrowth.

Figure 11 shows cathodoluminescence photomicrographs from Franciscan metagraywacke. In all examples the detrital quartz grains show up as homogeneously luminescent grains. None of the analyzed grains shows evidence of a rim of nonluminescent material. This result is of particular importance for this study, since it demonstrates that no material precipitated in the form of rinds around the detrital grains. Therefore, it can be argued that all precipitated material in the rock occurs as fibrous overgrowths.

SMT Deformation-Metamorphism Relationships

In metagraywacke of the Yolla Bolly Mountains, quartz, as well as relatively insoluble minerals, such as muscovite, phengite, chlorite, and lawsonite, make up the fibers (Fig. 12). The Si content of fibrous phengite from the Valentine Springs

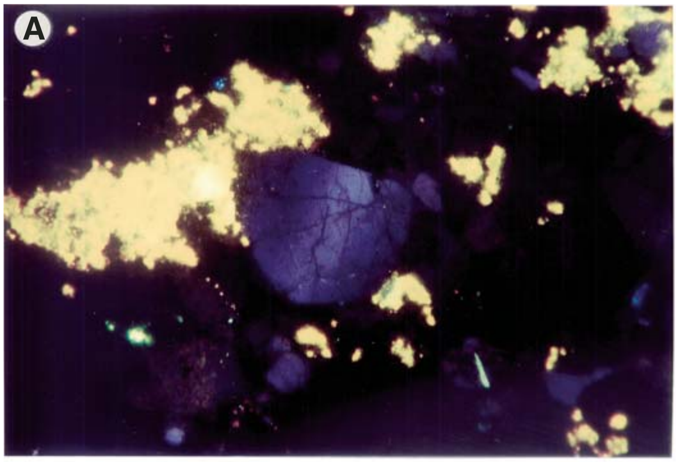

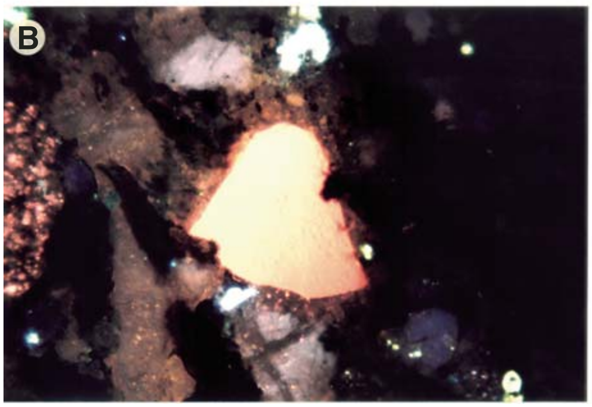

Figure 11. Cathodoluminescence photomicrograph images: (A) Blue quartz crystals in nonluminescent matrix; yellowish luminescent minerals are iron oxide precipitates; sample 93-44. (B) Yellow to brown luminescent quartz in center, and smaller, blue luminescent quartz grains; sample 93-19; in both cases, no secondary growth of quartz was detected.

Formation and the Yolla Bolly terrane is 3.50–3.58 p.f.u. (Table 1). Fibrous chlorite has a daphnitic to ripidolithic-brunsvigitic composition and is partly intergrown with phengite. Crosscutting veins in the metaclastic rocks contain pumpellyite, aragonite, calcite, albite, and quartz.

For metagraywacke in the Diablo Range, Ernst (1965, 1972, 1993) showed that tiny, fibrous jadeite overgrowths project into matrix phases that possess the same chemical compositions as the host clinopyroxene. Euhedral jadeite and aragonite occur in quartzose veins. Coarsely crystalline, concentrically and oscillatory zoned jadeite prisms replace host grains of plagioclase plus quartz. Sodic amphibole occupies stringers and fracture-related patches (Ernst, 1987). Microprobe work revealed that the fibers are composed of quartz, lawsonite, aragonite, phengitic white mica, muscovite, and chlorite (Fig. 12). The Si content of phengite is between 3.49 and 3.51 p.f.u. (Table 2). Chlorite has the same composition and shows the same textural relationships as that in the Yolla Bolly Mountains.

In the Central Belt, Terabayashi and Maruyama (1998) showed that aragonite occurs in veins. Our observations show that these veins have mutual crosscutting relationships with cleavage.

The high Si content of phengite and the occurrence of lawsonite, aragonite, and jadeite in veins and fibers demonstrate that SMT deformation commenced at the peak of high-pressure metamorphism; i.e., the rocks were deformed by the SMT mechanism as they were accreted onto the overriding plate at the maximum depth of burial. SMT deformation continued to operate as the Franciscan rocks were exhumed.

METHODS OF STRAIN ANALYSIS, SAMPLING, AND DATA COLLECTION

Kinematics of Brittle Fault Zones

Large-slip brittle fault zones are commonly composed of an array of fault surfaces with widely varying orientations and slip directions. The collective slip on these surfaces accounts for the overall offset across the fault zone. Many fault surfaces in a fault zone belong to the same class (i.e., reverse, normal, or strike-slip) as the fault zone itself. However, as was pointed out by Hancock (1985), this relationship is not universal; i.e., reverse fault zones may contain normal faults and vice versa.

A primary focus of analyzing brittle fault zones is to deduce the average direction and sense of relative transport at the regional scale. The geometry of fibers and secondary fractures on slickensided surfaces can be used to infer the slip direction (e.g., Hancock, 1985). Fault surfaces in serpentinite display local crystallization of fibrous serpentine; in graywacke, fibrous quartz occurs. The fibers are subparallel to the fault surface and are inferred to have grown in the direction of slip into spaces that formed behind steps or irregularities in the fault plane (e.g., Durney and Ramsay, 1973). The accretion of fibrous serpentine occurs in a steplike fashion. These accretion steps face toward the movement of the missing block. Other useful kinematic indicators in brittle fault zones include asymmetric folds (Hansen, 1971; Cowan and Brandon, 1994) and Riedel structures (Riedel, 1929).

Another goal of kinematic analysis of brittle fault zones is to infer the principal axes of strain, using regional arrays of small-scale fault surfaces. Recent investigations of brittle fault zones show that there is a power-law distribution of fault sizes and slip magnitudes so that small faults, as judged by their size and slip magnitude, greatly predominate in number over large faults. Furthermore, these studies demonstrate that slip on individual faults can be integrated to determine the bulk brittle strain within the zone (Marrett and Allmendinger, 1990; Scholz and Cowie, 1990). The slip direction on the small faults can be used to estimate directions of brittle strain and bulk internal rotation for the overall fault zone.

Kinematic analysis of faults has to assume that continuum mechanics can be applied to an inherently discontinuous phenomenon (Marrett and Allmendinger, 1990). If the observational scale relative to the size of the faults is increased, the defor-

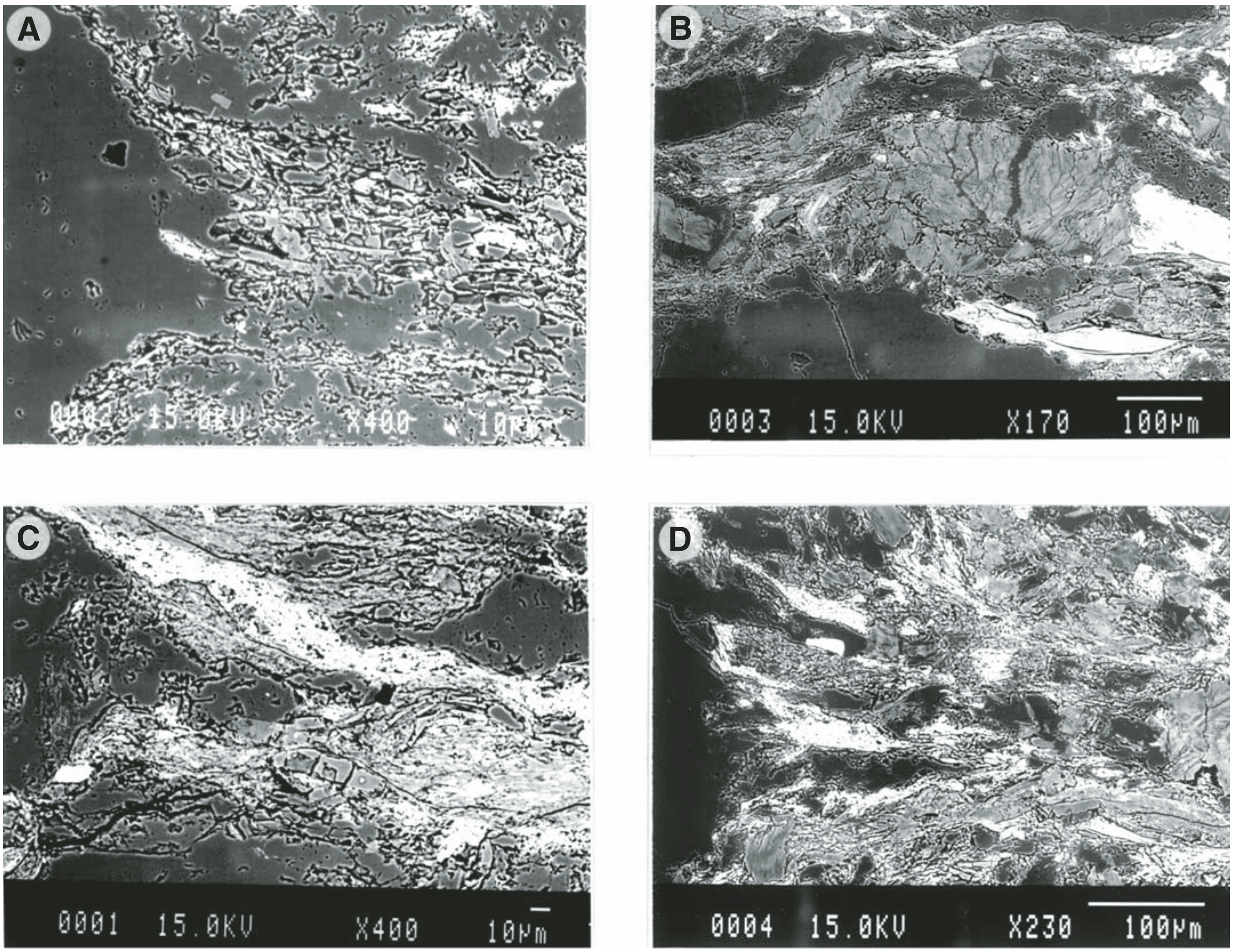

Figure 12. Backscattered photomicrograph images. (A) Euhedral lawsonite in fiber shadow behind quartz (big, dark mineral at lefthand side of micrograph); plucked-off relicts of host quartz grains also occur in fiber shadow; sample 93-19. (B) Lawsonite, chlorite (whitish), and phengite (gray) behind jadeite crystal (center of photograph); jadeite host is cracked and pulled apart, and quartz fills vein in jadeite crystal; sample 93-44. (C) Lawsonite prisms, phengite, and chlorite behind quartz grain; sample 93-53. (D) Phengite, chlorite, and jadeite in fibers between quartz (left) and small jadeite crystal (right); jadeite grains in fiber shadow appear to have been plucked off jadeite host to right; sample 93-44.

mation may be described by a continuum mechanics approach (Reches, 1987; Molnar, 1983; Cladouhos and Allmendinger, 1993). Essentially, the initial shape and the finite shape of the faulted region are regarded as continuous, not the deformation process itself (Wojtal, 1989).

Marrett and Allmendinger (1990) proposed that the strain in a faulted region can be directly related to the geometric moment, which can be expressed as the product of the average displacement and the fault surface area. This approach requires weighting the fault-slip data with the displacement and the fault surface area. These parameters can be estimated in the field via empirical scaling relationships for faults, such as fault-gouge thickness or the width of a fault (Elliott, 1976; Scholz, 1987). The pressure-tension (PT) method estimates directions of brittle strain (Marrett and Allmendinger, 1990). Slip on each fault can be viewed as contributing a small part of the total strain that occurred in the fault zone. The direction and sense of slip on a fault are defined by a slip vector, which indicates the motion of the hanging-wall block with respect to a fixed footwall block. The directions of maximum shortening and maximum extension associated with fault strain will bracket the slip direction to the fault surface (Fig. 13). Because slip on the measured faults is small in comparison with the bulk slip on a large-scale fault zone, the average incremental displacement gradient accommodated by each fault can be calculated. The average incremental displacement gradients for all observed faults can then be added. Marrett and Allmendinger (1990) use the infinitesimal-strain assumption to decompose symmetric and antisymmetric

TABLE 2. REPRESENTATIVE MICROPROBE ANALYSES OF FIBROUS PHENGITE AND LAWSONITE FROM DIABLO RANGE

Sample	YBT 93-44 phengite	YBT 93-51 phengite	YBT 93-51 lawsonite	YBT 93-53 phengite	YBT 95-53 lawsonite
SiO_2	54.56	53.71	36.89	51.58	37.82
TiO_2	0.22	0.27	0.48	0.16	0.36
Al_2O_3	28.19	27.99	32.34	26.12	31.88
FeO	2.82	4.41	0.67	4.30	0.42
MnO	0.09	0.02	0.14	0.00	0.07
MgO	3.28	3.11	1.01	3.48	0.13
CaO	0.07	0.05	16.75	0.00	16.29
Na_2O	0.00	0.02	0.00	0.00	0.00
K_2O	6.78	6.19	0.11	6.21	0.05
Total	96.01	95.77	88.39	91.85	87.02

Note: YBT—Yolla Bolly terrane.

parts. The eigenvectors of the symmetric part yield the orientations of the principal strain axes for brittle strain. Cladouhos and Allmendinger (1993) investigated the finite-strain case, showing that the results are approximately equivalent.

Cladouhos and Allmendinger (1993) argued that the moment-tensor approach may not be appropriate to represent the cumulative displacement on faults because it assumes infinitesimal strain. Another shortcoming of the PT method is that it cannot correctly calculate block rotations and is therefore not really capable of yielding unambiguous information about the rotational aspect of deformation in the fault zone.

Symmetry-based methods for analyzing the kinematics of brittle fault zones were proposed by Hansen (1971), Twiss and Gefell (1990), and Cowan and Brandon (1994). Symmetry methods, as well as the above outlined tensor-based methods, rest on symmetry principles (Paterson and Weiss, 1961); e.g., the monoclinic symmetry of a noncoaxial fault zone is recorded in the fabric of the fault zone (Cowan and Brandon, 1994). The fabric is determined not only by the symmetry of the deformation but also by the symmetry of processes preceding and attending deformation.

Symmetry methods first try to find the symmetry plane(s) of the overall deformation. Three general cases have to be distinguished: (1) Monoclinic symmetry, as characterized by one mirror plane. The intersection of this symmetry plane and the fault plane defines the slip direction (Hansen, 1971). In association with sense of shear criteria, the slip vector for the fault zone can be deduced. (2) Orthorhombic symmetry, as displayed by three orthogonal mirror planes. In this case, only the slip direction can be deduced. (3) Triclinic symmetry with no mirror plane. A kinematic interpretation is not possible.

We employ the internal-rotation-axis (IRA) method of Cowan and Brandon (1994), which provides a direct way to determine the bulk sense of shear on the fault zone. The internal rotation axis for a fault is shown in Figure 13. The data can be shown as either S– or Z–internal rotation axes, depending on the relative sense of rotation when viewed in the down-plunge direction of the fold axis (cf. Hansen, 1971). Plotting the S- and Z-rotation axes for all faults from a fault zone yields information about the structural symmetry and overall sense of shear for the fault zone. An alternative method for viewing these data is to

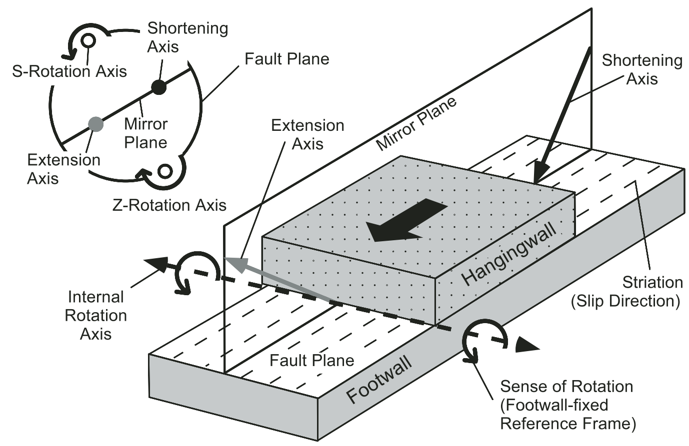

Figure 13. Schematic diagram illustrating relationship of fault and its slip direction to orientations of shortening, extension, and internal rotation axes used to represent brittle strain; geometry of structural features portrayed in stereogram on left; mirror plane defined as lying normal to average orientation of Z-transformed axes, assuming that shear zone formed by unidirectional tectonic transport, which, in ideal case, would be characterized by monoclinic structural symmetry.

convert the internal rotation axes so that they all have a common Z sense of rotation (i.e., a right-handed rotation). These directions will include both positive and negative plunges (down and up, respectively). Therefore the data must be portrayed and contoured, using both the lower and upper hemispheres of the stereogram. If the structures within the fault zone were formed by a single direction of offset across the zone, and if the structures were not significantly affected by preexisting structures (i.e., antecedent processes of Cowan and Brandon, 1994), then the statistical symmetry of the structures within the fault zone should be monoclinic. Basically, the approach attempts to find the average internal rotation axis for bulk shear across the fault zone. The Fisher vector mean and contouring method is used to determine the average orientation for each set of strain axes. The average orientation of the Z-sense axes is used to define the mirror plane and the overall sense of shear for the fault zone. The slip direction is indicated by the intersection of the mirror plane with the attitude of the overall fault zone (Cowan and Brandon, 1994).

Proper averaging of the bulk brittle shear would require weighting each measurement proportional to the amount of slip on the fault. We have no information about slip magnitudes for our study, so we are forced to assume equal weight for all of our slip directions. This approach is justified practically because there is only a limited variation in size among the exposed faults, and because fault size is correlated with slip magnitude (e.g., Marrett and Allmendinger, 1990). In this respect the symmetry-based IRA method is more robust because symmetry does not depend on the relative magnitudes of the observed faults, but on their geometry. A critical assumption, of course, is that the measured faults are representative of all faults within the zone, regardless of size. Relating the estimated directions of bulk brittle strain to the deformational history of the fault zone should be straightforward as long as the fault zone and its component structures are the result of a single direction of tectonic transport.

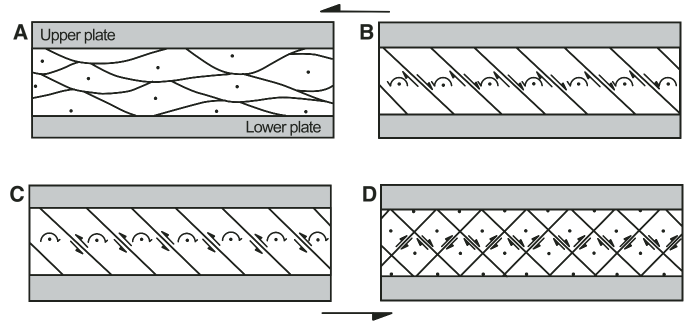

Figure 14. (A) Elongate fault slices aligned parallel to fault zone; shear sense indicated by synoptic Z-axis will be equal to overall shear sense of fault zone. (B) Obliquely oriented rotating fault slices, with rotation of fault slices antithetic to overall shear-induced rotation associated with fault zone. (C) Same as B, but rotation of fault slices are synthetic with fault zone. (D) Set of equant blocks rolling like ball bearings within fault zone (modified from Twiss et al., 1993).

Preferred Method of Analysis

We prefer the symmetry method for interpreting fault-zone kinematics. The symmetry principle states that the synoptic symmetry for the fault-zone fabric will be equal to or higher than the combined symmetry of the deformational process and any antecedent processes (Paterson and Weiss, 1961; Twiss and Gefell, 1990; Cowan and Brandon, 1994). The slip or shear sense is defined by the sense indicated by the synoptic Z-axis. Twiss et al. (1993) noted that the internal rotation within the fault zone is partitioned between rotation of blocks within the fault zone and shear resolved by slip on the slickensided surfaces, which surround the blocks. Four simple cases are illustrated in Figure 14. The first shows elongate fault slices aligned parallel to the fault zone. In this case, the shear sense indicated by the synoptic Z-axis will be equal to the overall shear sense of the fault zone. The second and third cases show obliquely oriented rotating fault slices, with the rotation being antithetic and synthetic with respect to the overall shear-induced rotation associated with the fault zone. The synoptic Z-axis indicates the correct shear sense for antithetically rotating slices but indicates the opposite shear sense for synthetically rotating blocks (the usage here of antithetic and synthetic rotations are after Passchier and Trouw, 1996, p. 113). The final example is a set of equant blocks, which roll like ball bearings within the fault zone. In theory, this type of fault zone would entirely lack internal fault surfaces if the fault blocks rolled with compatible tangential velocities at their surfaces, much like ball bearings. This case is a null example because there would be no slickensided surfaces and thus no shear-sense indicators.

We conclude that the examples in 1–3 span the range of possible conditions for the generation of shear-sense indicators in brittle fault systems. It is well recognized that regional-scale fault systems can have well-organized networks of internal faults dominated by either synthetic or antithetic geometries (Wernicke and Burchfiel, 1982; Cowan et al., 1986; Ring, 1995b). By analogy, shear-sense interpretation of brittle fault zones would be hampered if a systematic system of synthetically rotating fault slices were present. This possibility must be assessed to ensure a reliable kinematic analysis.

Sites of Fault Studies

Our kinematic studies at the Coast Range fault zone were done in two areas, which were specifically identified as extensional structures by Jayko et al. (1987) and Harms et al. (1992): (1) in the Yolla Bolly Mountains of northern California at Beehive Flat and Salt Creek near the town of Paskenta (Fig. A1 in Appendix[1]), and (2) in the northern Diablo Range of central California at Del Puerto Canyon (Fig. A2) and Mount Diablo (Fig. 2). The fault-slip studies within the Franciscan subduction complex cover the Coast Range fault zone, the Redwood Mountain fault, the Grogan fault, and the Bald Mountain fault east of Eureka, as well as the Coastal Belt thrust between Cloverdale and Garberville and the San Andreas fault near Cazadero (Fig. A3).

Ductile Strain

The methods used for quantifying ductile strain that accumulated during SMT deformation were outlined in Brandon et al. (1994) and Ring and Brandon (1999). Important here is to note that these methods allow quantifying ductile strain absolutely and also allow quantifying the amount of rotation during the accumulation of ductile strain.

As will be shown below, the ductile strain analysis yielded a heterogeneous data set. For addressing questions of regional significance, we found it necessary to calculate regional averages of the data. To obtain reliable strain tensor averages for SMT deformation on a regional scale, the sampling strategy must be

[1]The Appendix begins on p. 44.

representative for all deformation fields of that particular region. To accomplish this goal the strategy was to sample randomly in regions where the rock types are homogeneous at the scale of sampling. We sampled at three different scales in the Eastern and Central Franciscan Belts: (1) random sampling at a relatively large scale (Figs. A4–A6): (2) more detailed sampling in selected areas of the Eastern and Central Belts (Figs. A6–A8), and (3) detailed sampling at Leech Lake Mountain (Fig. A9) and in the proposed Del Puerto Canyon shear zone of Harms et al. (1992) (Fig. A10) (Ring and Richter, 2004).

Field measurements of cleavage, bedding, and, in rare cases, the stretching lineation have been taken in order to qualitatively compare the field measurements to the finite-strain results as produced in the laboratory.

Seven samples from lithic sandstones of the Great Valley Group have also been collected (four from the Yolla Bolly Mountains and three from the Diablo Range, Figs. A7, A8). These rocks show no internal deformation, and measurements of the dimensions of quartz grains indicate that the aspect ratios of the grains are close to 1 (Table 3). Therefore, it is assumed that the initial aspect ratios of quartz from the lithologically similar Franciscan metagraywacke samples were also close to 1.

Calculation of Exhumation by Vertical Ductile Thinning

As will be shown, the regional averages of our strain measurements indicate that SMT deformation resulted in vertical shortening. To properly estimate the contribution that this process made to the total exhumation of the Eastern and Central Franciscan Belts, both the vertical rate at which the rocks moved through the wedge and the rate of thinning of the remaining overburden at each step along the path have to be considered. For this purpose the model of Feehan and Brandon (1999), which calculates exhumation and ductile strain for particles moving through a steady-state wedge (Fig. 6), is used. By steady state it is meant that the rates of basal accretion, ductile strain, normal faulting, and erosion all remain constant with time.

The model integrates the acquired ductile strain of a rock over the thickness of an orogenic wedge and thereby calculates the fraction of the total exhumation caused by ductile thinning of the overburden. The rate of basal accretion, $\dot{\alpha}$, equals the rate of denudation (expressed as the rate of normal faulting plus erosion [$\dot{\varepsilon} + \dot{\mu}$] in Fig. 6). In the model the particle is first accreted at the base of the wedge unstrained and then moves through the interior of the wedge, where it accumulates ductile strain and leaves the wedge at the Earth's surface with a specific amount of ductile finite strain. That is, if the rock ascends through the column it acquires its finite ductile deformation. In order to investigate the exhumation history of the Eastern and Central Belts on a regional scale, strain tensor averages are considered to represent the finite ductile deformation of these belts.

TABLE 3. FINITE STRAIN DATA OF UNDEFORMED SAMPLES FROM GREAT VALLEY GROUP

Finite strain data	S (ab)	S (ac)	S (bc)
Sample			
GV 93-1	0.958	1.101	1.096
GV 93-2	1.034	1.057	1.147
GV 93-5	0.996	1.197	1.333
GV 93-6	1.113	0.991	1.060
GV 93-45	1.012	0.993	1.078
GV 93-52	0.978	1.011	0.989
GV 93-55	1.067	0.981	0.998

Note: ab—bedding plane; ac, bc—sections that are normal to each other and normal to bedding.

Elliott (1972) and Rutter (1983) argued that the rate-controlling step for SMT deformation is diffusion, which implies that the strain rate is a linear function of deviatoric stress. This suggests that the strain rate should scale approximately with depth, i.e., approximately uniform. However, these studies consider only closed-system behavior. In the case of open-system deformation, the rate of mineral dissolution or the rate of fluid advection will control the rate of deformation, making it difficult to specify a constitutive flow law. In this study the model calculations are based on a ductile-strain-rate law that is either uniform or proportional (Fig. 6) with depth. We think that the proportional strain-rate law approximates within-wedge deformation more closely, because both the rate of mineral dissolution and the rate of fluid advection are temperature and pressure dependent and increase with depth.

To solve for the best-fit parameters, we iterate the model and search for parameters that give the correct amount of exhumation and finite strain while the rocks of the Eastern and Central Belts resided within the wedge.

BRITTLE STRAIN ON THE COAST RANGE FAULT ZONE

Overview

Over most of California, the Coast Range fault zone has been steeply tilted and locally overturned to the east. The Great Valley sediments immediately above the Coast Range fault zone are also steeply tilted, indicating that the fault zone and the forearc sediments were rotated after deposition of the strata. The fault zone is commonly decorated by brittle serpentinite-rich shear zones, presumably derived from ultramafic rocks of the overlying Coast Range ophiolite (Fig. 15).

Based on kinematic data from the Coast Range fault zone, Ring and Brandon (1994) proposed that the fault formed by horizontal shortening, presumably by postaccretion out-of-sequence thrusting. There is growing evidence that the tectonic evolution of the Franciscan convergent margin included a significant component of backthrusting ("tectonic wedging" of Wentworth et al., 1984). These models envision the Coast Range fault zone as the roof thrust of an eastward-driven tectonic wedge of Franciscan material and postulate a component of top-W motion on the fault zone that has been active during the Quaternary and may have started as early as the latest Cretaceous (Unruh et al., 1995; Wakabayashi and Unruh, 1995).

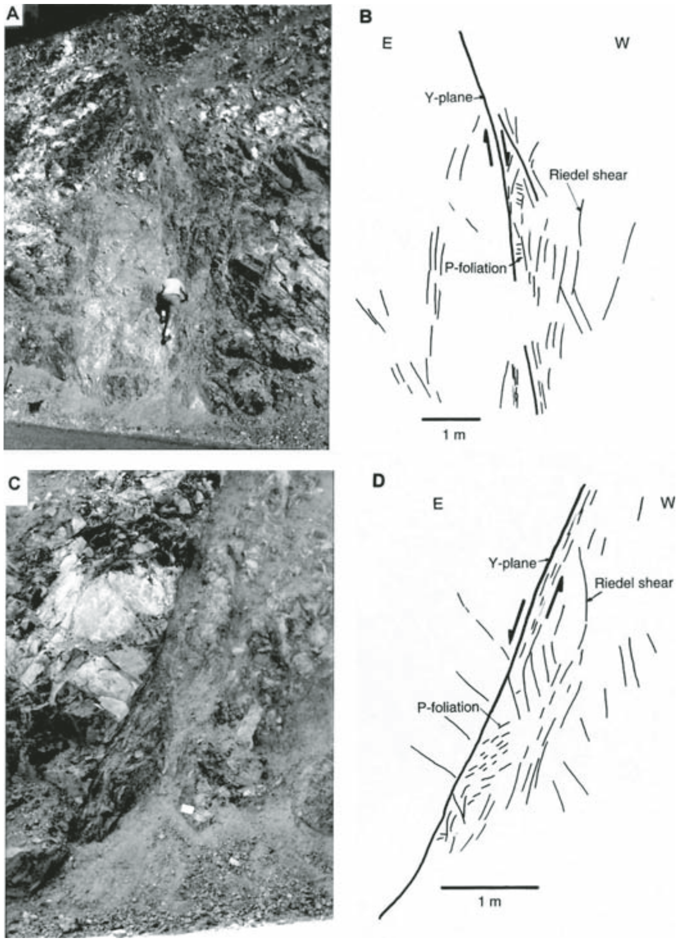

Figure 15. Photographs and line drawings of outcrop-scale faults within Coast Range fault zone (locations indicated in Fig. A2). (A, B) Steep, W-dipping, serpentinized fault zone; note variability in fault attitudes. (C, D) E-dipping fault zone, separating block on left of partially serpentinized harzburgite from highly sheared serpentinite matrix to right. Riedel shears and P-foliations provide information about sense of slip.

Our previous paper (Ring and Brandon, 1994) was criticized on a number of points. We summarize these issues here because they will help the reader to understand the focus we have taken in this paper.

(1) *The kinematic analysis presented in Ring and Brandon failed to provide an unambiguous indication of the shear sense for the Coast Range fault zone.* We agree on this point and have reviewed methods of kinematic analysis for brittle fault zones, above. We emphasize, like Twiss and Gefell (1990) and Cowan and Brandon (1994), that symmetry-based methods are the soundest and most robust methods. We use the internal-rotation-axis (IRA) method of Cowan and Brandon (1994) to get a direct estimate of the average sense of shear within the fault zone.

(2) *Major fault zones only preserve evidence of the latest stages of motion because faulting tends to abrasively remove and obliterate older structures.* This is a widely held view. Even so, we cannot identify any studies in which this interpretation has been demonstrated. This notion might be reasonable for fault zones where slickensides have formed in association with gouge-rich slip surfaces. The abrasion that formed the gouge material provides evidence that older structures may have been removed. However, we think it is important to note that many slickensides form by the accretion of fibrous overgrowth. In this case, much if not all of the slip history that occurred on the slip surfaces is preserved in the slickensides. The slickensides within the Coast Range fault zone studied by Ring and Brandon (1994) formed by the accretion of fibrous serpentine. The fiber directions are straight and unidirectional. Thus, we conclude that these kinematic indicators provide a fairly complete record of the slip history within the structure called the Coast Range fault zone. Furthermore, the general absence of curved fibers or overlapping fiber directions indicates a relatively simple single-phase history for this fault zone.

(3) *Contractional motion on the Coast Range fault zone cannot account for the metamorphic gradient that used to sit between the Great Valley forearc basin and the subjacent Franciscan subduction complex.* The point that may have been missed here is that forethrusts can place low-grade rocks over high-grade rocks in those cases where the metamorphic section was tilted prior to thrusting. More specifically, the metamorphic section must dip in the direction opposite of the transport direction for the thrust (see Fig. 1 of Wheeler and Butler, 1994; see Fig. 1 in Ring and Brandon, 1994; Ring, 1995a). We maintain that the problem of structural omission must be distinguished from that of exhumation. Platt's (1986) proposal of omission of crustal section by normal faulting accounts for both attenuation across the Franciscan subduction complex–Great Valley transition and exhumation of the complex. Our proposal of omission of structural section by thrust faulting does *not* account for exhumation. Instead, we argue that the Franciscan subduction complex was already largely exhumed prior to thrusting on the Coast Range fault zone. We attributed the exhumation largely to erosion of an evolving forearc high. Eastward tilting of the Great Valley Group–Coast Range ophiolite–Franciscan subduction complex section is considered to have occurred at that time. Subsequent out-of-sequence forethrusting on the Coast Range fault zone would have been responsible for omission of the tilted metamorphic section within the eastern flank of the uplift, creating the overall structural relationships we see today.

(4) *Erosional exhumation of the Franciscan subduction complex is unlikely because large amounts of ultramafic detritus have not been detected in Great Valley and Franciscan sandstones of appropriate age.* This argument is based on the assumption that a thick mantle section underlay the Coast Range ophiolite after the initiation of Franciscan subduction (Wakabayashi, 1992). The higher-temperature metamorphism of the Pickett Peak terrane, in comparison with the tectonically underlying Yolla Bolly terrane, is attributed to heating from the adjacent hot mantle hanging wall. This is an interesting idea, but it has little direct support. One problem is that initial metamorphism in the Pickett Peak terrane was concluded at ca. 150–125 Ma, whereas metamorphism in the Yolla Bolly terrane occurred at ca. 90 Ma and later (see above). Therefore, the

different degrees of metamorphic temperatures in both terranes must not have been related to heating from an overlying mantle wedge. The review of the alternate origins of the Coast Range ophiolite by Dickinson et al. (1996) also envisions scenarios in which the mantle section would have been lost at the start of subduction, leaving the Coast Range ophiolite as a thin structural lid. Hence, we think it is also pertinent to assume that the Cretaceous Franciscan subduction complex was filled with voluminous clastic debris, as proposed by Ernst and Liou (1995). This reasoning, and the argument that the Coast Range ophiolite was attenuated, imply that erosional exhumation of the Franciscan high-pressure rocks must not have been associated with large amounts of ultramafic detritus.

(5) *The kinematic data of Ring and Brandon (1994) are most likely related to the relatively young deformation associated with the formation of an E-directed wedge or triangle zone along the eastern flank of the Coast Range uplift.* We agree that the evidence for E-directed wedging is compelling and that this deformation has been active since the middle Cenozoic and possibly the latest Cretaceous as well (Unruh et al., 1995). Furthermore, we do not discount the possibility that our kinematic data are related to this relatively young deformation. The problem is that motion within the Coast Range fault zone is only broadly constrained to the interval between the latest Cretaceous to the present. Unruh et al. (1995) provide unambiguous evidence of wedging during the Neogene. Evidence for wedging during the latest Cretaceous and early Cenozoic is ambiguous because there is almost no stratal discordance between Cretaceous and Paleogene strata (Dickinson, 1971; Dickinson et al., 1979). Thus, the wedging-related structures and the structures reported by Ring and Brandon (1994) may overlap in time and are likely related. We emphasize that this possibility, whether right or wrong, has little or no bearing on the analysis of our kinematic data or the basic features of our interpretation of the exhumation of the Franciscan subduction complex.

Structures in the Coast Range Fault Zone

This fault zone is typically 3–4 km thick and is dominated by angular blocks of serpentinized harzburgite and serpentinite-rich shear zones (Fig. 15). A dense array of variably oriented fault surfaces is generally present. The fault surfaces display well-developed slickensides, which are mantled by striations defined by fibrous serpentine. The direction of fiber overgrowth and the orientation of extensional fractures cutting the fibers provide an excellent record of the local direction and sense of slip. In almost all observed cases, each slickensided surface is covered by only one set of straight, unidirectional fibers. We consider the slickensides to preserve a nearly complete record of fault-zone deformation, because the slickensided surfaces formed by the accretion of new fibrous serpentine rather than by the abrasion and comminution of existing wall rock. These observations suggest that the fault zone and component structures that define the *present* Coast Range fault zone formed as a result of a single direction of tectonic transport.

If a shear zone thickens or thins during its evolution, strain compatibility requires that the materials within the zone must undergo volume strain, or the walls of the shear zone must deform in a compatible manner (Ramsay and Huber, 1983). Because in three out of four cases, the maximum extension axis lies subperpendicular to the surface of the Coast Range fault zone, and the brittle strain data indicate that the Coast Range fault zone thickened during its evolution. We propose that strain compatibility was maintained, at least in part, by volume strain associated with serpentinization. Serpentinite itself has an average density of ~2520 kg m^{-3}, and the density of the original unaltered harzburgite is ~3240 kg m^{-3} (Christensen, 1978). Thin sections show that the degree of serpentinization within the fault zones is on the order of 40% in the weakly deformed areas and up to 100% in the more severely deformed shear zones, indicating a serpentinization-related volume increase of 12%–29% (see Eq. 4 in Brandon, 1995).

Brittle Strain Analysis

The raw fault-kinematic data for each particular outcrop are shown and described in the Appendix (Figs. A11–A20). Here only summaries of the data will be given (Fig. 16).

Yolla Bolly Mountains

The contoured shortening directions for all sampled faults in the Beehive Flat area (Fig. 16B) have a well-defined point maximum oriented in a nearly vertical direction, subparallel to, but somewhat more steeply inclined than, the present downdip direction of the fault. The contoured extension axes (Fig. 16C) depict a girdle pattern suggestive of a flattening type of deformation; a maximum is apparent, with a subhorizontal direction trending ESE. The orientations of the principal extension and shortening axes are subparallel to the contoured maxima. As a result of the smaller number of measured faults and the relatively high percentage of strike-slip faults, the contoured maxima at Salt Creek (Figs. 16E, 16F) are weak and are therefore statistically less meaningful. However, the same general pattern is indicated.

Diablo Range

The contoured shortening and extension directions for Del Puerto Canyon (Figs. 16H, 16I) are nearly identical to those at Beehive Flat (Figs. 16B, 16C), although the extension axes show a better-developed point maximum, and the shortening axes depict a slight girdle distribution. For Mount Diablo, the sparse data set also indicates fault-parallel shortening (Fig. 16K) and subhorizontal E-W extension (Fig. 16L) when viewed in the present reference frame.

At Del Puerto Canyon the Coast Range fault zone and the Del Puerto ophiolite are cut by a set of NW-striking subvertical faults (Fig. A2) with strike-slip motion (Figs. A15A, 15B). We found a few faults that had two sets of slickenside striae, with the younger of the sets indicating strike-slip offset (faults with dashed great circles in Figs. A13A–C). The strike-slip motion indicated by these structures is therefore interpreted to postdate the formation of the Coast Range fault zone, and hence might be related to the modern San Andreas fault system.

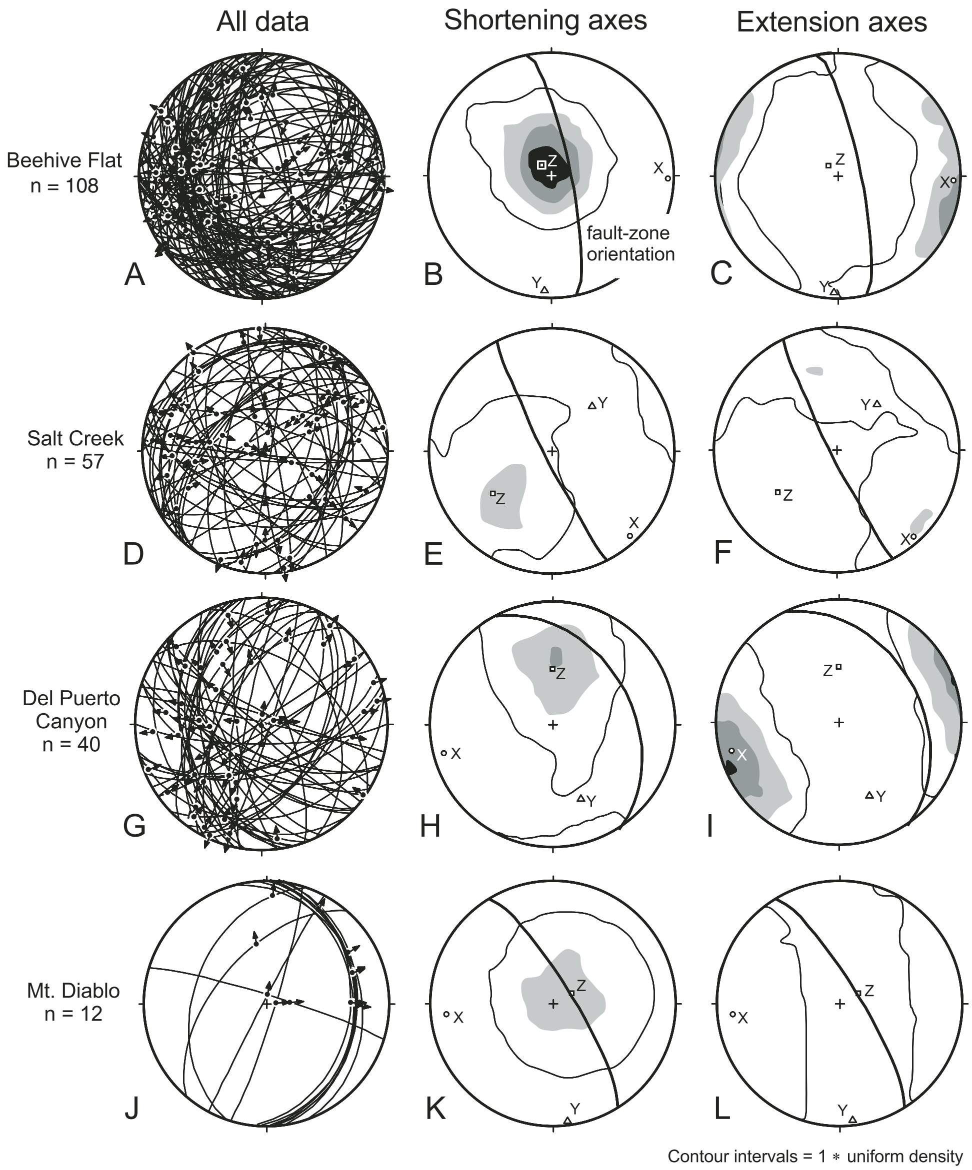

Figure 16. Stereograms showing all fault data in present coordinates for Coast Range fault zone at Beehive Flat, Salt Creek, Del Puerto Canyon, and Mount Diablo areas; stereograms in left column show attitude and direction of slip for all measured faults; right two columns of contoured stereograms show distributions of shortening and extension axes inferred for each of kinematic measurement (PT method of Marrett and Allmendinger, 1990); great circles in contoured stereograms show regional attitude of Coast Range fault zone at each of study areas. Contours were determined using method of Kamb (1959) and are reported in multiples of expected density for uniform distribution; lowest contour is 1 times uniform density, and contour interval is 1 times uniform density as well. Beehive Flat and Del Puerto Canyon areas are dominated by W-dipping normal faults; Mount Diablo area is dominated by E-dipping normal faults; Salt Creek area is characterized by highly variable fault orientations. Contoured stereograms indicate that Beehive Flat and Del Puerto Canyon areas have well-developed preferred orientation of principal axes of brittle strain (maxima are >3 times uniform density); principal axes at Salt Creek and Mount Diablo show much weaker maxima (<3 times uniform density), but patterns are similar to those for Beehive Flat and Del Puerto Canyon areas.

Interpretation of Data

There is no clear evidence that the Coast Range fault zone is dominated by a systematic set of synthetically rotating fault slices. As a consequence, we consider the average direction of the synoptic Z-axis to be a reliable indicator of the sense of slip on the Coast Range fault zone.

Constraints for Physical Setting of Fault Slip

For interpreting the kinematic data, it is useful to view the data in a fault-parallel reference frame (Fig. 17) with the primitive circle of the stereogram oriented parallel to the regional attitude of the fault zone (Ring and Brandon, 1994). This reference frame emphasizes the fact that the shortening axes lie at a low angle (~10°–15°) to the fault zone, and the extension axes define a girdle that lies in a plane approximately perpendicular to the shortening direction and at a high angle to the fault zone. This pattern suggests that brittle strain has resulted in a flattening style of deformation within the fault zone. Moreover, this pattern argues for a component of contraction across the fault zone. The low angle between the principal shortening direction and the mean fault plane caused thickening of the fault zone, probably due to distributed general shear on a system of faults.

The fact that the PT method indicates a maximum extension axis oriented almost perpendicular to the downdip direction of the fault zone needs some explanation. In large-slip fault zones the finite extension axis should rotate toward the fault plane. As was shown by Cladouhos and Allmendinger (1993), the results of the PT method do not fully represent the finite deformation associated with faulting; they only record aspects of strain associated

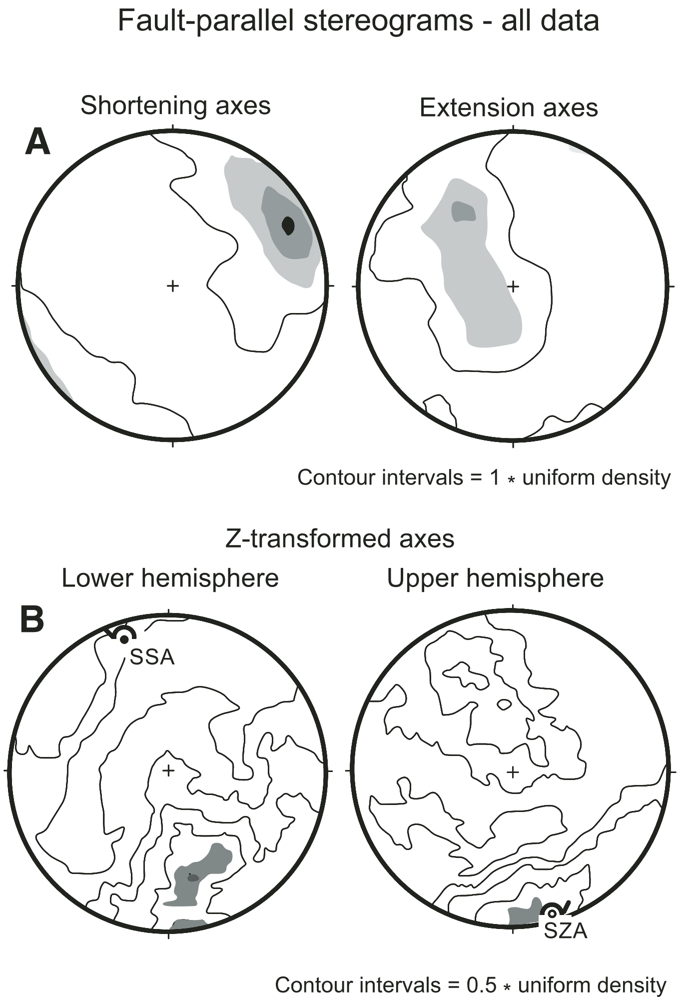

Figure 17. Summary fault-parallel stereograms showing (A) principal axes of brittle strain and (B) Z-transformed internal-rotation axes for all four study areas at Coast Range fault zone; stereograms were prepared by rotating data in Figure 16 by amount necessary to rotate Coast Range fault to primitive circle of stereonet; shortening axes show well-defined cluster oriented at low angle (~10°–15°) to fault zone, and extension axes define girdle that lies approximately perpendicular to average shortening direction and at high angle to fault zone; Z-transformed internal-rotation axes show maximum oriented in subhorizontal direction trending southeast; results indicate that Coast Range fault zone formed as top-W contractional fault zone.

with deformation. Therefore, a rotation analysis should help to shed light on the rotational aspect of the deformation that occurred with the Coast Range fault zone.

Rotation Analysis

The fault plane in each stereogram (Fig. 18) corresponds to the average orientation of the Coast Range fault zone in that area. Note that this orientation is commonly different from the average orientation of the measured faults, which lay within the fault zone (Figs. A11–A14). In this respect, we are interested in determining the bulk shear indicated by the population of faults within the fault zone and in relating this shear to the overall displacement across the fault zone.

The internal-rotation axes for the measured faults are displayed in two different ways in Figure 18. The left column of the stereograms shows all axes as projected into the lower hemisphere; the sense of rotation is designated by a Z or an S (clockwise and counterclockwise, respectively). An easier way to portray these data is to convert all internal rotation axes to a common Z sense of rotation, and to display them on the full sphere, which is shown by two stereograms, one showing the lower hemisphere, and the other, the upper hemisphere (center and right columns in Fig. 18). Cowan and Brandon (1994) refer to this type of distribution as Z transformed. One can think of the average Z direction as akin to the average “rolling” direction in the fault zone.

If the internal-rotation axes were due to unidirectional general shear, we would expect that the distribution of the Z-transformed axes should show a single well-defined maximum corresponding to the average Z-axis or the synoptic Z-axis (SZA). The equivalent rotation is also indicated by an S-sense of rotation in the antipodal direction, which is called the synoptic S-axis (SSA). Cowan and Brandon (1994) discussed cases in which internal-rotation-axis distributions might show departures from this expected result; the reader is referred there for further details. For our analysis here, we adopt the simplest interpretation that a well-defined unimodal cluster of Z-axes reflects the monoclinic symmetry of a unidirectional general shear that affected the entire fault zone. The SZA direction, which can be determined from the density maximum or the Fisher vector mean of the Z-axes, defines the normal to the mirror plane for the shear zone. We infer that the direction of slip lies at the intersection of this mirror plane with the attitude of the overall fault zone. The slip vector, which includes both the direction and sense of slip, is then deduced from the relative orientation of the SZA with the slip direction.

For the Beehive Flat area, the Z-axes (Fig. 18B) show a well-defined unimodal cluster, which defines an SZA direction plunging gently to the south. It should be pointed out here that only areas >2 times uniform density are statistically significantly overpopulated. This orientation indicates an E-up (or top-W) sense of motion for the Coast Range fault zone in this area. The large dispersion of the Z-transformed axes around the SZA direction appears to be typical of brittle fault zones and is attributed by Cowan and Brandon (1994) to stochastic processes associated with fault-zone deformation.

At first glance, the indicated E-up sense of motion for this area appears at odds with the predominance of normal faults among the measured fault data (Fig. A11). However, normal slip generally occurs on moderately W-dipping faults, whereas the Coast Range fault zone dips steeply to the east. When the slip vectors for the measured faults are considered in relationship to the geometry of the overall fault zone, it becomes apparent that the W-dipping normal faults caused thickening of the fault zone, as indicated by the orientation of the principal axes of brittle strain determined above by the PT method. Thus, faults that show normal slip in present coordinates are in fact

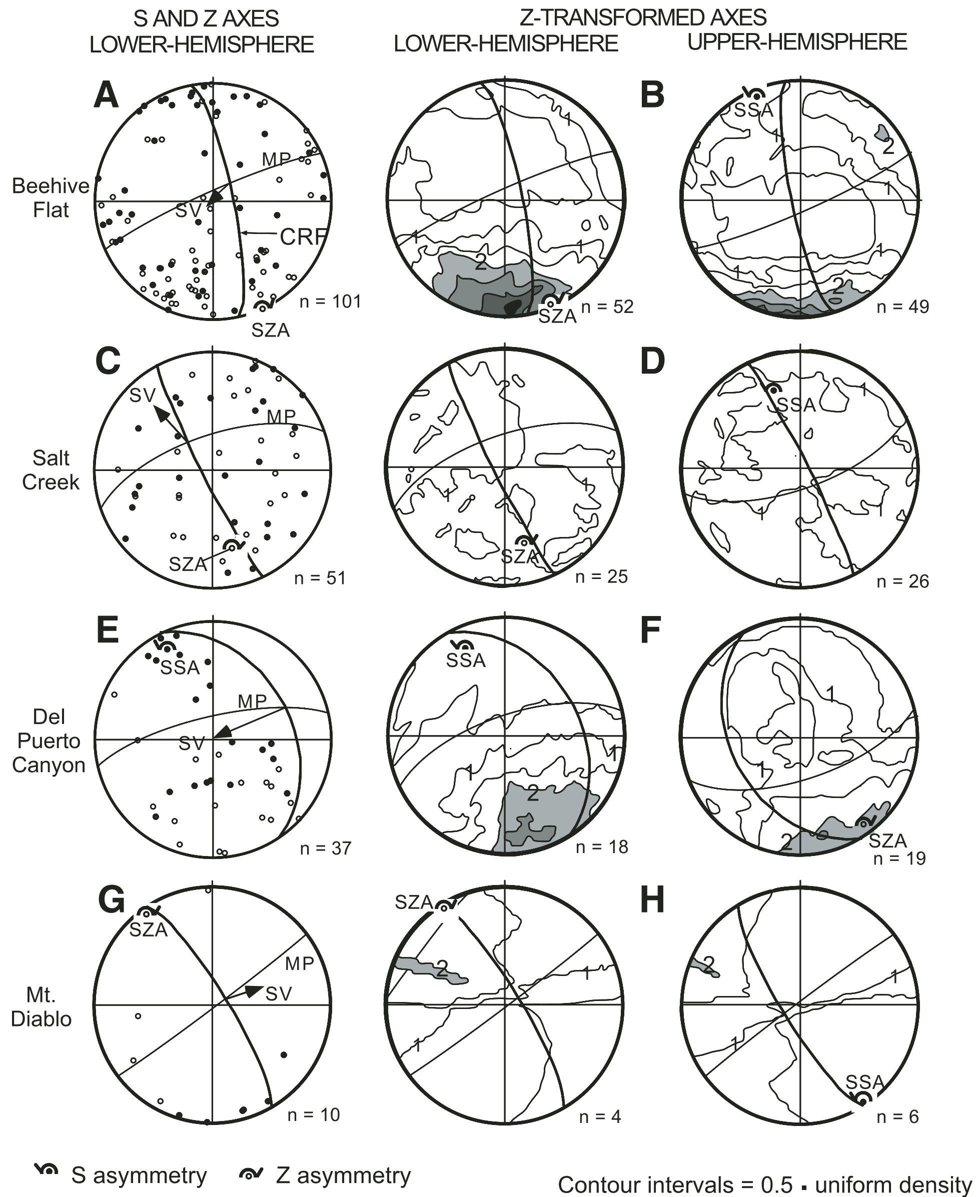

Figure 18. Stereograms showing internal rotation axes in present coordinates for all four study areas at Coast Range fault zone; left column of stereograms shows internal-rotation axes in lower-hemisphere projection with sense of rotation designated as Z (clockwise) or S (counterclockwise); right two columns of stereograms show internal-rotation axes after conversion to common Z sense of rotation; note that Z-transformed axes can have orientations in both lower and upper hemispheres; average direction for Z-transformed distribution called the synoptic Z axis (SZA) and antipodal direction called synoptic S axis (SSA); mirror plane (MP) for distribution of Z-transformed directions defined to be perpendicular to SZA direction; regional attitude of Coast Range fault zone (CRF) indicated by heavy great circle in each stereogram; slip vector (SV) for Coast Range fault zone is interpreted to lie at intersection of mirror plane and attitude of fault zone. Contours were calculated using method of Kamb (1959), modified to account for fact that Z-transformed axes are unidirectional vectors distributed over entire sphere (to contour density on full sphere, one must account for fact that Z axes are directed vectors and not bidirectional lines as typically is case in structural geology); lowest contour and contour intervals both 0.5 times uniform density. Contour diagrams show presence of well-defined cluster of Z-transformed axes for Beehive Flat and Del Puerto Canyon areas; Salt Creek and Mount Diablo areas show much weaker preferred orientation for Z-transformed axes; SZA directions for Beehive Flat, Salt Creek, and Del Puerto Canyon are all oriented in subhorizontal direction trending to SSE, which indicates top-WSW sense of shear for Coast Range fault zone in these areas; SZA direction for Mount Diablo is oriented in subhorizontal direction trending to NW, indicating top-NE sense of shear; latter result would be consistent with normal slip on Coast Range fault, but note small size of data set (n = 10).

compatible with a Coast Range fault zone that formed as an E-side-up contractional fault. This conclusion is true regardless of the present orientation of the fault.

For the Salt Creek area, the Z-transformed axes (Fig. 18D) are more scattered and display only a weak cluster plunging to the south. For the Del Puerto area the Z-transformed axes (Fig. 18F) show a well-defined maximum, once again plunging gently to the south. The Mount Diablo area provides an anomalous result. The SZA direction (Fig. 18H) plunges gently to the northeast, indicating an E-down sense of motion for the Coast Range fault in this area. This result is based on a very small data set (n = 10) and therefore is difficult to trust. However, we note that Unruh et al. (2007) described their Paleocene normal faults in the westernmost Great Valley basin from the Mount Diablo area.

BRITTLE STRAIN IN THE FRANCISCAN SUBDUCTION COMPLEX

The kinematic data from the Coast Range fault zone indicate contractional E-side-up motion at this structure. This brings up the question as to whether the faults within the Franciscan subduction complex have kinematics that are compatible with this interpretation.

The fault zones are typically only a few meters thick and are dominated by angular blocks of graywacke and shale. The array of variably oriented fault surfaces is much less dense than in the serpentinite fault zones in the Coast Range fault zone. The fault surfaces display well-developed slickensides, which are mantled by striations defined by fibrous quartz. As in the Coast Range fault zone, the direction of fiber overgrowth and the orientation of extensional fractures cutting the fibers provide a record of the local direction and sense of slip. In almost all observed cases, each slickensided surface is covered by only one set of straight, unidirectional fibers. Therefore, our interpretation of the structures is akin to that of the structures in the Coast Range fault zone—i.e., the structures formed as a result of a single direction of tectonic transport. The technique applied is the same as that used for the Coast Range fault zone.

The fault zones within the Franciscan subduction complex in general dip at moderate angles and have not been rotated into a subvertical position as in the Coast Range fault zone. The sense of shear at the intra–Franciscan subduction complex faults as deduced from small-scale structures is top-W-SW for the Coast Range fault zone west of the Klamath Mountains, the Grogan fault, the Redwood Mountain fault, and the Bald Mountain fault. Bolhar and Ring (2001) studied asymmetric folds at the Redwood Mountain fault in the Yolla Bolly Mountains farther south and also reported a top-W sense of movement.

The Coastal Belt thrust was interpreted by Ring and Brandon (1997) as a top-SW thrust, juxtaposing the higher-grade Central Belt against the underlying weakly metamorphosed Coastal Belt, thereby cutting out 15–20 km of section. If an original dip of 15°–20° for the Coastal belt thrust was assumed, the metamorphic hiatus would indicate a displacement of 40–80 km.

Outcrops near Cazadero close to the San Andreas fault and in the Potter Valley northeast of Cloverdale have fault planes associated with subhorizontal slickensides indicative of strike-slip faulting. In one single outcrop (CBT1) at the Coastal Belt thrust we observed that faults with subhorizontal slickensides overprint earlier thrust-related faults. We assume that the strike-slip faults are associated with the San Andreas fault system.

Brittle Strain Analysis

Northern California

The contoured shortening axes from all outcrops analyzed east of Eureka (Titlow Hill, Hoopa Valley, Bald Hill Road, Klamath River, and Humboldt Lagoons; Fig. A3) show a bimodal distribution, with the maximum of the shortening axes in an E-W direction (Fig. 19). The maximum of the shortening axes lies at ~20°–30° to the main fault planes of the Coast Range fault zone, the Grogan fault, the Redwood Mountain fault, the Bald Mountain fault, and the minor faults at and south of Humboldt Lagoons and at Titlow Hill. The vertical maximum of the extension axes indicates reverse faulting.

Coastal Belt Thrust

Contouring of the data from road cuts between Cloverdale and Garberville (Fig. A3) show that the shortening axes cluster in a NE-SW direction and that the extension axes are subvertical (Figs. 19E, 19F). In conjunction with the small-scale kinematic indicators, the data indicate top-SW tectonic transport on the Coastal Belt thrust.

Faults Related to the San Andreas Fault System

Contouring of the data from outcrops near Cazadero, in Potter Valley and at the Coastal belt thrust, show NE-trending shortening axes and NW-trending extension axes (Figs. 19H, 19I).

DUCTILE STRAIN AND MASS LOSS IN THE EASTERN AND CENTRAL FRANCISCAN BELTS

Some of the results reported in this section from the Yolla Bolly Mountains and from Del Puerto Canyon have been already published in Ring and Brandon (1999) and Ring and Richter (2004). Here we intend to show our entire data set, which consists of 99 samples from the Eastern Belt and 43 samples from the Central Belt. Despite the fact that the data show a wide scatter in orientations of the principal strain axes and of the magnitudes of the principal stretches, tensor averages of the data sets yield consistent results.

Directions and Magnitudes of the Finite Stretches

In general, strains in the rocks from the Eastern Belt are greater than those from the Central Belt (Table 4). The data are described in geographic order from northern California to the Diablo Range (see Figs. A4–A10 for sample localities) and then are summarized and discussed. Cleavage in all rock units dips moderately, and the maximum stretching direction is subhorizontal.

Northern California

The four samples from the Yolla Bolly terrane show variable orientations for X, Y, and Z (Table 4). The measurements of the modal abundance of fibers in the rock indicate that the metasandstones contain between 6% and 35% fiber per volume of rock. Therefore, the absolute stretches (Table 4) show a wide scatter and range from 1.06 to 1.54 for S_X. S_Z ranges from 0.48 to 0.77, and S_Y ranges from 0.56 to 1.03, indicating a constrictional (S_Y <1) strain type. The tensor average shows that $S_X \approx 1$ (S_X: S_Y: S_Z = 1.01: 0.77: 0.71) (Table 4). This surprising result stems from the highly variable orientations of the principal finite strain axes; the individual strain tensors do not share the same principal directions. The overall deformation at a regional scale is constrictional ($S_Z < S_Y < 1$), and plane strain ($S_X \approx 1$) (note that the term *plane strain* is used here as originally proposed in the literature for the deformation of metals (e.g., Nadai, 1950, 1963) indicates that one principal axis remains unchanged.

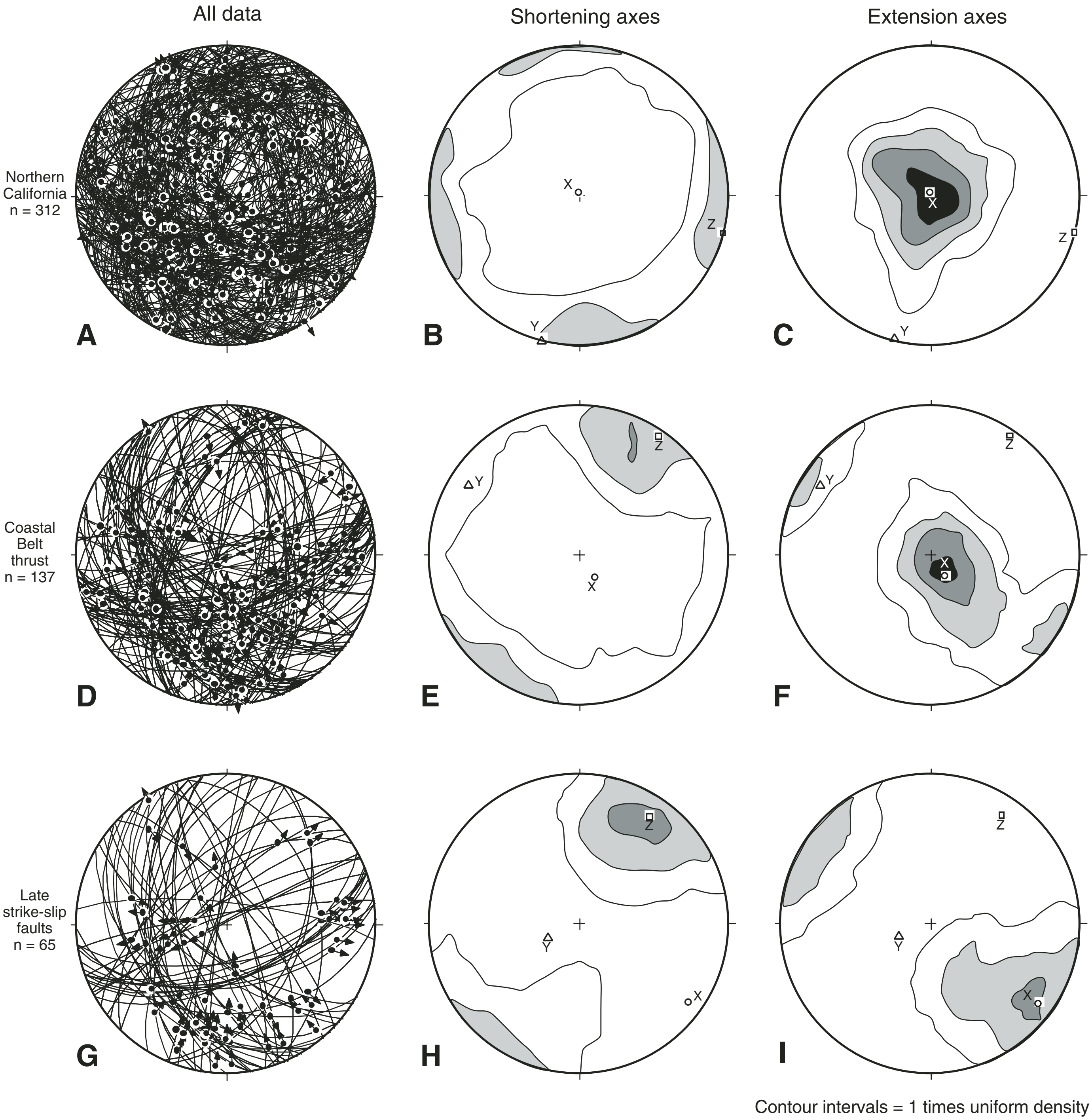

Figure 19. Stereograms showing all fault data in present coordinates; stereograms in left column show attitude and direction of slip for all measured faults; right two columns of contoured stereograms show distributions of shortening. Extension axes inferred from kinematic measurements (PT method of Marrett and Allmendinger, 1990). Contours were determined using method of Kamb (1959) and are reported in multiples of expected density for uniform distribution; lowest contour 1 times uniform density, and contour interval 1 times uniform density as well. (A, B, C) Faults with slickensides and shortening and extension axes for Coast Range fault zone, Redwood Mountain fault, Grogan fault, Bald Mountain fault, and minor faults in northern California; most faults have reverse kinematics; shortening axes show bimodal distribution with overall E-W–directed shortening. (D, E, F) W-, SW-, and S-dipping reverse faults dominate data set from Coastal Belt thrust; accordingly, shortening axes show pronounced maximum in NE-SW direction (maximum >3 times uniform density). (G, H, I) Fault-slip data of late strike-slip faults associated with NW-striking subvertical faults that cut across Franciscan accretionary assemblage in northern California; kinematic pattern shows NE-directed shortening and NW-directed extension. Note that summary plots contain more data than sum of individual plots because some data sets were too small, and data from these individual outcrops are not shown.

TABLE 4. PRINCIPAL STRETCHES

No.		Extension Tr.	Pl.	S_X	Intermediate Tr.	Pl.	S_Y	Shortening Tr.	Pl.	S_Z	γ_{oct}	Volume S_V	Internal rotation Tr.	Pl.	Angle	Kinematic numbers Wn	Wn*	An*
1. Northern California																		
96-49	CB	161	48	1.09	351	41	0.91	256	5	0.56	0.60	0.56	--	--	--	--	--	–0.85
96-50	CB	132	0	1.04	41	69	1.04	222	21	0.57	0.60	0.62	--	--	--	--	--	–0.70
96-51	CB	11	47	1.03	142	32	1.26	249	27	0.59	0.69	0.77	--	--	--	--	--	–0.34
96-52	CB	28	8	1.11	118	5	0.93	242	81	0.64	0.48	0.66	--	--	--	--	--	–0.74
96-53	YBT	262	18	1.54	9	43	0.56	155	42	0.48	1.26	0.41	11	42	–2.5	0.06	0.07	–0.70
96-54	YBT	40	8	1.47	303	44	0.69	138	45	0.51	1.03	0.52	301	47	–3.2	0.09	0.10	–0.60
96-55	YBT	172	69	1.06	17	20	1.03	285	8	0.52	0.71	0.57	--	--	--	--	--	–0.70
96-56	YBT	20	3	1.10	111	10	1.04	276	80	0.57	0.64	0.65	--	--	--	--	--	–0.59
96-57	CB	327	37	1.12	218	23	0.82	103	44	0.74	0.36	0.68	--	--	--	--	--	–0.89
96-58	CB	162	32	1.08	282	39	0.73	46	35	0.73	0.38	0.58	--	--	--	--	--	–1.22
96-59	CB	43	25	1.09	146	25	1.06	274	53	0.79	0.30	0.91	--	--	--	--	--	–0.26
96-60	CB	240	31	1.06	354	34	0.76	119	40	0.65	0.42	0.52	--	--	--	--	--	–1.30
96-63	YBT	90	80	1.08	267	11	0.81	357	1	0.77	0.30	0.67	--	--	--	--	--	–1.08
96-64	CB	25	32	1.03	216	58	0.68	118	5	0.66	0.42	0.46	--	--	--	--	--	–1.55
Average	CB	348	7	0.95	91	62	0.87	254	27	0.76	0.19	0.63	--	--	--	--	--	–3.41
Average	YBT	49	1	1.01	318	46	0.77	140	44	0.71	0.31	0.56	332	51	–2.4	0.08	0.09	–1.06
2. Yolla Bolly Mountains																		
93-7	VSF	5	14	1.49	102	27	0.82	251	59	0.47	1.11	0.57	103	31	+7.0	0.21	0.23	–0.48
93-9	VSF	348	26	1.35	104	42	0.70	239	38	0.58	0.80	0.55	255	9	+8.5	0.31	0.36	–0.68
93-14	YBT	69	13	1.17	174	49	0.94	328	38	0.33	1.38	0.36	326	42	+2.4	0.05	0.06	–0.75
93-13	YBT	202	17	1.13	80	60	1.06	300	24	0.60	0.60	0.72	--	--	--	--	--	–0.47
93-11	YBT	89	33	1.33	202	31	0.76	323	41	0.66	0.65	0.67	279	56	–9.8	0.43	0.47	–0.54
93-12	YBT	42	8	1.08	139	42	1.06	303	47	0.53	0.72	0.61	--	--	--	--	--	–0.62
93-17	YBT	241	25	1.52	148	7	0.70	44	64	0.69	0.82	0.73	93	61	–5.6	0.21	0.22	–0.34
93-18	YBT	65	3	1.34	156	20	0.81	327	70	0.74	0.55	0.80	159	56	+3.7	0.19	0.20	–0.34
93-19	YBT	63	1	1.21	153	12	1.10	326	78	0.59	0.69	0.79	167	84	–9.0	0.39	0.40	–0.31
93-20	YBT	104	1	1.06	194	26	1.05	11	64	0.58	0.60	0.65	--	--	--	--	--	–0.63
93-21	YBT	295	28	1.22	174	44	1.21	45	33	0.56	0.81	0.83	57	45	–6.3	0.24	0.25	–0.21
93-22	YBT	153	54	1.14	54	6	0.75	320	35	0.74	0.41	0.63	54	6	+0.0	0.00	0.00	–0.93
93-23	YBT	49	2	1.09	143	63	1.06	317	27	0.54	0.70	0.62	139	26	–1.1	0.04	0.05	–0.59
93-24	YBT	297	17	1.47	64	63	0.84	200	20	0.64	0.76	0.79	174	60	–1.2	0.05	0.05	-0.28
93-25	YBT	133	6	1.08	228	40	1.01	35	50	0.54	0.67	0.59	--	--	--	--	--	–0.69
93-27a	YBT	357	24	1.09	266	2	0.78	172	65	0.77	0.33	0.65	--	--	--	--	--	–1.08
93-27b	YBT	69	19	1.40	330	26	0.75	192	57	0.69	0.68	0.72	176	38	+3.4	0.15	0.15	–0.42
93-28	YBT	348	34	1.26	255	4	1.15	159	55	0.66	0.61	0.96	126	47	–11.3	0.56	0.56	–0.06
93-29	YBT	356	15	1.30	255	36	1.06	104	50	0.69	0.56	0.95	226	68	–5.3	0.29	0.29	–0.08
93-30	YBT	45	10	1.20	314	8	1.19	188	76	0.60	0.70	0.86	167	69	+4.0	0.17	0.18	–0.19
Average	YBT	56	3	0.99	146	16	0.92	317	74	0.76	0.23	0.69	69	70	–1.8	0.15	0.21	–0.51
3. Leech Lake Mountain																		
95-1	YBT	76	0	1.14	347	5	1.09	167	85	0.61	0.60	0.76	184	53	+4.9	0.23	0.25	–0.40
95-2	YBT	284	2	1.36	14	4	0.75	167	85	0.72	0.62	0.73	190	59	+8.9	0.43	0.46	–0.43
95-3	YBT	296	0	1.14	28	15	1.08	208	75	0.67	0.50	0.82	158	75	+2.4	0.14	0.14	–0.33
95-4	YBT	101	26	1.07	350	37	1.06	217	42	0.64	0.50	0.73	212	36	–1.6	0.09	0.09	–0.54
95-5	YBT	137	2	1.10	45	30	1.08	230	60	0.61	0.58	0.72	258	86	+1.3	0.06	0.07	–0.48
95-6	YBT	91	19	1.32	183	6	1.06	290	70	0.61	0.70	0.85	336	50	–8.0	0.35	0.35	–0.20
95-7	YBT	284	3	1.17	193	25	0.66	20	65	0.63	0.60	0.49	190	61	–18.4	0.72	0.94	–1.03
97-8	YBT	329	11	1.36	92	71	0.67	236	15	0.61	0.79	0.56	61	10	–7.0	0.24	0.28	–0.67
95-9	YBT	106	13	1.33	5	37	0.70	212	50	0.54	0.84	0.50	294	76	+6.7	0.23	0.27	–0.74

(*continued*)

TABLE 4. PRINCIPAL STRETCHES (*continued*)

No.		Extension Tr.	Pl.	S_X	Intermediate Tr.	Pl.	S_Y	Shortening Tr.	Pl.	S_Z	γ_{oct}	Volume S_V	Internal rotation Tr.	Pl.	Angle	Kinematic numbers Wn	Wn*	An*
3. Leech Lake Mountain (*continued*)																		
95-10	YBT	15	22	1.10	109	11	1.01	225	65	0.65	0.48	0.72	139	55	+0.9	0.05	0.06	–0.58
95-11	YBT	59	8	1.10	325	27	0.83	164	62	0.64	0.46	0.58	168	67	+1.1	0.06	0.06	–0.99
95-12	YBT	6	24	1.20	98	6	1.00	202	65	0.53	0.77	0.64	108	26	–1.1	0.04	0.04	–0.53
95-13	YBT	319	21	1.03	64	35	1.03	204	48	0.55	0.63	0.58	119	68	–0.1	0.00	0.00	–0.74
95-14	YBT	312	10	1.13	51	43	1.07	212	45	0.50	0.82	0.60	211	49	–1.5	0.05	0.06	–0.55
95-15	YBT	296	11	1.31	38	47	0.66	196	41	0.62	0.74	0.54	202	24	+5.8	0.21	0.24	–0.75
95-16	YBT	225	2	1.01	134	26	1.00	320	64	0.54	0.62	0.55	316	19	+0.0	0.00	0.00	–0.85
95-17	YBT	328	43	1.00	110	41	0.72	218	20	0.63	0.40	0.45	70	13	+0.0	0.00	0.00	–1.66
95-18	YBT	3	43	1.12	131	34	1.11	243	29	0.62	0.59	0.77	263	10	–0.2	0.01	0.01	–0.38
95-19	YBT	337	12	1.12	98	67	0.87	243	19	0.81	0.28	0.70	223	62	+0.0	0.00	0.00	–1.63
95-20	YBT	287	22	1.28	28	25	0.82	161	56	0.61	0.65	0.61	42	46	+3.5	0.14	0.15	–0.63
Average	YBT	300	0	1.07	30	28	0.91	210	62	0.66	0.41	0.64	208	16	+0.5	0.03	0.03	–0.87
4. Mendecino Pass traverse																		
96-40	CB	208	83	1.03	10	6	0.87	100	2	0.67	0.36	0.60	--	--	--	--	--	–1.18
96-41	YBT	258	18	1.23	349	3	0.68	87	72	0.47	0.89	0.39	357	4	–0.2	0.01	0.01	–0.96
96-42	YBT	211	35	1.20	333	36	0.74	92	34	0.54	0.71	0.48	333	36	+0.5	0.02	0.02	–0.91
96-43	YBT	69	9	1.11	333	9	0.83	199	81	0.61	0.51	0.56	--	--	--	--	--	–0.96
96-44	YBT	36	24	1.12	164	54	0.66	294	25	0.55	0.65	0.41	--	--	--	--	--	–1.22
96-45	YBT	109	54	1.19	250	28	0.66	348	20	0.52	0.76	0.49	231	20	+2.8	0.09	0.11	–1.05
96-46	CB	216	40	1.28	113	15	0.65	7	46	0.47	0.95	0.39	111	17	+2.1	0.06	0.07	–0.92
96-47	CB	273	11	1.05	16	49	0.72	174	39	0.66	0.42	0.50	--	--	--	--	--	–1.41
96-48	CB	159	27	1.03	23	55	0.66	260	21	0.65	0.44	0.44	--	--	--	--	--	–1.56
97-93	CB	176	11	1.11	267	0	0.84	356	79	0.74	0.35	0.69	--	--	--	--	--	–0.89
97-95	CB	110	1	1.07	21	23	0.93	201	67	0.82	0.22	0.82	--	--	--	--	--	–0.76
97-96	CB	160	22	1.12	48	43	0.91	268	39	0.77	0.31	0.78	--	--	--	--	--	–0.65
97-98	CB	89	49	1.17	266	41	1.08	358	1	0.67	0.52	0.85	57	1	–0.1	0.01	0.01	–0.39
97-99	CB	144	3	1.22	56	1	1.18	305	86	0.91	0.91	1.31	39	32	–3.1	0.28	0.34	+0.84
97-101	CB	292	10	1.09	30	31	1.04	185	55	0.64	0.50	0.73	--	--	--	--	--	–0.54
97-102	CB	68	24	1.10	327	22	1.02	200	57	0.89	0.18	1.00	--	--	--	--	--	–0.01
97-103	CB	82	15	1.08	350	10	1.00	229	72	0.64	0.48	0.69	--	--	--	--	--	–0.71
97-106	CB	52	0	1.07	322	2	1.03	142	89	0.91	0.14	1.00	--	--	--	--	--	+0.02
97-107	CB	248	50	1.12	345	7	1.10	335	70	0.83	0.28	1.02	--	--	--	--	--	+0.02
97-111	CB	100	10	1.05	191	3	0.93	300	80	0.90	0.13	0.88	--	--	--	--	--	–0.80
97-112	CB	45	10	1.04	134	1	0.89	231	79	0.79	0.23	0.73	--	--	--	--	--	–1.14
97-113	CB	67	12	1.13	331	9	0.83	201	79	0.85	0.29	0.80	--	--	--	--	--	–0.66
97-114	CB	10	0	1.07	99	49	0.99	280	40	0.91	0.13	0.96	--	--	--	--	--	–0.23
97-115	CB	299	20	1.02	204	14	0.95	82	66	0.87	0.13	0.84	--	--	--	--	--	–1.07
97-116	CB	26	7	1.04	117	11	0.83	264	78	0.79	0.24	0.68	--	--	--	--	--	–1.31
97-117	CB	77	1	1.06	171	14	0.89	354	74	0.73	0.31	0.69	--	--	--	--	--	–1.00
97-120	CB	128	32	1.08	29	13	1.06	280	56	0.86	0.21	0.98	--	--	--	--	--	–0.06
97-121	CB	151	34	1.10	40	28	1.03	282	43	0.84	0.23	0.95	--	--	--	--	--	–0.18
97-126	CB	68	12	1.12	332	27	1.08	178	61	0.72	0.41	0.87	--	--	--	--	--	–0.28
Average	CB	68	5	0.97	158	6	0.94	299	83	0.84	0.12	0.77	357	20	–1.0	0.08	0.09	–0.36
Average	YBT	235	5	0.91	140	40	0.72	331	50	0.68	0.26	0.45	236	25	+1.0	0.04	0.09	–2.34
5. Cloverdale traverse																		
96-23	CB	334	8	1.03	234	51	0.79	71	38	0.75	0.28	0.61	--	--	--	--	--	–1.45
96-24	CV	94	6	1.02	196	64	0.82	1	25	0.69	0.33	0.58	--	--	--	--	--	–1.40
96-25	YBT	290	53	1.03	157	28	0.96	55	23	0.92	0.09	0.91	--	--	--	--	--	–0.83
96-27	YBT	222	70	1.33	106	9	1.26	13	18	0.55	0.91	0.92	109	9	–2.0	0.07	0.07	–0.08

(*continued*)

TABLE 4. PRINCIPAL STRETCHES (*continued*)

No.		Extension Tr.	Extension Pl.	Extension S_X	Intermediate Tr.	Intermediate Pl.	Intermediate S_Y	Shortening Tr.	Shortening Pl.	Shortening S_Z	γ_{oct}	Volume S_V	Internal rotation Tr.	Internal rotation Pl.	Internal rotation Angle	Kinematic numbers Wn	Kinematic numbers Wn*	Kinematic numbers An*
5. Cloverdale traverse (*continued*)																		
96-28	YBT	15	1	1.04	284	50	0.78	106	40	0.69	0.35	0.56	--	--	--	--	--	–1.38
96-29	CB	255	62	1.10	71	28	1.06	162	2	0.71	0.41	0.83	--	--	--	--	--	–0.39
96-30	CB	255	66	1.08	135	13	0.79	40	20	0.62	0.47	0.53	--	--	--	--	--	–1.14
96-34	CB	345	51	1.09	245	8	0.81	149	38	0.77	0.31	0.68	--	--	--	--	--	–1.03
96-35	CB	246	9	1.02	151	30	1.02	351	58	0.81	0.22	0.84	--	--	--	--	--	–0.64
96-36	CB	317	26	1.20	132	64	1.01	225	2	0.63	0.58	0.76	132	64	+0.0	0.00	0.00	–0.40
96-37	YBT	161	21	1.06	36	56	1.03	262	26	0.66	0.45	0.72	--	--	--	--	--	–0.62
96-39	YBT	49	18	1.14	140	4	0.89	245	71	0.63	0.51	0.64	--	--	--	--	--	–0.75
Average	CB	292	48	0.96	128	41	0.89	31	8	0.80	0.15	0.68	297	27	–8.3	0.46	0.35	–0.51
Average	YBT	128	36	0.94	36	4	0.90	301	54	0.87	0.63	0.74	109	9	–1.9	0.07	0.07	–0.45
6. Bay area																		
96-16	YBT	202	1	1.59	294	50	0.69	111	40	0.54	1.08	0.59	299	51	–0.7	0.02	0.02	–0.56
96-17	CB	289	10	1.12	44	67	0.93	196	21	0.81	0.27	0.84	--	--	--	--	--	–0.52
96-18	CB	292	10	1.04	194	46	0.76	31	43	0.70	0.35	0.53	--	--	--	--	--	–1.42
96-19	CB	180	9	1.04	276	32	0.78	76	56	0.78	0.28	0.63	--	--	--	--	--	–1.38
96-20	YBT	261	9	1.43	164	38	0.73	2	51	0.72	0.69	0.75	164	38	+3.1	0.13	0.14	–0.36
96-21	YBT	114	7	1.32	206	19	0.80	5	70	0.76	0.52	0.80	206	20	–0.7	0.04	0.04	–0.36
96-22	YBT	334	24	1.28	236	25	0.86	106	54	0.78	0.44	0.86	235	25	–0.1	0.01	0.01	–0.29
Average	CB	301	7	0.98	208	22	0.84	49	67	0.80	0.17	0.67	--	--	--	--	--	–2.16
Average	YBT	226	4	1.03	317	10	0.97	116	79	0.72	0.32	0.72	141	24	+0.6	0.05	0.06	–0.39
7. Diablo Range																		
Mount Hamilton																		
93-33	YBT	21	54	1.27	142	20	0.71	243	28	0.54	0.78	0.49	221	34	+3.3	0.11	0.13	–0.82
93-34	YBT	33	14	1.06	300	14	1.06	168	70	0.49	0.80	0.55	167	70	+0.5	0.02	0.02	–0.67
93-35	YBT	168	50	1.06	318	36	0.78	59	15	0.50	0.66	0.41	--	--	--	--	--	–1.17
93-36	YBT	323	46	1.04	202	26	1.04	94	32	0.63	0.49	0.68	--	--	--	--	--	–0.66
93-37	YBT	315	34	1.22	201	31	0.77	80	40	0.64	0.57	0.60	47	3	–0.8	0.04	0.04	–0.77
93-38	YBT	111	54	1.19	249	28	0.66	350	20	0.52	0.76	0.49	234	21	+2.8	0.11	0.14	–1.00
21-3	YBT	317	36	1.04	213	19	1.04	100	48	0.62	0.51	0.67	206	27	–0.9	0.05	0.05	–0.67
93-39	YBT	7	61	1.09	253	13	0.84	157	25	0.56	0.58	0.51	--	--	--	--	--	–1.00
93-40	YBT	158	35	1.02	56	17	0.79	304	50	0.50	0.63	0.40	--	--	--	--	--	–1.26
93-41	YBT	219	61	1.10	1	24	1.09	98	16	0.70	0.44	0.84	--	--	--	--	--	–0.34
93-42	YBT	187	19	1.22	74	49	0.83	291	35	0.60	0.62	0.61	8	71	–2.7	0.12	0.13	–0.70
93-43	YBT	232	60	1.30	119	12	0.76	23	27	0.59	0.71	0.58	130	6	+7.1	0.29	0.33	–0.67
21-4	YBT	232	30	1.06	140	4	0.96	43	60	0.66	0.42	0.67	--	--	--	--	--	–0.80
93-54a	YBT	192	17	1.07	101	4	0.75	357	72	0.46	0.76	0.37	--	--	--	--	--	–1.18
93-54b	YBT	234	26	1.01	134	17	1.01	15	57	0.45	0.85	0.46	--	--	--	--	--	–0.83
93-53	YBT	235	26	1.05	61	64	1.04	325	3	0.61	0.53	0.67	33	63	–4.7	0.23	0.26	–0.65
Average	YBT	199	31	0.89	305	25	0.81	66	49	0.77	0.12	0.55	358	16	–1.4	0.10	0.21	–1.68
Pacheco Pass																		
93-46	YBT	245	8	1.14	338	17	1.03	130	72	0.66	0.50	0.77	128	70	+1.7	0.10	0.10	–0.44
93-47	YBT	36	24	1.02	164	54	0.66	294	25	0.50	0.63	0.34	--	--	--	--	--	–1.52
93-48	YBT	248	35	1.04	148	14	1.01	40	51	0.57	0.59	0.60	--	--	--	--	--	–0.76
93-49	YBT	245	2	1.25	155	7	1.05	355	83	0.51	0.87	0.67	342	72	+4.6	0.16	0.17	–0.42
93-50	YBT	18	15	1.15	270	51	0.60	119	35	0.49	0.80	0.34	119	35	+9.1	0.27	0.38	–1.22
93-51	YBT	103	32	1.17	10	5	0.89	272	58	0.62	0.55	0.65	271	58	+1.9	0.09	0.10	–0.69
21-5	YBT	280	8	1.14	184	35	0.97	21	54	0.53	0.72	0.59	21	54	–4.0	0.15	0.17	–0.66
21-6	YBT	191	7	1.21	98	23	0.69	297	66	0.66	0.58	0.55	--	--	--	--	--	–0.88
Average	YBT	206	5	0.99	116	4	0.84	344	84	0.65	0.35	0.54	135	55	+2.4	0.13	0.18	–1.25

(*continued*)

TABLE 4. PRINCIPAL STRETCHES (*continued*)

No.		Extension Tr.	Extension Pl.	Extension S_X	Intermediate Tr.	Intermediate Pl.	Intermediate S_Y	Shortening Tr.	Shortening Pl.	Shortening S_Z	γ_{oct}	Volume S_V	Internal rotation Tr.	Internal rotation Pl.	Internal rotation Angle	Kinematic numbers Wn	Kinematic numbers Wn*	Kinematic numbers An*
7. Diablo Range (*continued*)																		
Del Puerto Canyon																		
P1/1	YBT	303	52	1.16	103	36	1.01	200	10	0.68	0.47	0.80	103	36	–25.9	1.55	1.63	–0.41
P1/2	YBT	334	14	1.16	231	34	0.84	86	50	0.74	0.39	0.72	--	--	--	--	--	–0.71
P1/3	YBT	123	35	1.24	234	24	0.96	350	45	0.75	0.42	0.89	234	24	+4.5	0.31	0.31	–0.23
P2/2	YBT	171	40	1.37	52	30	0.80	297	36	0.62	0.72	0.68	52	30	+3.2	0.13	0.14	–0.48
P2/3	YBT	82	38	1.22	315	38	0.92	199	30	0.84	0.32	0.94	315	38	–5.4	0.48	0.48	–0.15
P3/3	YBT	198	16	1.11	301	40	0.78	91	46	0.74	0.37	0.64	--	--	--	--	--	–1.01
P3/4	YBT	73	77	1.10	206	9	0.71	297	9	0.71	0.43	0.55	--	--	--	--	--	–1.17
P4/1	YBT	90	60	1.25	270	30	0.94	360	0	0.68	0.52	0.80	270	30	–2.3	0.13	0.13	–0.37
P4/3	YBT	200	4	1.26	291	13	1.06	91	76	0.83	0.35	1.10	291	13	–12.0	0.98	1.00	+0.25
P5/1	YBT	82	58	1.16	286	30	1.03	190	11	0.79	0.33	0.94	286	30	–4.7	0.41	0.41	–0.15
P5/2	YBT	148	48	1.08	54	4	0.91	320	42	0.73	0.33	0.72	--	--	--	--	--	–0.85
93-44	YBT	230	60	1.30	120	12	0.76	23	27	0.59	0.71	0.58	120	11	+7.0	0.29	0.33	–0.67
DPC106	YBT	142	26	1.08	32	36	1.02	266	45	0.55	0.66	0.60	--	--	--	--	--	–0.67
DPC115	YBT	176	17	1.22	81	15	0.81	313	67	0.62	0.59	0.61	81	15	–3.5	0.15	0.18	–0.72
DPC117	YBT	60	53	1.21	304	19	1.08	202	31	0.86	0.29	1.12	--	--	--	--	--	+0.34
DPC119	YBT	165	72	1.02	333	18	0.86	64	3	0.80	0.21	0.71	--	--	--	--	--	–1.42
Average	YBT	135	50	1.00	35	9	0.88	298	39	0.86	0.13	0.76	249	45	–3.0	0.38	0.50	–1.72
Average	YBT	185	24	0.91	90	10	0.85	340	64	0.80	0.19	0.63	292	26	–1.3	0.12	0.47	–4.36
Grand average	CB	141	4	0.93	50	11	0.90	250	79	0.85	0.07	0.71	66	52	1.1	0.13	0.14	–1.60
Grand average	YBT	72	7	0.92	163	4	0.90	283	82	0.77	0.64	0.64	341	53	–0.7	0.06	0.10	–2.46
Grand average	ALL	97	8	0.91	7	0	0.90	276	82	0.80	0.12	0.66	342	51	–0.7	0.06	0.10	–1.96

Abbreviations: CB—Central Belt; VSF—Valentine Springs Formation; YBT—Yolla Bolly terrane; Tr.—trend; Pl.—plunge. Principal stretches are $S_X \geq S_Y \geq S_Z$ (S = final length/initial length); γ_{oct}—natural octahedral shear strain; Wn—kinematic vorticity number; Wn*—modified kinematic vorticity number; An*—modified kinematic dilatancy number (modified numbers include possible volume strains).

The results for rocks from the Central Belt in northern California are similar, but extensional stretches are smaller. S_X ranges from 1.03 to 1.12 (3%–11% fiber per volume of rock), S_Z ranges from 0.56 to 0.79, and S_Y ranges from 0.68 to 1.26, with most data indicating again a constrictional strain type. The principal stretches of the tensor average are S_X: S_Y: S_Z = 0.95: 0.87: 0.76 (Table 4) and largely similar to those of the Yolla Bolly terrane.

Yolla Bolly Mountains

All samples belong to the Yolla Bolly terrane. The field orientations of the measured finite-strain axes show considerable scatter (Table 4). S_X ranges from 1.06 to 1.52 (3%–34% fiber per volume of rock), S_Z varies from 0.33 to 0.77, and S_Y ranges from 0.70 to 1.21, with the data evenly split between constrictional and flattening (S_Y >1) strain types. The principal stretches of the tensor average are S_X: S_Y: S_Z = 0.99: 0.92: 0.76 (Table 4). Although margin-parallel shortening in the Y direction is less in the Yolla Bolly Mountains, the average is largely similar to the one for the Yolla Bolly terrane in northern California.

Leech Lake Mountain

The field orientations of the measured finite-strain axes again show some scatter (Table 4). The measurements of the modal abundance of fibers in the rock are between 0% and 29% fibers per volume of rock, with an average of 19%. Therefore, the absolute extensional stretches scatter and range from 1.00 to 1.36 for S_X. S_Z ranges from 0.50 to 0.81, and S_Y from 0.66 to 1.11. The principal stretches of the tensor average are S_X: S_Y: S_Z = 1.07: 0.91: 0.66 and indicate again that $S_X \approx 1$.

Mendocino Pass Traverse

The five samples from the Yolla Bolly terrane show variable orientations for X, Y, and Z (Table 4). The modal abundance of fibers in the rock ranges between 10% and 19% fiber per volume of rock, and the absolute stretches range from 1.11 to 1.23 for S_X (Table 4). Values for S_Z are 0.47–0.61, and S_Y ranges from 0.66 to 0.83, indicating a constrictional strain type. The tensor average is S_X: S_Y: S_Z = 0.91: 0.72: 0.68 (Table 4) and shows again no absolute stretch in the rocks.

The results for rocks from the Central Belt are similar. S_X ranges from 1.02 to 1.28 (2%–22% fiber per volume of rock), S_Z is 0.47–0.91, and S_Y is 0.65–1.18, with most data indicating again a constrictional strain type. The principal stretches of the tensor average are S_X: S_Y: S_Z = 0.97: 0.94: 0.84 (Table 4) and show no extension and largely similar values for S_X and S_Y.

Cloverdale Transect

In the five samples from the Yolla Bolly terrane, S_X ranges from 1.03 to 1.33 (3%–25% fiber per volume of rock) (Table 4). S_Z ranges from 0.55 to 0.92, and S_Y from 0.78 to 1.26, with most of the data showing a constrictional strain type. The tensor average is S_X: S_Y: S_Z = 0.94: 0.90: 0.87 (Table 4) and again shows no absolute extensional stretch in the rocks.

The results from the Central Belt are similar. S_X ranges from 1.02 to 1.20 (2%–17% fiber per volume of rock), S_Z ranges from 0.62 to 0.81, and S_Y ranges from 0.79 to 1.06, indicating a plane to constrictional strain type. The principal stretches of the tensor average are S_X: S_Y: S_Z = 0.96: 0.89: 0.80 (Table 4) and show no extension.

Bay Area

The data set from the Bay area is small but, in general, shows similar results as the data from the other areas. The modal abundance of fibers in the four rocks of the Yolla Bolly terrane is between 22% and 37% fiber per volume of rock, and the absolute stretches are 1.28–1.59 for S_X, 0.54–0.78 for S_Z, and 0.69–0.86 for S_Y (Table 4), indicating again a constrictional strain type. The tensor average is S_X: S_Y: S_Z = 1.03: 0.97: 0.72 (Table 4).

The results for rocks from the Central Belt show generally smaller principal stretches. S_X ranges from 1.04 to 1.12 (2%–11% fiber per volume of rock), S_Z varies from 0.70 to 0.81, and S_Y from 0.76 to 0.93, indicating a constrictional strain type. The principal stretches of the tensor average are S_X: S_Y: S_Z = 0.98: 0.84: 0.80 (Table 4).

Diablo Range

Three study areas belonging to the Yolla Bolly terrane were investigated in the Diablo Range (Table 4). Modal abundances of fibers for individual samples are 1%–27%, and therefore the absolute stretches for S_X are 1.01–1.37. S_Z varies from 0.46 to 0.86, and S_Y from 0.60 to 1.09, with most samples indicating a constrictional strain type. The tensor averages for the three study areas indicates that S_X is between 0.89 and 1.00, S_Y ranges from 0.81 to 0.88, and S_Z from 0.65 to 0.86 (Table 4). The field orientations of the finite strain axes show the usual scatter. The tensor average for all three study areas in the Diablo Range is S_X: S_Y: S_Z = 0.91: 0.85: 0.80.

Summary of Data

The tensor averages indicate that SMT deformation at the regional scale was largely similar in all study areas in the Yolla Bolly terrane. The principal stretches of the tensor average for this terrane, based on 99 samples, is S_X: S_Y: S_Z = 0.92: 0.90: 0.77 (Table 4), indicating that SMT deformation records only contraction. Contraction in all three principal strain directions is balanced by volume strain, as discussed below.

For the Central Belt the tensor averages of the various study areas are also fairly similar to each other, and the grand average, based on 43 samples, is S_X: S_Y: S_Z = 0.93: 0.90: 0.85 (Table 4). The only difference for the Yolla Bolly terrane on the regional scale is that shortening in the Z direction is about one-third smaller (15% versus 23%).

Contouring of all data reveals an overall subhorizontal attitude for X and Y in the Yolla Bolly terrane and the Central Belt. Consequently, the Z-axes show a subvertical maximum. The principal directions of the average strain tensor (open symbols in Fig. 20) yield a similar result. However, the principal directions of the

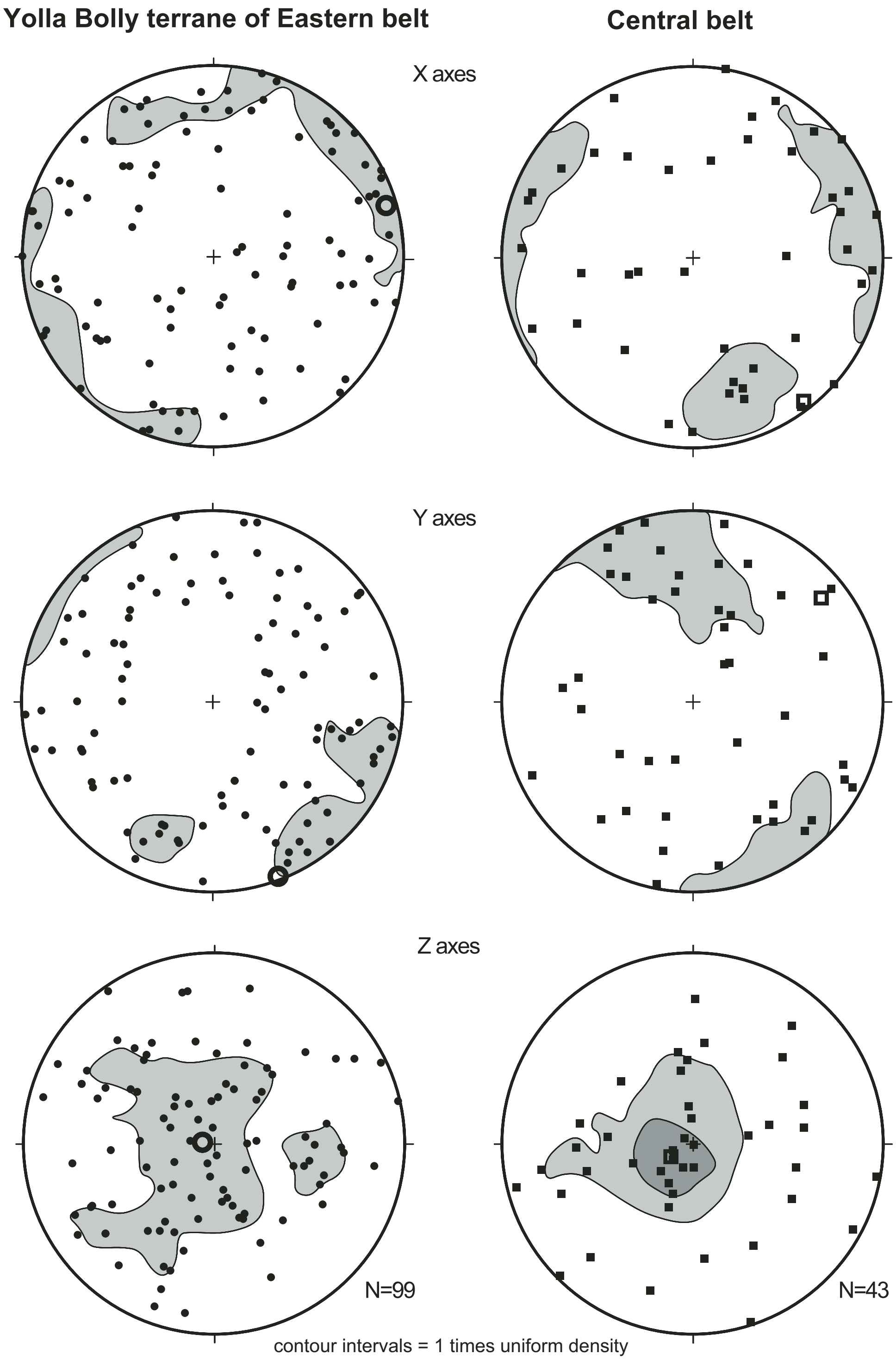

Figure 20. Lower-hemisphere equal-area plots for orientations of finite-strain axes in Yolla Bolly terrane of Eastern Belt (left) and Central Belt (right); also shown are axes of tensor averages (large open symbols). Contours determined using method of Kamb (1959) and represent multiples of expected density for uniform distribution, with lowest contour at 1, and interval for succeeding contours also 1.

tensor average show that the average X direction in the Yolla Bolly terrane is subparallel to the average Y direction in the Central Belt and that Y of the Yolla Bolly terrane is subparallel to X in the Central Belt. Given that the stretches in X and Y of the tensor averages differ insignificantly, and that the individual X- and Y-axes of the samples scatter considerably, the mutual interchange of the X- and Y-axes between the Yolla Bolly terrane and the Central Belt has no tectonic significance. Overall, the data show that SMT deformation did not accommodate any significant horizontal shortening perpendicular to the Franciscan margin in the NE direction, and also only a minor amount of horizontal contraction parallel to the Franciscan subduction complex in a NW direction.

Volume Strain and Strain Geometry

All but six analyzed samples have undergone volume loss (Table 4), which is between –2% and –64%. Two samples show no volume changes, and four samples underwent volume gain of +2% to +31%. Estimates of the kinematic dilatancy number also demonstrate the generally high volume loss (Table 4). In general, volume loss is more pronounced in the Yolla Bolly terrane, 36% against 29% in the Central Belt. However, in some of the study areas (Cloverdale transect, Bay area) (Table 4), volume loss in the Central Belt is greater than in the Yolla Bolly terrane. The volume strain is considered to have occurred largely by the loss of mass from individual detrital grains. As shown by Ring and Brandon (1999), the net loss of mass from the rock is equal to the total dissolved mass removed from the grains minus the mass of material precipitated as new fiber overgrowths.

The data indicate that about one-third of the rock volume was lost during SMT deformation in the Central and Eastern Franciscan Belts. On a regional scale the volume has been removed mainly by vertical contraction in the Z direction, and to a lesser degree by margin-perpendicular and margin-parallel shortening in the X and Y directions. The stretch parallel to the X direction, and in case of a flattening strain type also in the Y direction, of the individual samples was too small to allow for precipitation of all dissolved material.

In a conventional strain-symmetry plot (Ramsay and Huber, 1983) the strain-magnitude data fall in both prolate and oblate fields (Fig. 21A). Strain type is best determined by plotting S_V

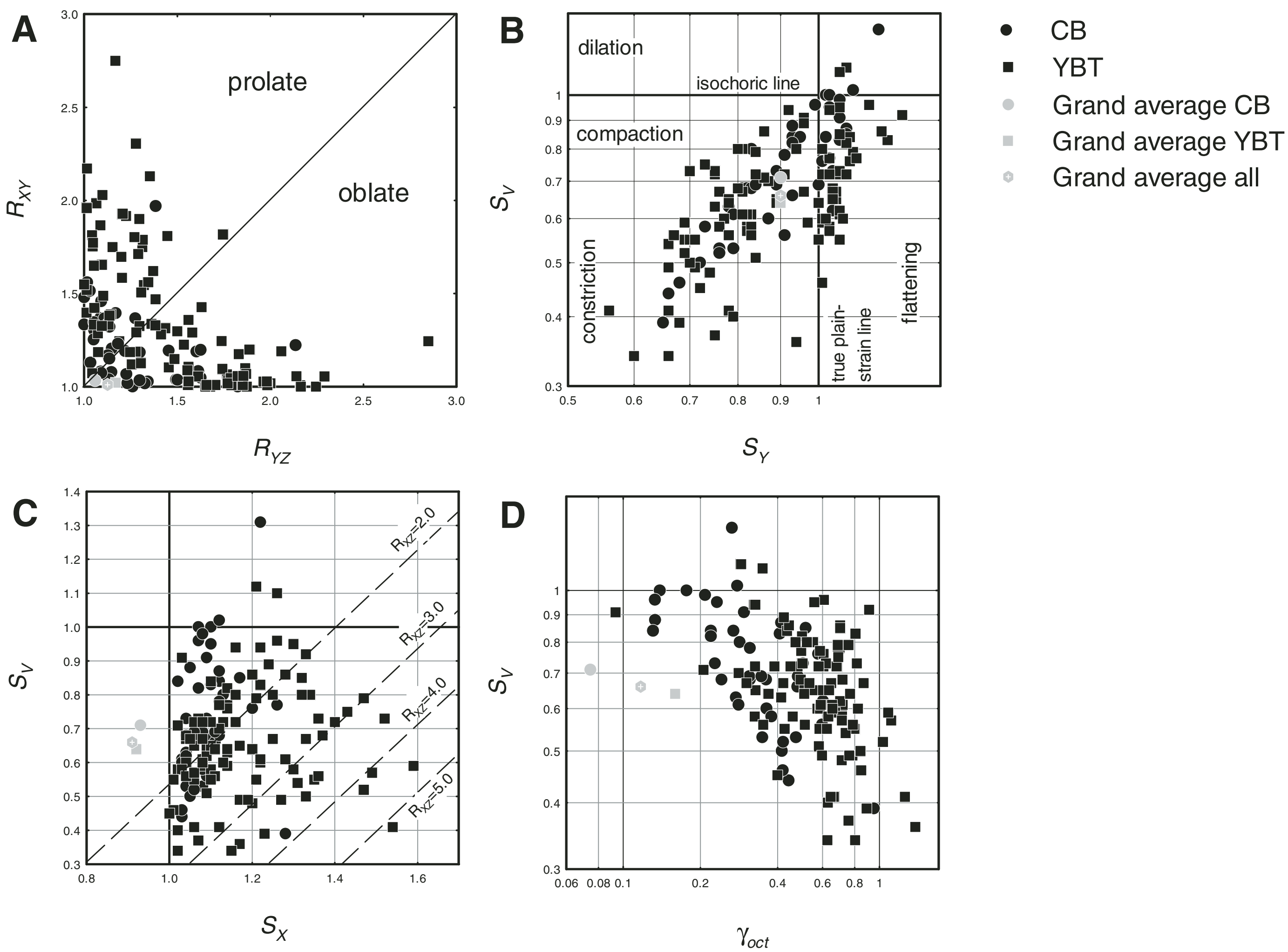

Figure 21. Finite-strain data. (A) Strain symmetry as graphic in Ramsay diagram (Ramsay and Huber, 1983), showing wide scatter of data points; note that strain tensor averages plot close to apparent plane-strain line in oblate field. (B) Strain type as indicated by S_V-S_Y diagram, illustrating true finite-strain geometry; note that data points depict considerable shift into constrictional field when compared to Ramsay plot; data show that with increasing stretch in Y, amount of volume loss decreases; strain tensor averages plot in constrictional field. (C) R_{XZ} ratios projected into S_V-S_X plot, indicating that relatively high aspect ratios in XZ section, which provide measure of cleavage intensity, do not correspond to large stretches in X when volume strains are considered. (D) Natural octahedral shear strain, γ_{oct}, plotted against volume strain, showing that volume loss increases with increasing strain magnitude. CB—Central Belt; YB—Yolla Bolly terrane.

versus S_Y (Brandon, 1995). This plot shows that the strain type is, in fact, constrictional (Fig. 21B). The S_V versus S_Y diagram shows that the amount of volume loss decreases with increasing S_Y; this trend does not emerge when one plots S_V against S_X.

Another important aspect of volume strain is highlighted in Figure 21C, in which isolines of aspect rations in the XZ section are projected into a diagram for absolute strain values. Such a diagram illustrates how volume strain and extension relate to cleavage formation, if cleavage is assumed to be perpendicular to the Z direction and the maximum axial ratio, R_{XZ}, is considered as a proxy for cleavage intensity (Brandon, 1995). S_V and S_X can be regarded as the open and closed components of the deformational system. Therefore, a strain path parallel to S_V would represent a pure volume strain, and a path parallel to S_X would characterize an isochoric plane-strain deformation where extension in the X direction is balanced by shortening in Z. As shown by Brandon (1995), and illustrated by the R_{XZ} isolines in Figure 21C, the closed-system case requires only half as much strain as the open-system case to produce the same R_{XZ} ratio. The data points in Figure 21C do not plot on either of these strain paths, indicating that deformation apparently involved both closed- and open-system behavior. The highest aspect ratios in the samples are slightly larger than 5; however, absolute stretches for these cases are between 1.5 and 1.6. Since this relationship is the same for all data points, it demonstrates that cleavage intensity is stronger than would be expected for the low extensional strains.

It is useful to compare the distortional and volume components of the strain, as shown in Figure 21D. The natural octahedral shear strain, γ_{oct}, represents a measure of the average distortional strain caused by the deformation (Nadai, 1963; Brandon, 1995). This measure is zero where $S_X = S_Y = S_Z$ and increases as R_{XY} and R_{XZ} increase. In Figure 21D, γ_{oct} is plotted against S_V. A steady-rate deformation would be shown on this plot as a path that extended at a constant rate. For a coaxial deformation, the distance from the origin is proportional to the amount of work expended in deforming the rock (Nadai, 1963; Brandon, 1995). The data show a weak negative correlation between these two measures. The work associated with volume strain varies greatly from sample to sample but generally exceeds the work associated with distorting the rock, suggesting that these two components are due to different processes. The tensor averages for volume strain are centered with respect to the distribution of the individual measurements, because volume change has no directional properties. This is not the case for the averages of the strain magnitude, because of the directional properties of strain. Also note that the tensor averages are centered with respect to the distribution of S_V but offset on the low side with respect to γ_{oct}. The reason is that variability in the principal directions at the local scale is averaged out at the regional scale so that the regional-scale average shows less distortional strain than the distribution of local values would suggest. Overall, Figure 21D suggests that removal of rock volume does not significantly affect the amount of work needed to deform the rock. This also implies that the strain recorded in the aspect ratios of deformed rocks is not simply related to the amount of work done in the rock.

The important conclusions are that if the large volume strains are ignored, one will be tempted to significantly overestimate the extension recorded in the rocks. Furthermore, regional strain in the Franciscan subduction complex is characterized by margin-parallel shortening, despite the fact of local flattening strain.

Internal Rotation and Strain Regime

Figure 22 shows the degree of internal rotation. Angles of internal rotation, Ω_i, are small, especially when compared with the angle of $\Omega_i = 42°$ for a simple-shear deformation (see Fig. 3 in Ring and Brandon, 1999). Only four samples have internal rotation angles larger than 10° (Fig. 22A; Table 4). Figure 22 illustrates that the degree of internal rotation increases slightly with increasing S_X and R_{XZ}. The average kinematic vorticity numbers of the individual samples show considerable scatter, but are, on average, small (below ~0.5), and the senses of

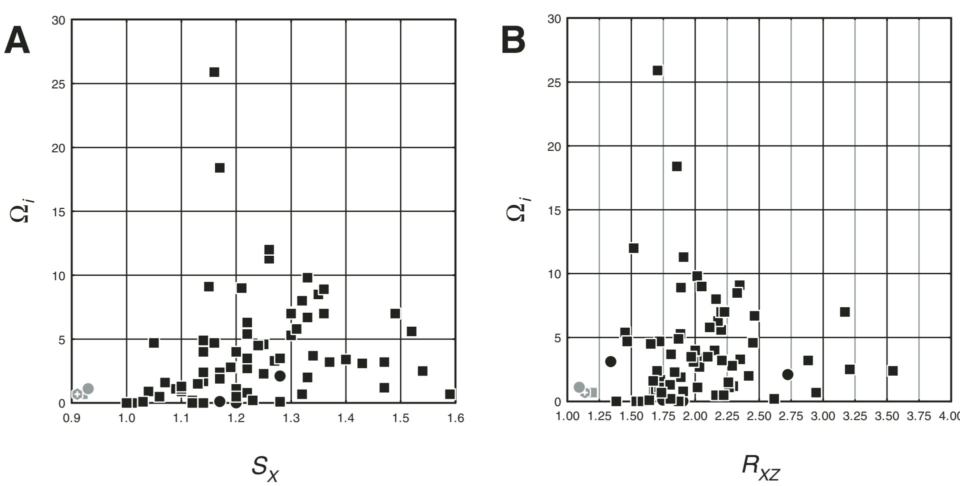

Figure 22. (A) Comparison of internal rotation angles, Ω_i, versus S_X, showing increasing angles of internal rotation with increasing stretches in X direction. (B) Internal rotation versus R_{XZ}, showing same positive correlation; note that internal rotation could only be determined for some samples of Yolla Bolly terrane and very few samples from Central Belt; all other samples had too few fibers for this analysis.

TABLE 5. OROGENIC PARAMETERS

	Depth of initial accretion
Yolla Bolly terrane	~30 km
Central Belt	~25 km
	Residence time
Yolla Bolly terrane	~40 m.y.
Central Belt	~30 m.y.
Average strike of wedge	155°

rotation are alternating (Table 4). The average mean rotation tensor on a regional scale shows almost no internal rotation for the rocks of the Yolla Bolly terrane; the small internal rotation is compatible with a top-WSW sense of rotation. The amount of volume loss is highest in samples with the highest degree of coaxial deformation (Table 4). From the neglectable internal rotation on the regional scale, we conclude that the data indicate an overall coaxial strain regime.

ROLE OF DUCTILE THINNING OF THE OVERBURDEN TO EXHUMATION OF THE HIGH-PRESSURE METAMORPHIC ROCKS

Residence Times of High-Pressure Rocks in the Franciscan Subduction Complex

In summarizing timing information above, it was estimated that the rocks of the Eastern and Central Belts resided between ~60 and 30 m.y. within the Franciscan subduction complex. The Eastern Belt rocks resided somewhat longer in the wedge than did the rocks of the Central Belt. For the exhumation calculations below, we use an average time span of 40 m.y. for the Eastern Belt and 30 m.y. for the Central Belt (Table 5). Deformation-metamorphism relationships indicate that cleavage formation and SMT deformation commenced at the peak of high-pressure metamorphism and thus when the rocks were accreted onto the overriding plate. SMT deformation and cleavage formation continued as the rocks moved upward within the wedge. Thus, we envision that SMT strain accumulated while the Eastern Franciscan rocks moved through the wedge.

Results

The regional averages of our strain measurements indicate that SMT deformation resulted in vertical shortening of ~15%–23% (Table 4). For the exhumation calculations we envision that particles are first accreted at depths of 30 and 25 km, respectively, and then moved through the interior of the wedge, reaching the surface 40–30 m.y. later (Table 4).

The results are summarized in Tables 6 and 7. They indicate that ductile strain contributed ~12% (uniform rate) to 8% (proportional rate) to the overall exhumation of the Eastern Belt and 8% (uniform rate) to 5% (proportional rate) to the overall exhumation of the Central Belt. Ring and Brandon (1999) and Ring and Richter (2004) reported similar results from local areas in the Eastern Belt. The other >90% of the exhumation was due to shallow normal faulting and/or erosion.

In Table 7 we list the vertically averaged strain rates associated with SMT deformation. The across-strike horizontal strain rate for the Franciscan subduction complex is estimated to be 0.22%–0.36% $m.y.^{-1}$. Given an across-strike dimension of 100–200 km for that portion of the complex that deformed by the SMT mechanism, one can estimate the amount of plate convergence that was accommodated by SMT deformation by considering the across-strike horizontal strain rate and multiplying it by the width of the actively deforming accretionary wedge. The estimated rate of horizontal shortening is between 0.22 and 0.72 km $m.y.^{-1}$ (0.22% $m.y.^{-1} \times$ 100 km, and 0.36% $m.y.^{-1} \times$ 200 km, as the lower and upper limits). In comparison, Engebretson et al. (1985) estimated that the convergence rate for the Franciscan subduction zone during the Late Cretaceous was >100 km $m.y.^{-1}$. In other words, SMT deformation appears to have accounted for <1% of the total convergence across the Franciscan margin. Thus, SMT

TABLE 6. RESULTS OF EXHUMATION CALCULATIONS FOR ROCKS FROM YOLLA BOLLY TERRANE BASED ON PROPORTIONAL STRAIN-RATE LAW

	Rates (km/m.y. or mm/a)			**Integrated values** (km and %)		
	χ_{dot}	ϕ_{dot}	a_{dot}	χ	ϕ	$\phi/(\chi+\phi)$
Uniform strain-rate law						
Yolla Bolly terrane	0.66	0.19	0.85	26.3	3.7	12%
Central Belt	0.77	0.13	0.90	23.1	1.9	8%
All samples	0.70	0.17	0.88	24.6	2.9	11%
Proportional strain-rate law						
Yolla Bolly terrane	0.69	0.20	0.89	27.5	2.5	8%
Central Belt	0.79	0.14	0.93	23.7	1.3	5%
All samples	0.73	0.18	0.91	25.5	2.0	7%

χ_{dot}—rate of thinning owing to erosion and shallow normal faulting ($\delta_{dot} + \lambda_{dot}$).
ϕ_{dot}—rate of thinning for whole wedge owing to vertical ductile thinning.
a_{dot}—rate of basal accretion ($\chi_{dot} + \phi_{dot}$).
χ—total exhumation owing to denudation (i.e., erosion and normal faulting).
ϕ—total exhumation owing to ductile flow.
$\chi + \phi$—total exhumation.
$\phi/(\chi + \phi)$—fraction (%) of exhumation owing to vertical ductile thinning.

TABLE 7. VERTICALLY AVERAGED SMT STRAIN RATES FOR UNIFORM AND PROPORTIONAL STRAIN-RATE LAW FOR ROCKS FROM YOLLA BOLLY TERRANE, CENTRAL BELT, AND ALL ANALYZED FRANCISCAN SAMPLES IN OROGENIC COORDINATE FRAME

	Across-strike (T)	Parallel-strike (P)	Vertical (V)
Uniform strain-rate law			
Yolla Bolly terrane	–0.21% m.y.$^{-1}$	–0.27% m.y.$^{-1}$	–0.65% m.y.$^{-1}$
Central Belt	–0.35% m.y.$^{-1}$	–0.25% m.y.$^{-1}$	–0.53% m.y.$^{-1}$
All samples	–0.28% m.y.$^{-1}$	–0.30% m.y.$^{-1}$	–0.63% m.y.$^{-1}$
Yolla Bolly terrane	-6.7×10^{-17} s^{-1}	-0.5×10^{-17} s^{-1}	-2.1×10^{-16} s^{-1}
Central Belt	-1.1×10^{-16} s^{-1}	-7.9×10^{-17} s^{-1}	-1.7×10^{-16} s^{-1}
All samples	-8.9×10^{-17} s^{-1}	-9.5×10^{-17} s^{-1}	-2.0×10^{-16} s^{-1}
Proportional strain-rate law			
Yolla Bolly terrane	–0.22% m.y.$^{-1}$	–0.28% m.y.$^{-1}$	–0.67% m.y.$^{-1}$
Central Belt	–0.36% m.y.$^{-1}$	–0.25% m.y.$^{-1}$	–0.54% m.y.$^{-1}$
All samples	–0.29% m.y.$^{-1}$	–0.31% m.y.$^{-1}$	–0.65% m.y.$^{-1}$
Yolla Bolly terrane	-7.0×10^{-17} s^{-1}	-8.8×10^{-17} s^{-1}	-2.1×10^{-16} s^{-1}
Central Belt	-1.1×10^{-16} s^{-1}	-8.0×10^{-17} s^{-1}	-1.7×10^{-16} s^{-1}
All samples	-9.3×10^{-17} s^{-1}	-9.8×10^{-17} s^{-1}	-2.1×10^{-16} s^{-1}

Note: Strain rates in % m.y.$^{-1}$ and in s^{-1}; negative numbers indicate contractional strain rates.

deformation is considered to have been a background deformation process. The subduction thrust at the base of the wedge must have largely decoupled the wedge from the rapidly subducting oceanic plate. The fact that rocks within the wedge might have accumulated significant amounts of strain is apparently due to the long residence time of these rocks within the wedge and not a high degree of coupling across the subduction zone.

The finite-strain results show that shortening in the Z direction is of the order of 23% in the Yolla Bolly terrane and 15% in the Central Belt. The contribution of ductile thinning to exhumation is much less than these values. For a particle being accreted at the base of the wedge, vertical thinning of the overburden can only contribute that amount of vertical thinning to exhumation, which the overlying column of rock undergoes after the particle has been accreted. If the overlying rocks have already acquired any strain by the time the particle is accreted, the contribution of ductile flattening will be less than the total finite strain. This means that the fraction of ductile thinning of the overburden is not simply related to the acquired total finite strain but is mainly a function of the instantaneous integrated strain along the exhumation path, which is a function of the depth dependence of the strain rate. In the case of a proportional strain-rate law, the amount of ductile flattening of the overburden strongly depends on the thickness of the overburden and the upward decrease in the strain rate. Most of the finite strain of the accreted and upward moving particle is acquired in the lower part of the wedge, where the strain rate is highest. Therefore, the shortening in the Z direction will always be (significantly) higher than the amount of ductile thinning of the overburden.

The contribution of ductile flattening to exhumation depends strongly on the orientation of the finite strain axes during deformation. Vertical thinning requires a shallowly plunging extension direction and a subvertical shortening direction. Many high-pressure orogenic belts do fulfill this requirement (e.g., the Alps, Selverstone, 1985, 2005; the Aegean subduction system, Lister et al., 1984; Ring et al., 2001a; the Franciscan subduction complex, Ring and Brandon, 1999; the San Juan–Cascade nappes of northwestern Washington State, Feehan and Brandon, 1999). This qualitative statement also works if subvertical shortening is more or less compensated by volume loss and no net extension occurs, such as in the Franciscan complex. Nevertheless, settings like the Olympic Mountains (Brandon and Calderwood, 1990; Brandon and Vance, 1992), the Taiwan Alps (Suppe, 1980, 1981), or the Southern Alps of New Zealand (Kamp et al., 1989) have steeply plunging extension directions, indicating vertical thickening where subhorizontal shortening was not wholly compensated by volume loss. Wedge models (Willett et al., 1993) indicate that both the orientation of the principal strains during deformation, and the magnitudes of the corresponding stretches, can evolve during the life of an orogen. Hence, it is likely that during periods of exhumation the relative contributions of erosion, normal faulting, and ductile thinning vary over time.

DISCUSSION: DUCTILE DATA

Our discussion will be threefold and is meant to present supporting arguments for the envisioned tectonic history presented later. We start with discussing the ductile data, followed by a discussion of brittle and sedimentologic aspects. Our main conclusion is that the ductile data do not support the development of a supercritically tapered Franciscan wedge that promoted normal faulting in its upper rear part.

Mass Loss, Pattern, and Magnitude of Ductile Deformation

We showed that ductile deformation in the Franciscan subduction complex was largely accommodated by SMT deformation, thus confirming the assumptions of Platt (1986) about ductile deformation mechanisms in orogenic wedges. SMT deformation within the Franciscan complex is characterized by considerable mass loss, averaging –34%. The volume strains can be considered a form of internal erosion within the accretionary wedge. SMT deformation involved both closed and open exchange, expressed by local precipitation of fiber overgrowths and wholesale loss of mass from the rock. The open-system behavior was probably driven by dissolution and bulk removal of the more soluble components of the rock, owing to flow of a solvent fluid phase on a regional scale. The closed-system behavior apparently reflects grain-scale transport of the relatively insoluble components of the rock, which have crystallized as fiber overgrowths. Despite quartz, Al-bearing minerals with a relatively low solubility make up the fibers (e.g., phengite, chlorite, lawsonite), suggesting that transport of these components must have been restricted to diffusion length scales.

The pattern of the principal finite strain axes shows considerable scatter for the Eastern and Central Franciscan Belts. Individual samples show maximum extensional stretches of up to 59%. Values for the natural octahedral shear strain, which represents the strain magnitude in the rock, are surprisingly low (Table 4). On a regional scale the highly variable strain pattern is averaged out; there is no extension associated with SMT deformation at the local and regional scale. Instead, our data indicate shortening in all three principal directions. Furthermore, the overall internal rotation on a regional scale is negligible, because the variable vorticity at the local scale is averaged out. Models involving simple-shear deformation are therefore not applicable to the Franciscan subduction complex. Rather, the overall deformation in this complex can be approximated as a distributed, heterogeneous, coaxial deformation characterized by overall shortening, which was balanced by negative volume strain. Heterogeneous pure-shear deformation is manifested by various components of general shear with variable senses of vorticity.

Our results challenge many of the casual assumptions about ductile deformation in accretionary wedges. The first assumption is that wedge settings are characterized by wholesale noncoaxial flow (Cloos and Shreve, 1988). The second is the more widespread assumption that deformation at the regional scale is isochoric, and plane strain with the Y direction oriented parallel to the margin and $S_Y = 1$ (e.g., Quinquis et al., 1978; Mattauer et al., 1981; Ramsay et al., 1983). On a regional scale the ductile strain data show no ductile extension parallel to the Franciscan subduction complex. Therefore, the strain data do not support large-scale orogen-parallel displacements and are therefore at odds with tectonic models that involve significant accretion of terrigenous terranes or fragments of accretionary prisms that originated south of the Franciscan margin.

Ductile Fabrics in Del Puerto Canyon

It is interesting to note that the highly variable finite strain pattern, as documented in this study, matches the pattern of "mylonitic lineations" as reported by Harms et al. (1992) from a small area south of Mount Oso (Fig. A10). We have recently completed an SMT strain study on quartz grains in the high-pressure graywacke from the proposed Del Puerto Canyon shear zone (Ring and Richter, 2004). Our work shows no evidence for a ductile shear zone in the uppermost Franciscan subduction complex as advocated by Harms et al. (1992). We have found no high strains and no evidence of strongly noncoaxial deformation. The strain does not increase toward and within the uppermost 10 m of Franciscan sandstone underneath the Coast Range ophiolite. The mapped maximum stretching directions depict a highly variable pattern, and there is no evidence for a preferred sense of rotation in the uppermost Franciscan subduction complex. A tensor average for the Franciscan graywacke in the Del Puerto Canyon shear zone (Table 4) shows that the maximum stretch direction did not involve any extension. There is a positive correlation between shortening and volume loss (Ring and Richter, 2004, their Fig. 6), which implies that shortening was balanced by volume loss and not by extension. Thus, there is no evidence for any net extension in the proposed Del Puerto Canyon shear zone.

One could argue that most of the deformation is partitioned into the lithic clasts or the shale sequences and thus was not captured by the strain analysis on quartz grains in graywacke by Ring and Richter (2004). We measured aspect ratios of the lithic clasts in sections perpendicular to the foliation and parallel to a weak linear fabric in the rocks in a reconnaissance fashion. In general the aspect ratios were 2–3, with highest values of ~5. As discussed above, the volume strains indicate that absolute stretches parallel to X for rocks with aspect ratios of 5 are <2 and comparable to our detailed strain measurements of the clastic quartz grains. We did not perform quantitative strain measurements in the shales. Nonetheless, Richter et al. (2007) compared strain data from quartz grains in graywacke to those obtained by X-ray texture goniometry on phyllosilicate grains in shale in the Paleozoic accretionary wedge of coastal Chile. The latter wedge is similar in lithology and tectonic style to the Franciscan. Richter et al. (2007) found no systematic differences between the quartz and phyllosilicate strains. Such a finding is in line with the general lack of any refraction of the foliation between the sandstone and shale layers in the Del Puerto Canyon area and elsewhere in the Franciscan. Therefore, we conclude that the strain analysis of Ring and Richter (2004) adequately represents ductile strain in the proposed Del Puerto Canyon shear zone.

We contend that the average direction of the lineations themselves cannot be used to infer the extension direction at the regional scale nor the direction of tectonic transport in Del Puerto Canyon. The substantial deviation from simple shear in the Eastern Franciscan Belt implies that the lineations should not, a priori, be regarded as displacement trajectories that track regional-scale tectonic transport directions in mylonites. The strain data from Del Puerto Canyon, and the Franciscan subduction complex in general (Table 4), suggest that the development of a linear fabric is due to a combination of volume loss and shortening in two directions rather than net extension of the rocks. We argue that the average direction of the lineations of Harms et al. (1992) cannot be used to infer the direction of tectonic transport and that the low-strain SMT fabric of the Franciscan subduction complex sandstones cannot be compared with S-C fabrics.

Ductile Strain, Exhumation of Franciscan High-Pressure Rocks, and the Role of SMT Deformation Mechanisms

According to the model of Platt (1986), subhorizontal extension caused the exhumation of the high-pressure metamorphic rocks of the Eastern Franciscan Belt (Fig. 23A). Subhorizontal extension is thought to be the result of vertical contraction driven by gravitational forces. However, extension would only be required if constant-volume deformation in the wedge was assumed. In the case of the Eastern and Central Franciscan Belts, vertical shortening occurred without horizontal extension, because shortening was compensated by mass loss (Fig. 23B). Large-scale mass loss obviously prevented the wedge from becoming supercritically tapered. This suggests that the model of Platt (1986) might not be strictly applicable to wedges that have undergone high volume strains during SMT deformation.

The absence of ductile extensional strains on the regional scale indicates that the deep parts of the wedge were not significantly thinned by ductile extensional flow. The results of the exhumation model argue that vertical ductile thinning of the overburden of the high-pressure rocks did not significantly contribute to the exhumation of the high-pressure rocks themselves.

The predicted strain rates for SMT deformation are fairly low. Vertically averaged strain rates for different directions in the wedge are relatively low in horizontal directions and greater in the vertical direction (Table 7). These strain rates are orders of magnitude smaller than the 1×10^{-14} s^{-1} strain rates assumed by Platt (1986). Expressing the strain rate in % $m.y.^{-1}$ illustrates the point more clearly. Platt (1986) envisions 31% $m.y.^{-1}$, and we derived strain rates <0.36% $m.y.^{-1}$, which are a factor of ~100 smaller. As a consequence of the slow strain rates and the high volume loss, ductile flow probably was not fast enough to significantly influence the stability of the wedge and form a supercritically tapered wedge.

The width of the actively deforming Franciscan subduction complex has been variably estimated to be 100–200 km across. Because the strain measurements come from the rearward part of the wedge, this calculation will tend to overestimate vertically averaged SMT strain rates for the thinner and more forward parts of the wedge. Using the numbers given above, estimated rates of across-strike horizontal shortening are no greater than 1 km $m.y.^{-1}$. Convergence rates at the Franciscan margin have been estimated by Engebretson et al. (1985) to be >100 km $m.y.^{-1}$. Hence, a fraction of <1% of orogenic convergence was taken up by SMT deformation. This means that <1% represents the entire ductile deformation within the Franciscan subduction complex and that >99% of the overall deformation in the presently exposed portion of the Franciscan plate margin was accommodated by other mechanisms.

The importance of our findings for the exhumation of the high-pressure metamorphic interior of accretionary wedges is twofold: (1) ductile deformation in the Franciscan subduction complex did not help to drive the wedge into supercritical mode; (2) the high volume strain also prevented the wedge from becoming supercritically tapered. Both points render the development of synsubduction normal faults in the wedge rather unlikely.

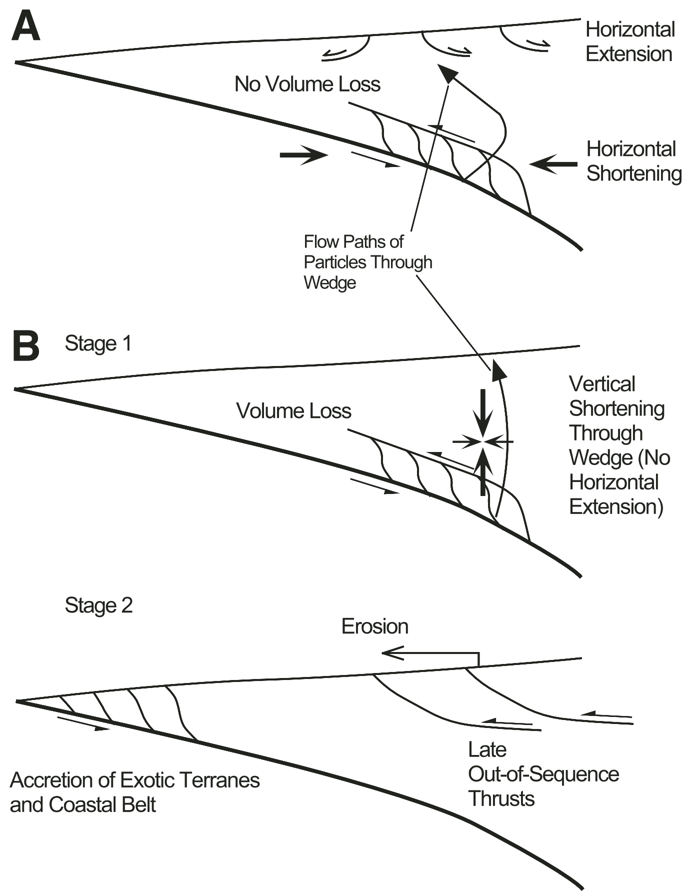

Figure 23. (A) Subhorizontal extension in upper rear part of wedge, thought to be result of vertical contraction driven by gravitational forces and, because isochoric within-wedge deformation is assumed, balances out subhorizontal contraction in lower part of wedge (strongly modified from Platt, 1986). (B) Proposed two-stage development of Franciscan subduction complex; in first stage, material that rises through wedge is vertically shortened, and this shortening is balanced by large-scale mass loss, not by subhorizontal extension; second stage shows late out-of-sequence thrusts that carry material into higher crustal levels where erosion takes place; note that considerations are restricted to two dimensions.

What structures took up the orogenic convergence, then? Part of the orogen-normal shortening may have been accommodated by late, out-of-sequence thrusts as reported by Suppe (1973), Cowan (1974), Platt (1975), and Worrall (1981) for the Franciscan subduction complex; Glen (1990) for the westernmost Great Valley Group; and Ring and Brandon (1994) from the Coast Range fault zone. Suppe (1979) and Glen (1990) depicted these thrusts as ramp-flat systems, indicating that they caused folding and, if temperatures during thrusting were high enough to activate SMT deformation mechanisms, internal deformation in Franciscan sandstone. According to the cross section of Suppe (1979, his Fig. 1), the out-of-sequence thrusts affected the Franciscan rocks at a depth of ~15 km. Assuming an average geotherm of 15 °C km^{-1} for higher levels of the Franciscan at that time indicates that temperatures should have been high enough to promote SMT mechanisms. Therefore, at least part of the thrust-related strain should have been accommodated by SMT deformation. If thrust-related deformation was associated with SMT deformation, and if the very low strain values for SMT deformation are considered, thrust-associated displacement in crustal levels deep enough to allow SMT deformation mechanisms to operate cannot have been large. Such an interpretation is corroborated by barometric data, which show only moderate breaks in metamorphic pressure of ≤~1 kbar, corresponding to displacement of ≤13.5 km (assuming a dip angle of 15°–20°) across the faults that juxtapose the South Fork Mountain Schist of the Pickett Peak terrane against the Valentine Springs Formation of the uppermost Yolla Bolly terrane, and the latter against the structurally deeper rocks of the Yolla Bolly terrane. If this argument is accepted, it will have implications for current tectonic models of the Franciscan subduction complex because it implies that no large-scale orogenic shortening has been accommodated within the Eastern and Central Franciscan Belts. However, as argued above, the Coastal Belt thrust probably accommodated 40–80 km of horizontal shortening and seems to be the only structure in the Franciscan that records considerable horizontal shortening.

We envision that slip along a major thrust between the subduction wedge and the downgoing plate accommodated most of the convergence at the Franciscan margin. If this was true, it would indicate that the subduction wedge was largely decoupled from the downgoing plate—that is, traction at the base of the wedge was low, and therefore no high stresses built up within the wedge. It follows that the relatively high convergence rate of >100 km $m.y.^{-1}$ (Engebretson et al., 1985) had almost no influence on the rate of deformation in the wedge and that the accumulation of ductile strain in the wedge was mainly a function of the residence time within the wedge. Such a scenario can also explain the low strain magnitudes within the Franciscan subduction complex.

Comparisons with Other Accretionary Wedges

Our work in other accretionary belts provides similar results. Feehan and Brandon (1999) reported a volume strain of ~47% from the San Juan–Cascade wedge of Washington State. Ring et al. (2001b) showed that a volume loss of ~36% accompanied cleavage formation in the Helvetic wedge of the frontal part of the Central Alps in Switzerland. Richter et al. (2007) reported a volume loss of ~20%–30% in the late Paleozoic accretionary wedge of coastal Chile. J. Rahl (2007, personal commun.) found ~20% volume loss in the low-grade flanks of the Torlesse wedge of New Zealand, and H. Deckert (2008, personal commun.) could show that volume loss in the high-grade interior of the Torlesse wedge (Otago schist) was of the order of ~15%.

In all these wedges the values for the natural octahedral shear strain and strain rates are low, and deformation was largely coaxial. Furthermore, there is no evidence for horizontal extension normal or parallel to the belts. In general, these data indicate that all of these accretionary wedges were largely decoupled from their downgoing plates. Strong coupling should have produced distinctly noncoaxial fabrics in the accreted rocks, a stronger preferred orientation of finite-strain axes, and generally larger strains. Synsubduction normal faulting did not play a significant role in the exhumation of the high-grade interior of these accretionary wedges. For the Torlesse wedge, Deckert et al. (2002) showed that late-stage normal faults are probably due to postsubduction rifting and did not form during subduction.

DISCUSSION: BRITTLE DATA

Tectonic Wedging

Results of seismic reflection and refraction profiles and thrust fault focal mechanisms of earthquakes in several transects across the east flank of the Coast Ranges have been interpreted by Wentworth et al. (1984), Wentworth and Zoback (1989), and Unruh and Moores (1992) as indicating the presence of a triangle zone that has been driven eastward beneath the Great Valley Group. In this interpretation the eastward dip of the Great Valley homocline is considered to mimic the dip of the underlying roof thrust for the triangle zone. According to Wentworth et al. (1984), the Coast Range fault zone has a top-E sense of displacement. According to a more recent interpretation of tectonic wedging (Unruh et al., 1995) the Coast Range fault zone is considered a top-W thrust.

Wentworth et al. (1984) originally proposed that wedging along the eastern flank of the Coast Ranges occurred during the middle Cretaceous, a view also expressed by Unruh et al. (1995). Most authors concluded that much, if not all, of this deformation was fairly young (Phipps, 1984; Namson and Davis, 1988; Wentworth and Zoback, 1989; Ramirez, 1992; Unruh and Moores, 1992; Jones et al., 1994).

The wedging model has gained support from geodynamic modeling by Malavieille (1984) and Willett et al. (1993), which shows that when an accretionary wedge develops a prominent forearc high, the wedge divides itself into two parts: a seaward-facing prowedge that accommodates the subduction of oceanic lithosphere and an arcward-facing retrowedge that is floored by thrust faults that allow the forearc high to override the inboard forearc basin. This phenomenon illustrates the important role that topographic slope plays in controlling the vergence of thrust faulting in areas undergoing horizontal contraction.

Kinematics of the Coast Range Fault Zone and Intra-Franciscan Faults

We believe that our kinematic data indicate that the present Coast Range fault zone is a contractional fault that accommodated E-side-up or top-W motion. The Z-transformed internal-rotation axes (Fig. 18) are clustered around an average orientation parallel to the fault zone and approximately perpendicular to the average shortening direction. The orientation of the SZA direction indicates a general top-W (~250°) sense of shear for the fault zone.

We propose that the Coast Range fault zone as now exposed is an out-of-sequence thrust fault that attenuated an already tilted metamorphic sequence, thus explaining the pronounced break in metamorphic grade across this fault. It is important to note that an abrupt downward increase in metamorphic grade, and also the presence of stratigraphically younger-over-older rocks, can be produced during overall contractional deformation, and thus are not unique indicators of normal faulting (cf. Wheeler and Butler, 1994). Kinematic data are therefore most critical for elucidating the slip history of a fault zone, and these data indicate that the Coast Range fault zone is a contractional fault. Furthermore, we have found no evidence for the 9–20 km of normal slip predicted by the extensional model of Platt (1986) and others.

Despite differences in the interpretation of the sense of slip, there seems to be general agreement that the Coast Range fault zone originated with a low dip and was rotated into its present steep orientation at a later time. If so, the shortening axes would have originally had a subhorizontal orientation, indicating ENE contraction. The raw fault data (Figs. A11–A14) show some evidence for conjugate sets of faults. After restoration of the tilt of the Coast Range fault zone, the conjugate sets appear as moderate to steep, E- and W-dipping reverse faults oriented at a high angle to the average shortening direction, as schematically illustrated in Figure 5. We infer that these faults originated at an acute angle to the average shortening direction and have been rotated into their present "high-angle" orientation as a result of distributed brittle strain within the fault zone. This interpretation is consistent with other evidence that the fault zone thickened during its evolution. When the fault zone is viewed in its original subhorizontal orientation (Fig. 5B), it is apparent that the thickening was caused by distributed deformation on a network of E- and W-dipping reverse faults. This style of deformation emphasizes the fact that the Coast Range fault did not form by simple shear but rather by general shear, involving thickening normal to the fault zone and positive volume strain within the fault zone owing to serpentinization. It seems also important to note that the top-W shear sense, as found in our study, is inconsistent with an interpretation that the Coast Range fault zone is a top-E normal fault, even after any restoration of dip (Fig. 5).

There is other evidence for top-W shear at or near the Coast Range fault zone. Unruh et al. (1995) place this contractional deformation into latest Cretaceous to early Tertiary time, whereas Glen (1990) argues that top-W motion in the westernmost Great Valley Group near Paskenta was Eocene or younger in age. The more recent work by Unruh et al. (2007) argues for earliest Tertiary high-angle normal faulting in the western Great Valley basin in the northernmost Diablo Range. Either the normal faults in the northern Diablo Range are local to this part of the basin, or Eocene or later thrusting followed Paleocene normal faulting.

Most of the intra–Franciscan subduction complex faults place higher-grade rocks over lower-grade ones and show evidence for top-W motion. The most prominent of these structures is the Coastal Belt thrust. Bolhar and Ring (2001) provided evidence for top-W thrust motion on the Red Mountain fault, which places the Eastern Belt onto the Central Belt. These authors also showed that faults within the Yolla Bolly terrane resulted from E-W shortening with thrusts having top-W kinematics. We envision that most of the intra–Franciscan subduction complex faults, as well as the Coast Range fault zone and associated faults in the forearc massif, resulted from the same E-W shortening event.

Top-W motion on the Coast Range fault zone would have caused structural burial of the underlying Eastern Franciscan Belt. As shown by the zircon fission-track ages of Tagami and Dumitru (1996), incipient exhumation-related cooling of the latter started immediately after the completion of high-pressure metamorphism in the Yolla Bolly terrane (ca. 90 Ma) and brought the Franciscan high-pressure rocks into shallower crustal levels, where they have been affected by the postmetamorphic out-of-sequence thrust faults. In any case, thrusting at the Coast Range fault zone and incipient steepening there should have occurred before the final exhumation and steepening of Great Valley rocks in the homocline during the Cenozoic.

One might argue that the slickensides analyzed by us might be of very young age and thus might postdate steepening of the Coast Range fault zone. The Neogene kinematics of coastal California are controlled by dextral transpression across the San Andreas fault. This kinematic pattern caused dextral strike-slip, coupled with E-directed contraction, and therefore cannot explain the present pattern of subvertical contraction and subhorizontal extension at the Coast Range fault zone. Moreover, we found evidence for a dextral strike-slip overprint in Del Puerto Canyon, which fits into the Neogene kinematic framework. This supplies further evidence for our argument that the main brittle deformation structures are pre-Neogene in age.

The lack of evidence for normal faulting in the Franciscan subduction complex and the Coast Range fault zone does not lend any support into the extrusion wedge model by Maruyama et al. (1996). In subduction settings these wedges usually form directly above the subduction thrust in the lower parts of the accretionary wedge or the subduction channel (Ring et al., 2007). Therefore, the normal faults described by Unruh et al. (2007) from the Great Valley basin also do not support the extrusion wedge model.

Possible Cause for Out-of-Sequence Thrusting in the Franciscan Subduction Complex

Contraction within the Franciscan subduction complex might have been caused by collision of exotic oceanic terranes. This complex contains evidence of only two major oceanic terranes, both of which collided with the margin at some time during the Late Cretaceous or early Cenozoic (Blake, 1984). The Marin headland terrane contains a thick chert sequence, indicating that it resided in a deep ocean setting from Early Jurassic through middle Cretaceous times, perhaps as an oceanic plateau (Murchey, 1984). The Laytonville limestones and other related limestones in the Central Belt were deposited as pelagic sediments at low latitudes in the Pacific basin during the middle Cretaceous (Alvarez et al., 1980). If either of these units were associated with a sufficiently large bathymetric feature, such as an oceanic plateau or seamount chain, the resulting collision would have forced the basal thrust of the wedge to steepen as it climbed over the subducting terrane. The predicted result would be to shift deformation rearward into the wedge with the formation of out-of-sequence thrust faults. These new faults would be expected to have migrated seaward with time, causing contraction within the wedge.

DISCUSSION: SEDIMENTOLOGIC ASPECTS

Emergence of Forearc High and Sedimentologic Record

Stratigraphic relationships provide some constraints for the timing of emergence of the forearc high and associated onset of erosional denudation. Sedimentologic data indicate that the surface of the Great Valley basin was at water depths of 3–6 km during the Late Jurassic and became shallow and locally emergent during the Late Cretaceous and early Tertiary (i.e., Eocene unconformity, Ingersoll, 1978, 1979; Dickinson et al., 1982; Moxon and Graham, 1987; Moxon, 1988). All of the paleocurrent data for the Great Valley Group indicate that a forearc high was present along the west side of the Great Valley basin from the Early Cretaceous through the Paleogene, as indicated by the dominant flow of turbidites parallel to the axis of the basin at these times (Ingersoll, 1978; Suchecki, 1984; Seiders, 1983, 1988). Ingersoll (1978, 1979), among others, argued that the forearc high did not become emergent above sea level until the Late Cretaceous. Such a view appears to be consistent with the onset of tectonically driven shoaling in the Great Valley basin at 84 Ma (Moxon and Graham, 1987).

The pronounced Eocene unconformity in the western Great Valley basin indicates no deposition in the basin during the latest Cretaceous and early Cenozoic. Overlying Eocene strata contain unambiguous evidence of Franciscan subduction complex detritus (Dickinson, 1976, p. 465; Page and Tabor, 1967, p. 3–4; Swe and Dickinson, 1970, p. 184; Berkland et al., 1972, p. 2396 and 2401). Although this Eocene unconformity precludes deposition of Franciscan material in the Great Valley basin in the Late Cretaceous and Paleocene, it does not preclude erosion of the Franciscan forearc high prior to the Eocene, as long as sediments were transported westward. Cowan and Page (1975) and Smith et al. (1979) reported occurrences of recycled Franciscan detritus in Late Cretaceous trench and trench-slope basins. These occurrences are scarce among the recognized conglomerates in the Franciscan subduction complex, but most of what is exposed of this complex are the more deeply exhumed parts of the subduction wedge. Trench-slope basins are rare, presumably because they would have mantled the top of the wedge and would have been the first units to be eroded away following subaerial emergence. Berkland et al. (1972, p. 2401) proposed that materials eroded from an emergent Franciscan forearc high were transported into the trench (cf. Brandon et al., 1998, for the Olympic subduction complex) and can now be found in the Coastal Belt of the Franciscan subduction complex. Another alternative is that the eroded sediment was subducted beneath the current exposures of the complex.

Erosional Exhumation

Ring and Brandon (1994) proposed that the Coast Range fault zone formed late in the evolution of the Franciscan subduction complex as a top-W out-of-sequence thrust fault. This type of structure can account for the break in metamorphic grade observed at the Coast Range fault zone, but only if the metamorphic isograds were dipping eastward at a steeper angle than the fault (Wheeler and Butler, 1994; Ring and Brandon, 1994; Ring, 1995a). This interpretation does not explain how the Franciscan subduction complex was exhumed. In fact, top-W motion on the Coast Range fault zone would have caused increased structural burial of the Eastern Belt. We prefer the interpretation that exhumation of the Franciscan was accomplished by erosion of an uplifted forearc high. The necessary rates of erosion are <1 km m.y.$^{-1}$ to exhume rocks from <30 km within ~40 m.y. Comparable rates of erosional exhumation have been documented for the Olympic Mountains (Brandon and Vance, 1992; Brandon et al., 1998). Because the Olympic Mountains and the adjacent forearc basin of Puget Sound occupy a similar tectonic position as the Franciscan subduction complex and the Great Valley forearc basin, they will serve as a modern example here.

The main argument against erosional exhumation is that the Great Valley Group shows little evidence of the eroded sediment (Platt, 1986). Provenance studies indicate that the Sierra Nevadan arc was the primary source for Great Valley sediments as well as those of the Franciscan (Dickinson et al., 1982). However, Dickinson et al. (1982) do recognize recycled sediments within the Central and Eastern Franciscan belts that were shed from other parts of the complex. Those recycled sedimentary rock fragments make up between 2% and 25% of the Franciscan sandstones. Among these rock fragments, chert makes up between 1% and 13% of the Franciscan sandstones. In particular, Cowan and Page (1975) and Cowan (1978) report the occurrence of blueschist clasts in conglomerates and pebbly mudstones that are interpreted to have been deposited in trench and trench-slope basin settings.

Among the numerous studies of sedimentary provenance at the Franciscan subduction complex–Great Valley margin, the Coastal Belt has received only limited study (Underwood and Bachman, 1986; Dickinson et al., 1982). Dickinson et al. (1982, p. 102–103) concluded that the possibility remains open that a significant fraction of sediments that make up the Coastal Belt were derived from erosion of the Franciscan forearc high. Notable is the fact that the recycled material would have been restricted mainly to the overburden of the currently exposed high-pressure metamorphic rocks. Thus, one might not expect to find much difference between first-cycle sediment and that derived from recycling of exhumed parts of the Franciscan subduction complex. The apparent absence of ultramafic detritus in the complex would suggest that the Coast Range ophiolite did not extend across the forearc high.

Unruh et al. (2007) criticized our model of erosional exhumation of the Franciscan high-pressure rocks by pointing out that the sediments of the Great Valley Group provide little support of the model. We note that our model does *not* argue that the eroded rocks were deposited in the Great Valley basin but that the bulk of the eroded material was shed to the west and was recycled into the trench.

A cornerstone of the proposed erosion model (Fig. 24) is that the critical at-yield mechanical state of the material in a deforming orogen implies a strong interdependence between the active deformation of the orogen and its topographic profile (e.g., England and Richardson, 1977). Surface processes that erode and denude mountains lead to large-scale removal of mass from an orogen and cause the velocity field to adjust in order to replace eroded material by material from within the wedge. Additional mass loss from within the wedge would enhance this trend. The at-yield behavior of modeled orogens requires that deformation adjusts instantaneously to replace removed material. Hence, denuded zones have increased exhumation rates.

On the basis of the aforementioned observations, we propose that the eroded cover of the Franciscan subduction complex may have been transported westward, down the seaward slope of the complex, as illustrated in Figure 24. This possibility is compatible with sediment transport patterns for the forearc high of the modern Cascadian margin. The rainfall is several times higher on the seaward flank of the Olympic Mountains. The rivers that drain this mountain range flow mainly to the west and north and ultimately link with submarine canyons that transport sediment down to the lower trench slope and onto the Cascadian abyssal plain. The landward side of the Olympic Mountains is drier and more poorly drained, so that little of the eroded sediment is deposited in Puget Sound. Hence, a situation like the one illustrated in Figure 24 occurs in orogens where precipitation is orographically controlled, giving the orogen a wet, more rapidly denuded, windward side and a dry, leeward side with little erosional denudation. Such an asymmetric pattern of erosion with a paleodrainage divide located close to the present-day position of the Coast Range fault zone is envisioned. Uplift of the forearc high was maintained by continued deep accretion beneath the Franciscan wedge.

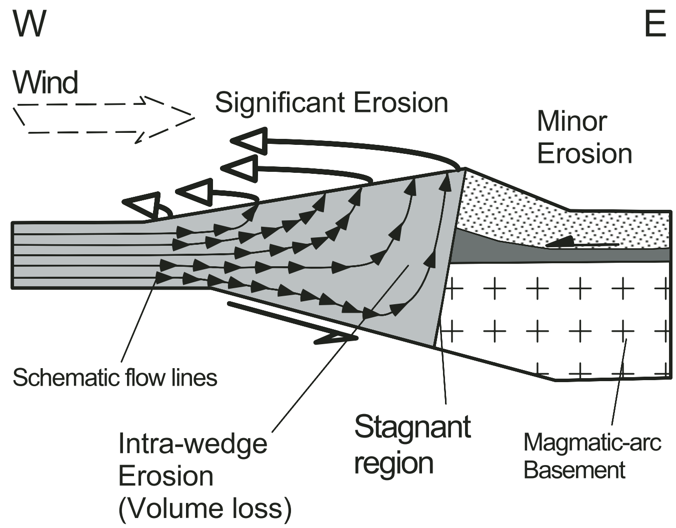

Figure 24. Idealized asymmetric pattern of erosion, which resulted in differential exhumation across eastern flank of Coast Ranges (after Willett et al., 1993); frontal part of wedge (which would be represented by Franciscan subduction complex) heavily denuded, creating nondeforming, noneroding rearward part (which would be represented by Great Valley Group) against which frontal wedge material is decoupled and exhumed, forming huge flexural fold near stagnant region. This response has effect of short-circuiting material trajectories and subsequently reducing path length and residence time in orogen; metamorphic grade of surface rocks increases across frontal wedge; note that finite strain data for Eastern and Central Belts indicate that deformation was accompanied by significant loss of mass, which can be viewed as type of internal erosion within wedge; physical erosion across western flank of Coast Ranges is thought to have triggered enhanced exhumation rates in frontal part (i.e., in front of stagnant region) of wedge.

PROPOSED TECTONIC EVOLUTION

Figure 25 shows three cross sections that illustrate the proposed evolution at the Franciscan subduction complex–Great Valley contact. Our approach is to focus on those relationships that are relevant to the exhumation problem.

The first section (Fig. 25A) shows a broad Great Valley basin that pinches out to the west on a forearc high during the Cretaceous. By Late Cretaceous time, the forearc high had become emergent in many areas, as indicated by an unconformity, breaks in stratigraphy, and some evidence of recycling (i.e., erosion of the forearc high commenced). Water depth was very shallow in those areas farther to the east where deposition was still going on (e.g., Campanian–Maastrichtian Sacramento shale, Fig. 7). Sediments onlapping the forearc high during the Cretaceous would have ensured that the bathymetric relief of the forearc high was insignificant. In other words, it probably remained only a structural high until the Late Cretaceous, when it became emergent. The Yolla Bolly and Pickett Peak terranes were already accreted and past their peak metamorphism, and they may have been cooling because of continued underplating. The vertical separation at this time between the top of the Coast Range ophiolite and the Pickett Peak and Yolla Bolly terranes was ~15 km (12 km of Great Valley Group and 1 km of Coast Range ophiolite, versus 25–30 km accretion depth for the Pickett Peak and Yolla Bolly terranes).

Over the interval from 100 to 70 Ma, the whole forearc area probably shoaled by 2–3 km. Some 5 km of stratigraphy was added to the center of the Great Valley basin, which requires that

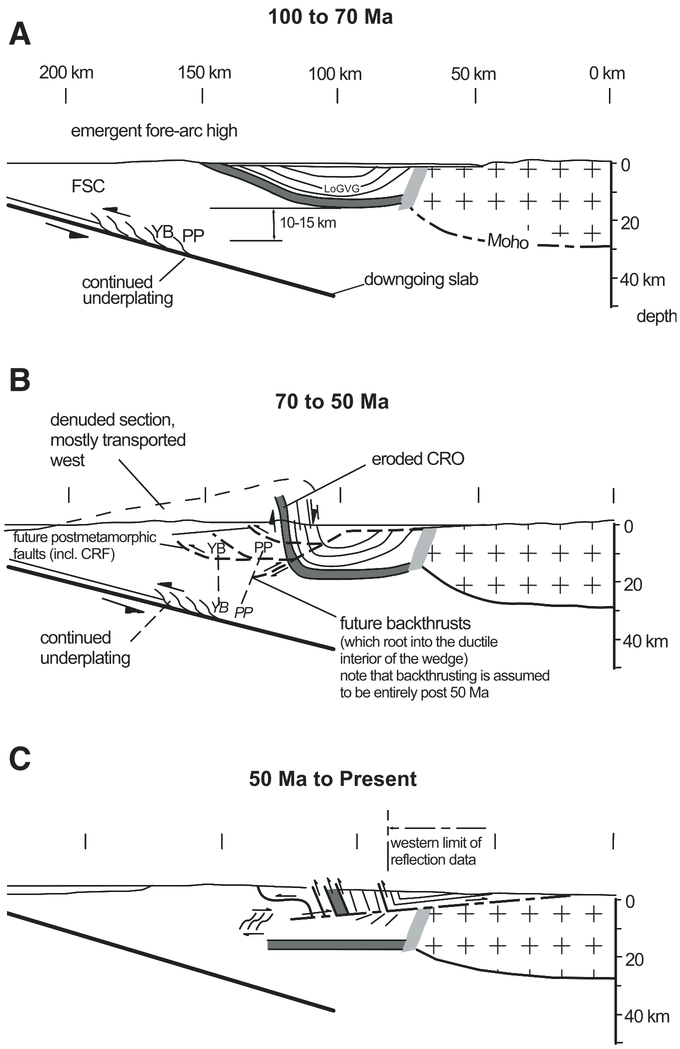

Figure 25. Proposed evolution at Franciscan plate margin. (A) Interval between 100 and 70 Ma; high-pressure metamorphism in Eastern Belt; forearc high became emergent probably at ca. 84 Ma (according to Moxon and Graham, 1987); based on age of 50–70 m.y. for oceanic crust (Engebretson et al., 1985), water depth was ~5.5 km (Sclater et al., 1971); this water depth has emergent thickness of 27.5 km, which approximates thickness needed to metamorphose Yolla Bolly terrane (note that emergent thickness means thickness of material required to fill water depth to sea level). (B) "Olympic phase" (an analogy to present situation of Olympic subduction complex in Washington State; Brandon et al., 1998); this phase is thought to reflect main phase of exhumation; high-angle normal faults in westernmost Great Valley basin (Unruh et al., 2007) interpreted here to have accommodated part of flexural shear associated with differential uplift and exhumation; Franciscan subduction complex (FSC) detritus occurs in Great Valley basin and in Franciscan itself. (C) Modern situation; E-directed back-thrusting envisaged to be entirely post-Paleocene in age; progressive accretion of younger Franciscan terranes indicates that in-sequence deformation occurred at same time in more frontal parts of evolving wedge; because deformation in forearc basin continued into Tertiary, forearc basin grew, and thus its surface slope was being reduced, causing concentration of deformation at forearc basin-wedge interface. Note that cross sections are schematic. CRF—Coast Range fault; CRO—Coast Range ophiolite; LoGVG—lower Great Valley Group; PP—Pickett Peak terrane; YB—Yolla Bolly terrane.

the top of the Coast Range ophiolite moved downward by ~2–3 km relative to the Pickett Peak and Yolla Bolly terranes. This effect does not contribute significantly to reduce the vertical separation between the Coast Range ophiolite and the Pickett Peak and Yolla Bolly terranes. Wakabayashi and Unruh (1995) suggested that the western Great Valley homocline was tilted and erosionally beveled during the Albian. The basis for this argument is the record of a sub-Cenomanian unconformity on the east side of the Great Valley basin (Dumitru, 1988). Because this unconformity is only developed in the eastern Great Valley basin, we suggest that the sub-Cenomanian unconformity was local to that part of the basin.

Between 70 and 50 Ma (Fig. 25B), uplift and erosion of the forearc high became pronounced. A large-scale flexure or back-fold developed at the Franciscan subduction complex–Great Valley contact. We interpret the high-angle normal faults, which developed at least in parts of the Great Valley basin (Unruh et al., 2007), to have aided the accommodation of differential erosion-exhumation between the accretionary wedge and the forearc basin. It is conceivable that high-angle normal faults also formed in the Coast Range ophiolite, but evidence for that is lacking. Great Valley rocks contain Franciscan detritus, but most of the eroded sediment is inferred to have gone to the west. We estimate that ~200-km^3-per-km strike length of the margin was eroded. About 1%–3% of that would have been the Coast Range ophiolite and ~15% the Great Valley Group, and the rest would have been the Franciscan subduction complex, mostly high-level rocks. During uplift and erosion the rocks of the Pickett Peak and Yolla Bolly terranes are inferred to have moved upward by ~15 km. At this time the wedge may have taken on a steady-state form, with accretion balanced by erosion. The location of the "retrowedge" fault system is also shown, but no slip had yet occurred. It is argued that this stage of development of the Franciscan is similar to the evolution of the Olympic Mountains over the last 15 m.y.

The section for the situation between ca. 50 Ma and the present (Fig. 25C) is simplified from Wakabayashi and Unruh (1995) and shows the final configuration. One can see how the retrowedge fault system evolved by comparing Figures 25B and 25C. Note that this fault system is not shown to root into the main subduction boundary, as envisioned by Wakabayashi and Unruh (1995). Instead, we think it is more likely that this fault system was resolved by ductile flow within the interior of the wedge, similar to backthrust geometries in other orogenic belts.

The present juxtaposing of the Franciscan subduction complex and the Coast Range ophiolite is attributed to E-directed wedging. How does one account for the uplift of the Franciscan relative to the Great Valley–Coast Range ophiolite? By various estimates, it seems agreed that the Franciscan subduction complex was displaced upward by ~15 km relative to the rocks that underlie the Great Valley Group. Almost all of this uplift can be accounted for by the growth of the forearc high west of the Coast Range fault zone, and subsidence of the Great Valley basement (i.e., the flexural-shear hypothesis). During the earliest Cretaceous the surface of the Great Valley basin lay at a water depth between 2 and 6 km. According to Ingersoll (1979, his Fig. 8), the area that would become the forearc high originated in even deeper water than that of the Great Valley basin. Because the Great Valley evolved into a bounded basin, one can conclude that the surface of the forearc high must have risen above the surface of the Great Valley basin. Thus, the thickness of the sedimentary fill in the Great Valley basin represents a minimum estimate of the differential uplift of the top of the forearc high relative to the top of the Coast Range ophiolite. At 90 Ma, the base of the Great Valley strata was ~9 km, as decompacted by Dickinson et al. (1982, his Figs. 1–5). At 65 Ma, it was ~12 km. These relationships show that the differential rise of the Franciscan subduction complex relative to the Great Valley can be accounted for solely by relative uplift of the forearc high and relative subsidence of the forearc basin. This estimate is a minimum, because the relief of the forearc high above the Great Valley basin and any erosion of the forearc high would have added to the differential uplift.

At this point, one can account for how the Eastern Belt rose to the same depth level as the Coast Range ophiolite. Note that there is no need to call for any exhumation or erosion, because the relative uplift is accommodated by the development of submarine topography and basin subsidence. It still has to be explained how the Coast Range ophiolite and the Eastern Belt became juxtaposed. Unruh et al. (1995) argued that E-directed thrusting started in the middle Cretaceous or even earlier, but this is based on the interpretation of deep reflections that are assumed to be from deeply buried and imbricated strata within the lower part of the Great Valley Group. Given that hardly any direct information about the deep reflections exist, a range of other interpretations remain open. At this time it seems safe to conclude that the deep reflections were truncated by an erosional unconformity sometime during the Late Cretaceous and that the floor fault for the Great Valley triangle zone lies along the unconformity. The Great Valley wedge itself was apparently initiated sometime during the Campanian to Eocene (i.e., Eocene unconformity).

Willett et al. (1993) showed that backthrusting within an accretionary wedge is controlled by the development of a forearc high that divides the high into a prowedge and a retrowedge. The reversal of vergence is controlled by the change in surface slope across the high. The intersection of the main subduction zone fault and the subsidiary shear zone that floors the retrowedge should underlie the crest of the forearc high. We attribute the initiation of the retrowedge to the growth of the forearc high. Thus, differential uplift would have preceded, at least in part, E-directed wedging. At this point the roof thrust of the wedge would have caused out-of-sequence imbrication of the Great Valley Group, the Coast Range ophiolite, and the Franciscan subduction complex. The differential uplift creates the situation where contractional thrust faulting can now thin the tilted “overburden section.”

CONCLUSIONS

This paper summarizes absolute finite-strain data from the Franciscan subduction complex and brittle strain data from important faults in and above this complex. The Franciscan is generally considered a prototypical sediment-rich subduction complex, and therefore our results may have broad implications for other subduction-zone settings as well. We have shown that ductile deformation within the complex was accommodated primarily by the SMT deformation mechanism. Our major conclusions are as follows:

1. The strain data indicate that convergence was accommodated by large-scale mass loss during SMT deformation within the subduction wedge.
2. The Franciscan high-pressure rocks show no extensional strains at the regional scale. On the basis of our deformation measurements and simple modeling, we conclude that exhumation of the metamorphic interior of the accretionary wedge was accomplished primarily by erosion of a subaerial forearc high.
3. Average strain rates and strain magnitudes for SMT deformation are surprisingly low for the high-pressure rocks of the Eastern and Central Franciscan belts. Ductile strain within the wedge can account for only a small percentage of the total orogenic convergence at the Franciscan margin. We infer that most of the convergence was probably accommodated by slip at the base of the subduction wedge.
4. Current wedge models, which do not take volume strains into account, do not appear to be strictly applicable to subduction wedges that have undergone SMT deformation, or that were dominated by the SMT deformation mechanisms.
5. Results from other accretionary wedges indicate that our results from the Franciscan subduction complex appear to be representative for accretionary belts in general.
6. The Coast Range fault zone resulted from horizontal crustal shortening, has a top-W sense of shear, and caused the Great Valley Group and the Coast Range ophiolite to override the Eastern Franciscan Belt. Top-W thrusting can account for the profound break in metamorphic grade at the Coast Range fault zone as long as the original metamorphic isograds had a steeper eastward dip than that of the Coast Range fault zone.
7. Intra–Franciscan subduction complex faults have similar kinematics as the Coast Range fault zone and appear to have resulted from the same shortening event.
8. Thrusting at the Coast Range fault zone and at the intra–Franciscan subduction complex faults would have caused further structural burial of the Eastern Franciscan Belt. Thus, we propose that mechanical erosion is responsible for the exhumation of the Eastern Franciscan.
9. Because the Great Valley Group shows little evidence of erosional exhumation of the Franciscan subduction complex, we conclude that most of the erosion occurred on the seaward slope of an emergent forearc high, with sediment transported to the coast and down submarine canyons to depositional sites on the lower slope and in front of the Franciscan. This denudation pattern led to large-scale material redistribution within the Franciscan complex, resulting in selective uplift of the Franciscan rocks and the development of a pronounced exhumation gradient, which is now exposed on the eastern flank of the modern Coast Ranges.

ACKNOWLEDGMENTS

This research was supported by the Deutsche Forschungsgemeinschaft (grant Ri538/8), a Feodor-Lynen fellowship by the German Alexander von Humboldt-Stiftung, and U.S. National Science Foundation grant EAR9005777. We appreciate discussions and support by Jeff Unruh, John Wakabayashi, Bill Dickinson, Ken Aalto, and Bob McLaughlin, and formal reviews by Bill Dickinson, Howard Day, John Wakabayashi, Gary Ernst, and Tekla Harms.

APPENDIX

Maps

The maps in Figures A1–A10 show localities for sampling for strain analyses, and also sites from which samples have been analyzed for brittle strain.

Brittle Strain Analysis

The raw fault-kinematic data for each particular outcrop are presented in stereograms in which each measured fault is indicated by a great circle and an arrow, representing the fault attitude and slip vector, respectively. The actual direction of slip corresponds to the intersection of the arrow and the great circle. The sense of slip is indicated by the direction of the arrow relative to the great circle and the center of the stereogram, assuming a footwall-fixed convention. For example, an arrow parallel to the downdip direction of the fault surface and directed outward from the great circle would indicate a normal fault (assuming a footwall-fixed convention). If the arrows were reoriented to point inward to the center of the net, the fault would be a reverse fault. Strike slip would show as an arrow parallel to the strike direction of the fault.

Coast Range Fault Zone

Yolla Bolly Mountains. At Beehive Flat (Fig. A1), most of the studied faults dip to the west and have a normal sense of slip, with the shortening axes subvertical when viewed in present coordinates (Fig. A11). Only 9 out of 108 faults (8% of all measured faults) have a reverse sense of slip. Fourteen faults can be classified as strike-slip faults (13% of all measured faults), 10 of which show sinistral slip and strike generally to the east, and 4 show dextral strike-slip and strike generally to the northwest.

At Salt Creek the density of faults is less, but there is still a preponderance of normal faults in present coordinates (Fig. A12). Overall, the percentage of strike-slip faults at Salt Creek (24% of all measured faults) is higher than at Beehive Flat.

Diablo Range. The Diablo Range data set contains a smaller number of faults than the Yolla Bolly data set. Nonetheless, the faults in the Diablo Range show the same general characteristics. Most of the faults we have studied are from the Del Puerto Canyon area (Fig. A2), in which the Del Puerto ophiolite is exposed (part of the Coast Range ophiolite). The studied faults dip to the west and have a normal sense of slip in present coordinates (Fig. A13). In Del Puerto Canyon there is a distinct strike-slip overprint of the first-phase dip-slip structures (Fig. A14). Farther north at Mount Diablo (Fig. 2), only 12 faults were measured at the Coast Range fault zone (Fig. A15), but they are similar to the fault distribution at Del Puerto Canyon.

Intra-Franciscan Faults

Northern California. Data were collected from a number of outcrops to the northeast of Eureka (Fig. A3). At Titlow Hill, faults prefer-

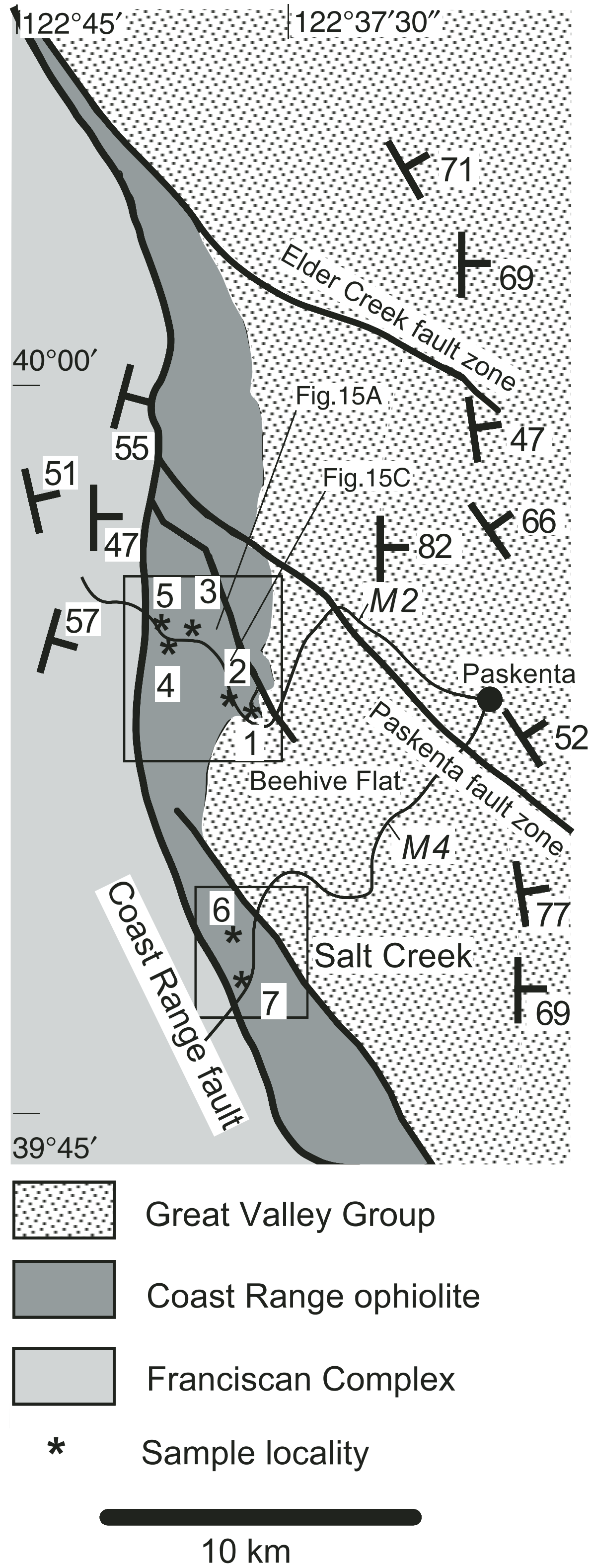

Figure A1. Geologic map of Paskenta area (for location refer to Fig. A3). Coast Range fault zone corresponds to heavy line; kinematic data come from Beehive Flat and Salt Creek; also indicated are locations of micrographs in Figure 15 and U.S. Forest Service roads M2 and M4, along which kinematic data were collected.

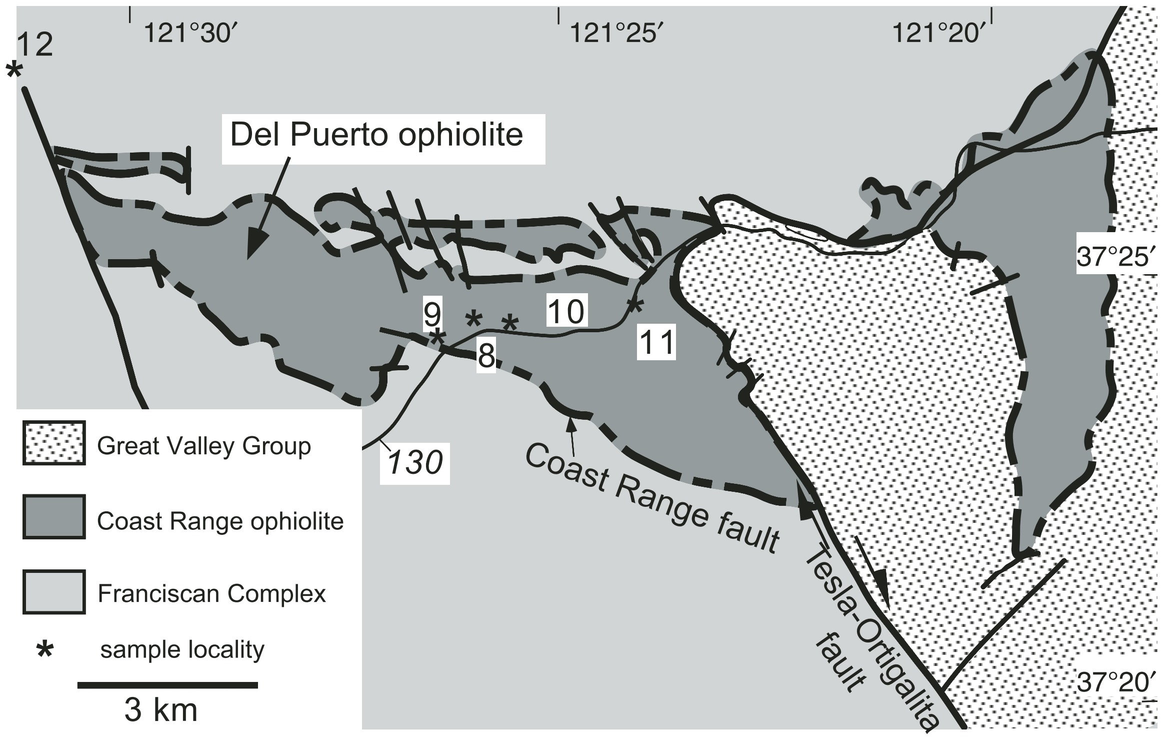

Figure A2. Geologic map of Del Puerto Canyon area (for location, refer to Fig. A8); kinematic data were collected along California State Route 130; note that Tesla-Ortigalita fault and associated minor faults cut across Coast Range fault zone (heavy dashed line); seismicity on Tesla-Ortigalita fault indicates that it is active.

entially strike N-S and record reverse kinematics (73 out of 103 faults); 20 faults are strike-slip faults, and 10 are normal faults (Fig. A16). The shortening directions for the nine studied outcrops scatter around the E-W direction. The NE-striking strike-slip faults appear to have dextral kinematics, and the NW-striking ones sinistral kinematics.

In Hoopa Valley the faults have similar kinematics: 86 out of 101 measured faults have reverse offsets; furthermore, 7 normal and 8 strike-slip faults occur (Fig. A17). The shortening directions are more varied than at Titlow Hill and in general trend about NE-SW. The kinematics of the latter are similar to those at Titlow Hill.

In the northernmost outcrops (Bald Hill Road, Klamath River, and Humboldt Lagoons) again show a similar pattern with a strong predominance of reverse faults (54 out of 62 faults). The kinematics of the seven strike-slip faults is different than in the previous outcrops, and the NE-striking faults have sinistral kinematics. Shortening directions for the seven outcrops again scatter around the E-W direction (Fig. A18).

Coastal Belt thrust. Data have been collected in a number of road cuts between Cloverdale and Garberville (Fig. A3). Most of the 112 faults shown in Figure A19 dip to the northwest and have reverse-slip kinematics. Most of the strike-slip faults strike E-W and have dextral kinematics; two sinistral strike slip faults strike NE. A few normal faults have been mapped, especially in outcrop CBT0.

Faults related to the San Andreas fault system. One outcrop near Cazadero close to the San Andreas fault is dominated by a NW-dipping fault with sinistral kinematics (Fig. A20A), whereas the second outcrop has N-striking faults with dextral oblique kinematics (Fig. A20B). In Potter Valley the fault population is mixed; S- to E-dipping normal faults occur together with E-dipping sinistral oblique faults, steeply NE-dipping sinistral strike-slip faults, and two S-dipping reverse faults (Fig. A20C). Outcrop CBT1 at the Coastal belt thrust, in which thrust-related faults are overprinted by strike-slip faults, shows a remarkably straightforward fault pattern with NNE-striking sinistral faults, ENE-striking sinistral oblique-slip faults, and NW-striking reverse faults (Fig. A20D).

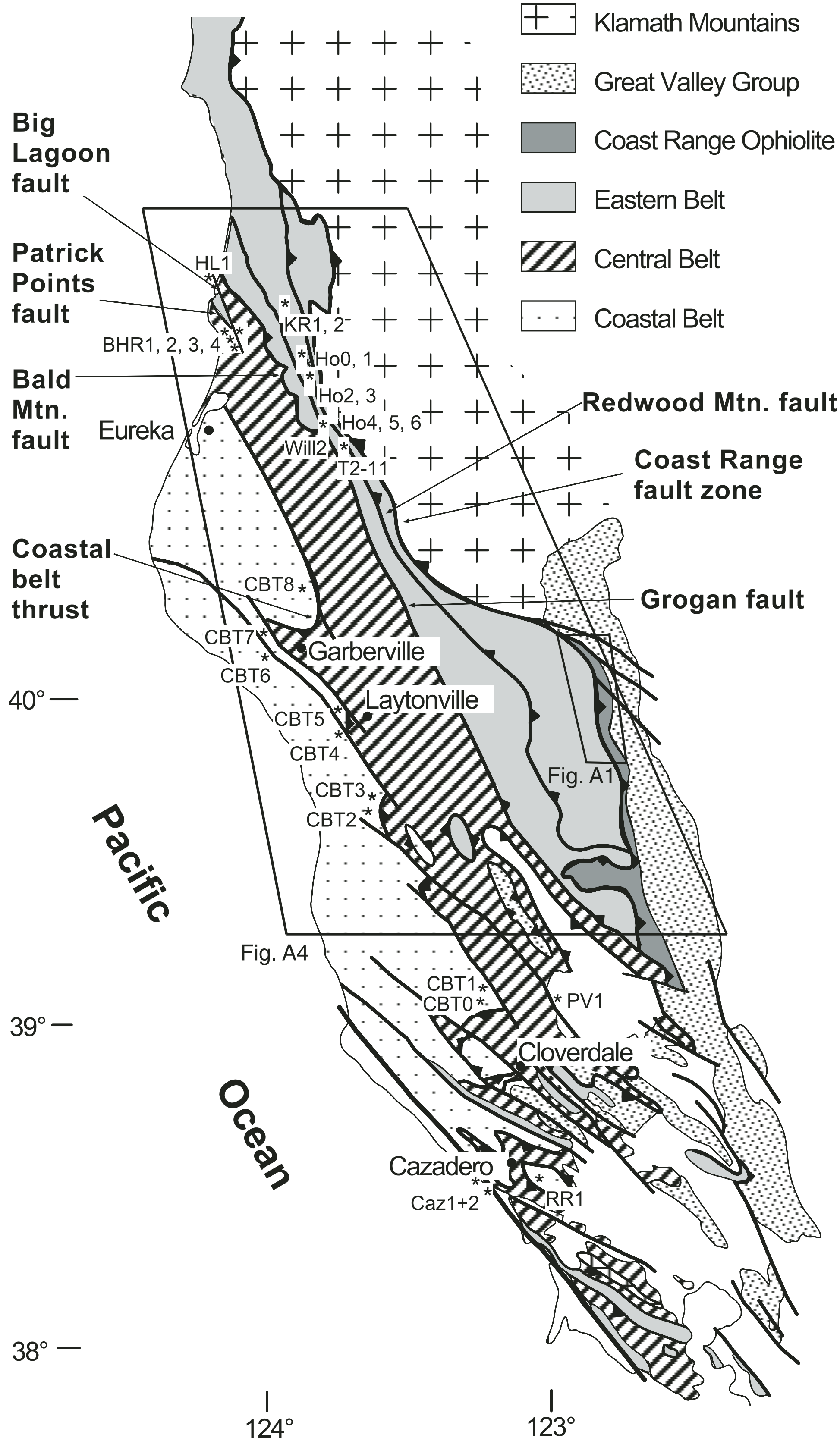

Figure A3. Geologic map of northern California (north of Golden Gate Bridge) with localities of outcrops (stars) where kinematic data were collected (locations of Figs. A1 and A4 are indicated).

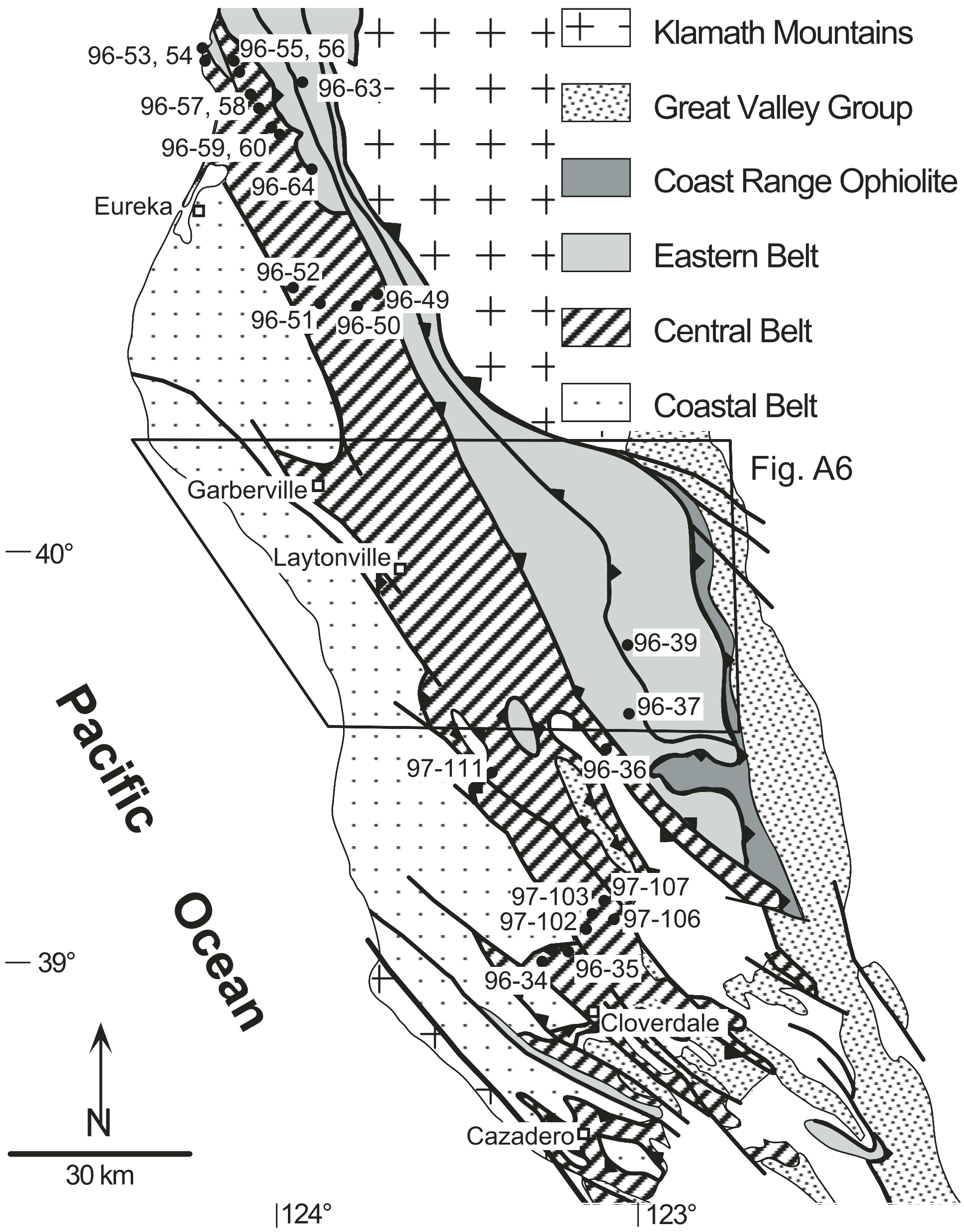

Figure A4. Geologic map of northern California (north of Golden Gate Bridge), with localities of samples for finite-strain analysis (location of Fig. A6 is indicated).

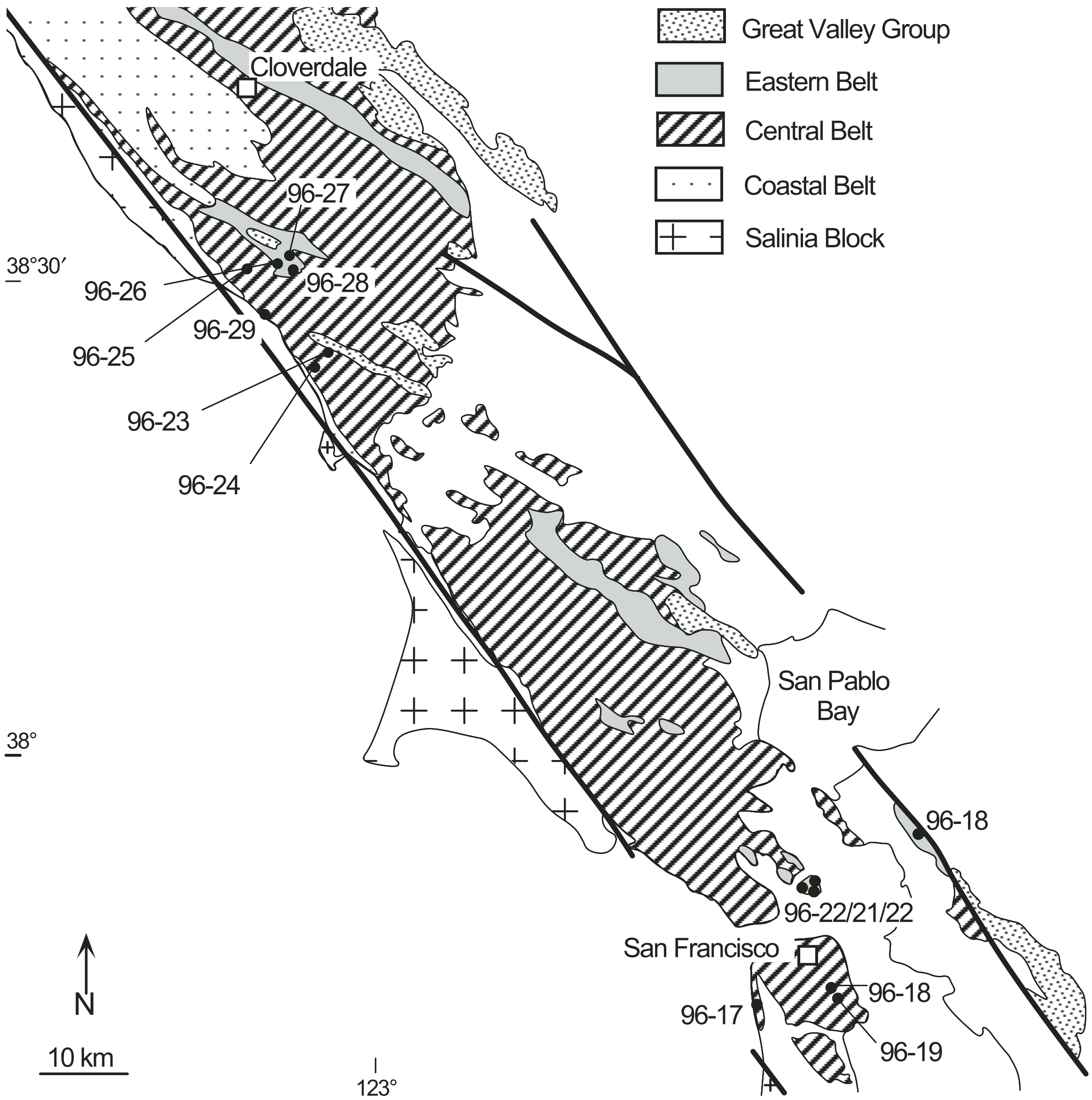

Figure A5. Geologic map of San Francisco–Cazadero area, with sample localities for finite-strain analysis.

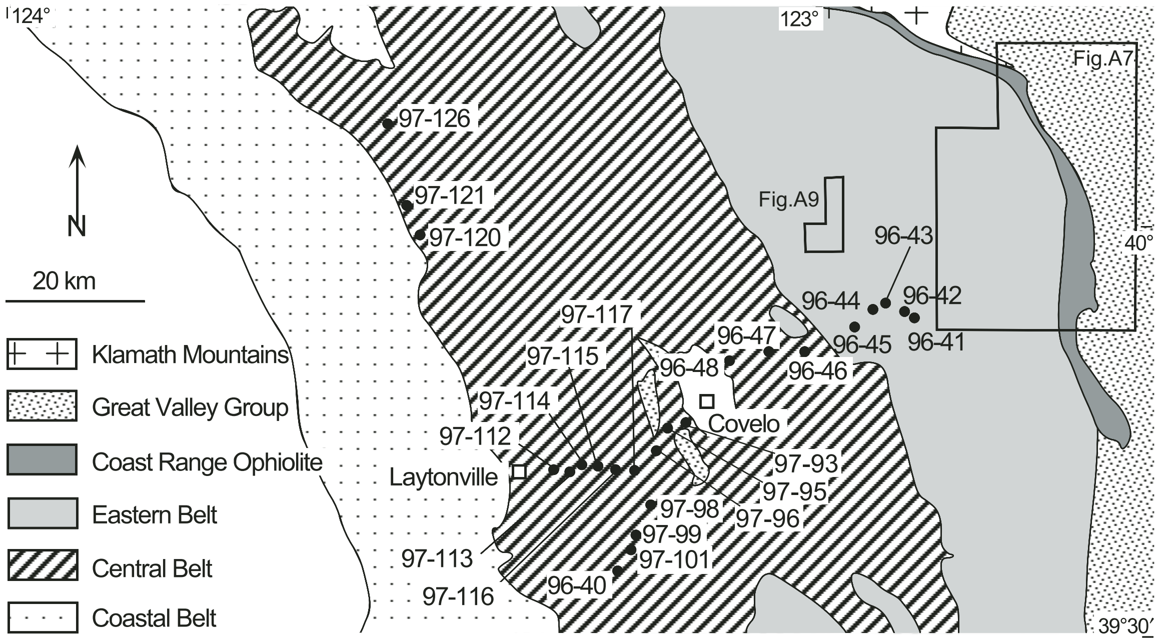

Figure A6. Geologic map of northern California between Laytonville and Paskenta, with localities of samples for finite-strain analysis between Laytonville and Mendocino Pass (locations of Figs. A7 and A9 are indicated).

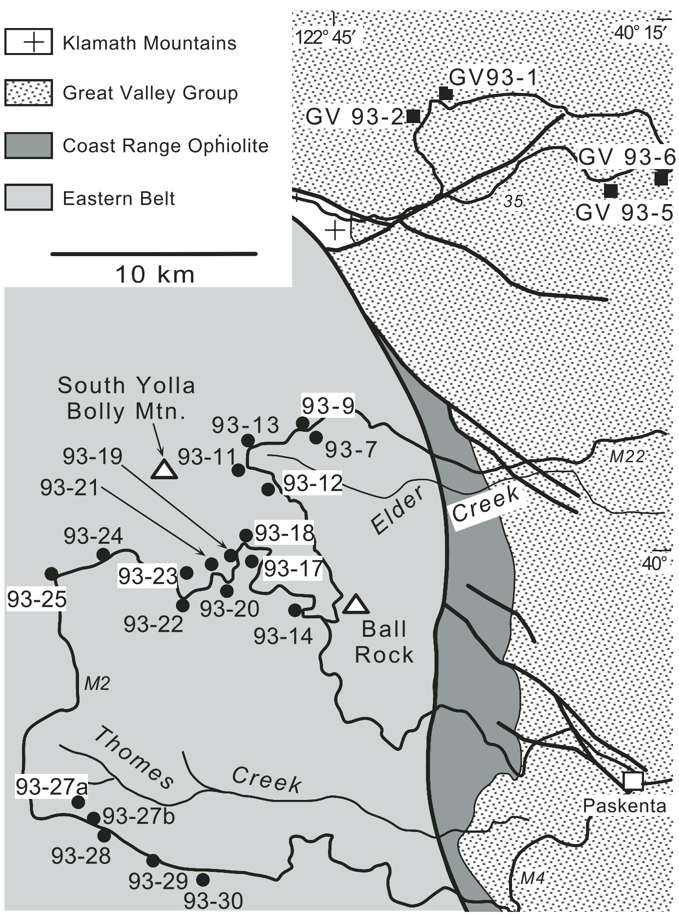

Figure A7. Geologic map of Yolla Bolly Mountains, showing localities of samples used for finite-strain analyses and major roads (M22 and M4) along which samples were collected.

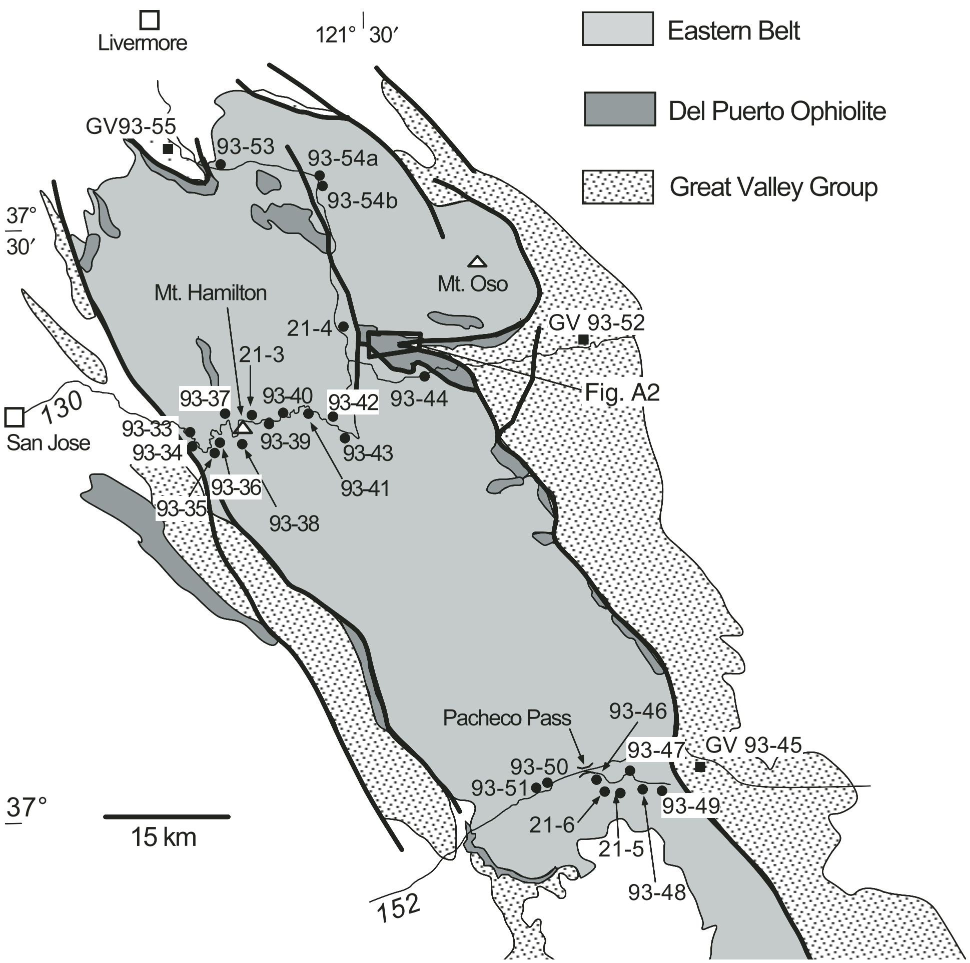

Figure A8. Geologic map of Diablo Range, with localities of samples used for finite-strain analyses and major roads along which samples have been collected (California Highways 130 and 152) are shown.

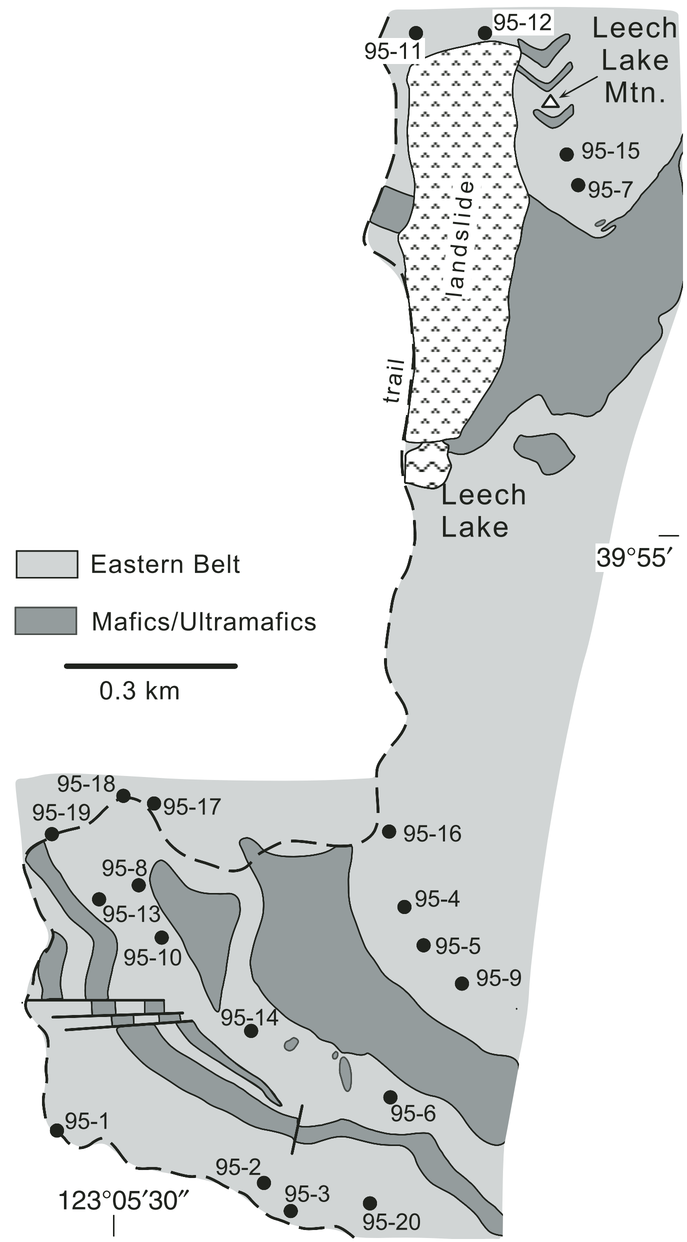

Figure A9. Geologic map of Leech Lake Mountain, showing sample localities for finite-strain analysis.

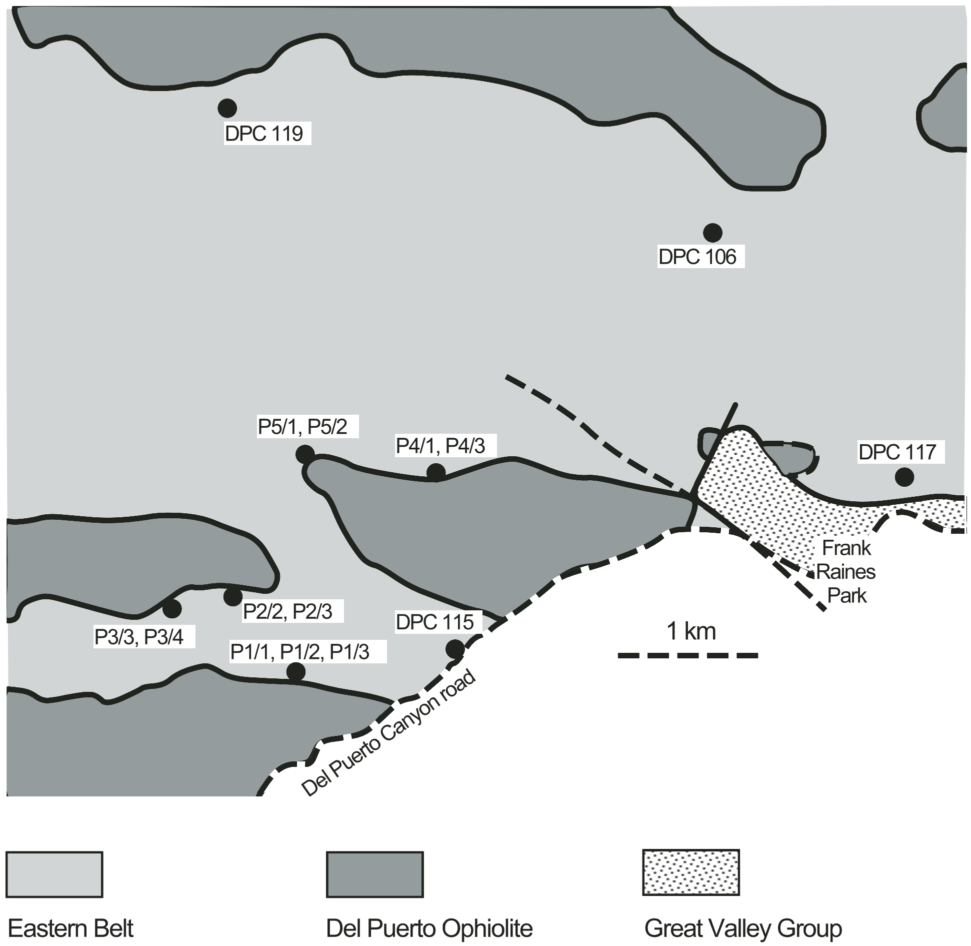

Figure A10. Geologic map of Del Puerto Canyon, with locations of sampling profiles (P prefix) in uppermost 10 m of Franciscan subduction complex, and other samples (DPC prefix).

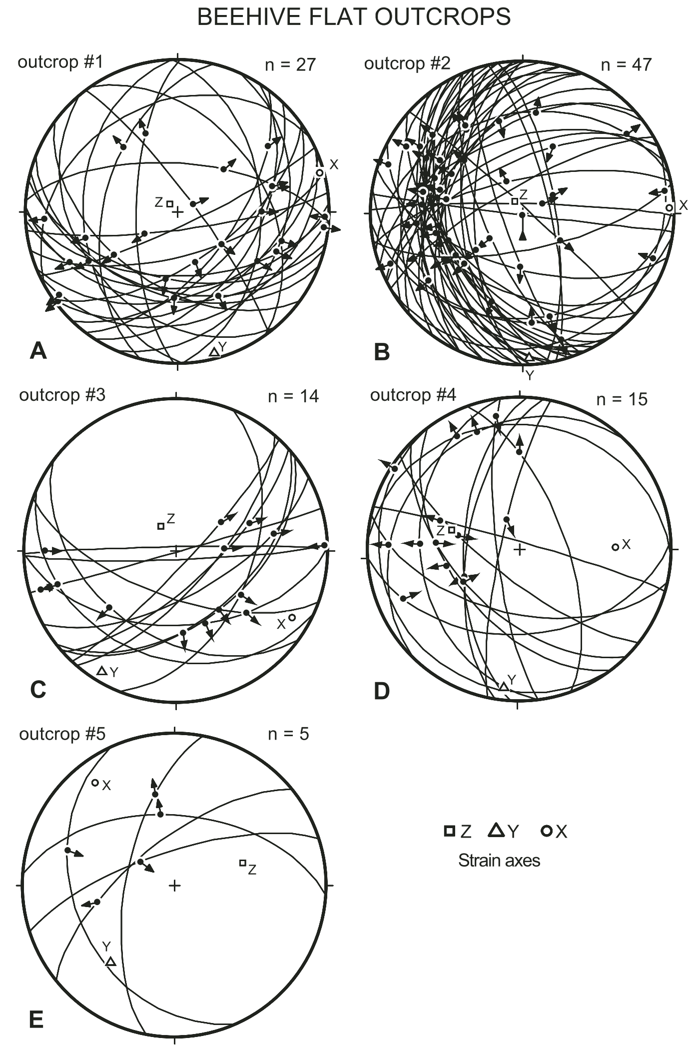

Figure A11. Stereograms showing fault data for present coordinates for five large outcrops at Beehive Flat in Yolla Bolly Mountains (see Fig. A1 for locations); each fault is illustrated by great circle marking attitude of fault and arrow indicating sense of slip. Average orientation of principal axes of brittle strain are indicated by Z—shortening; Y—intermediate; X—extension. Types of faults present at each outcrop are (A) 24 normal faults, 2 dextral faults, and 1 sinistral fault; (B) mainly W-dipping normal faults, but also 4 reverse faults, 1 dextral fault, and 1 sinistral fault; (C) 10 normal faults and 4 sinistral faults; (D) 7 normal faults, 4 reverse faults, and 4 sinistral faults; and (E) 3 normal faults and 2 reverse faults.

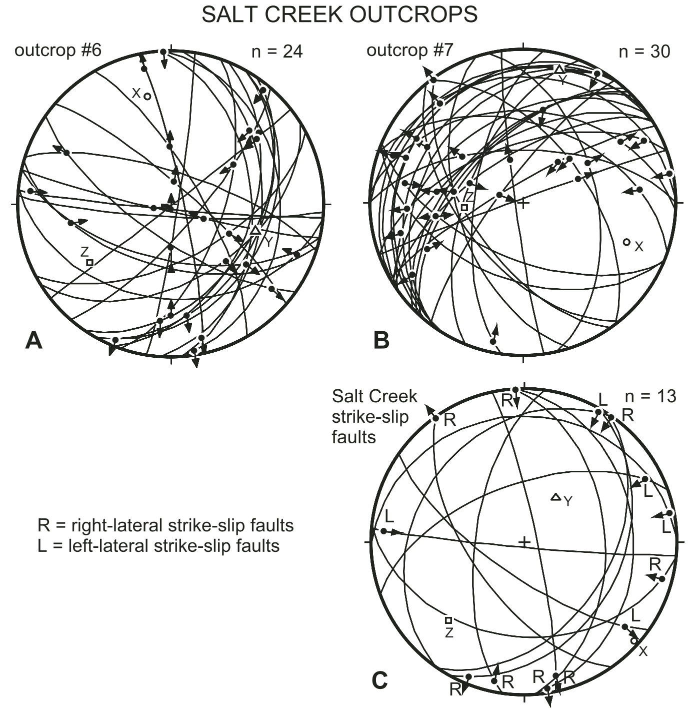

Figure A12. Stereograms showing fault data for present coordinates for two large outcrops in Salt Creek area of Yolla Bolly Mountains (see Fig. A1 for locations and Fig. A11 for explanation of symbols). Types of faults present at each outcrop are (A) mainly E-dipping normal faults, but also 5 dextral and 4 sinistral faults; (B) mainly NW-dipping normal faults, but also 9 NW-dipping reverse faults, 3 sinistral faults, and 1 dextral fault. All strike-slip faults at Salt Creek are shown together in (C) to highlight conjugate pattern of NNW-striking dextral faults and E-striking sinistral faults; note that this conjugate set is centered at high angle to average shortening direction.

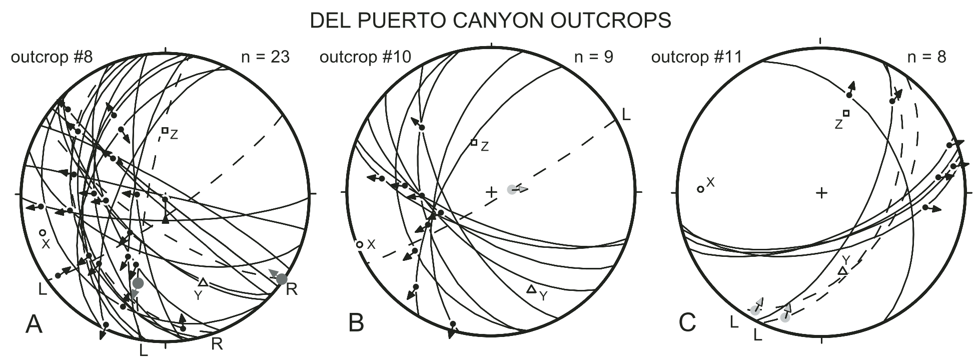

Figure A13. Stereograms showing fault data for present coordinates for three large outcrops from Del Puerto Canyon area (see Fig. A2 for locations and Fig. A11 for explanation of symbols); distinction made between older set of faults (solid great circles with black dots and arrows) and younger set of crosscutting strike-slip faults (dashed great circles with gray dots and arrows; L stands for left-lateral, and R for right-lateral offset). Types of faults at each outcrop are (A) mainly W-dipping normal faults, with 2 reverse faults, 2 sinistral faults, and 2 dextral faults; (B) W-dipping normal faults overprinted by 1 sinistral fault; and (C) oblique-slip normal faults and oblique-slip reverse faults, for which both sets have significant sinistral component of motion.

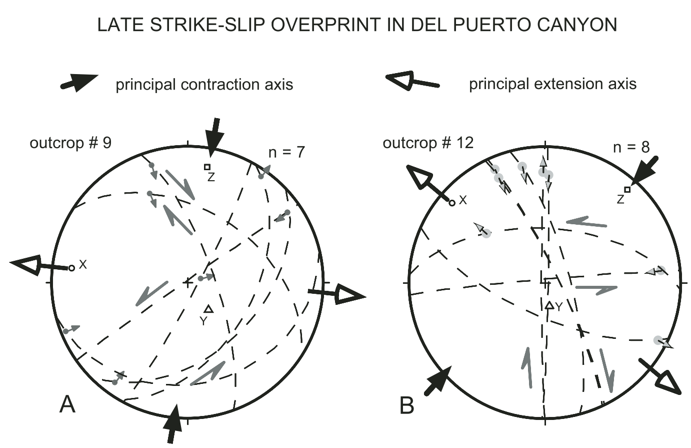

Figure A14. Stereograms showing fault data for present coordinates for young strike-slip faults in Del Puerto area (see Fig. A2 for locations and Fig. A11 for explanation of symbols); faults show conjugate geometry centered at high angle around shortening direction; these faults are attributed to strike-slip deformation associated with San Andreas fault system.

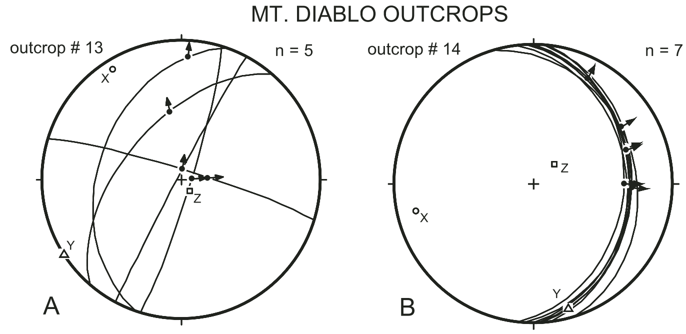

Figure A15. Stereograms showing fault data for present coordinates for two outcrops at Mount Diablo (see Fig. A11 for explanation of symbols); pattern of faulting at this location is similar to that in Del Puerto Canyon area.

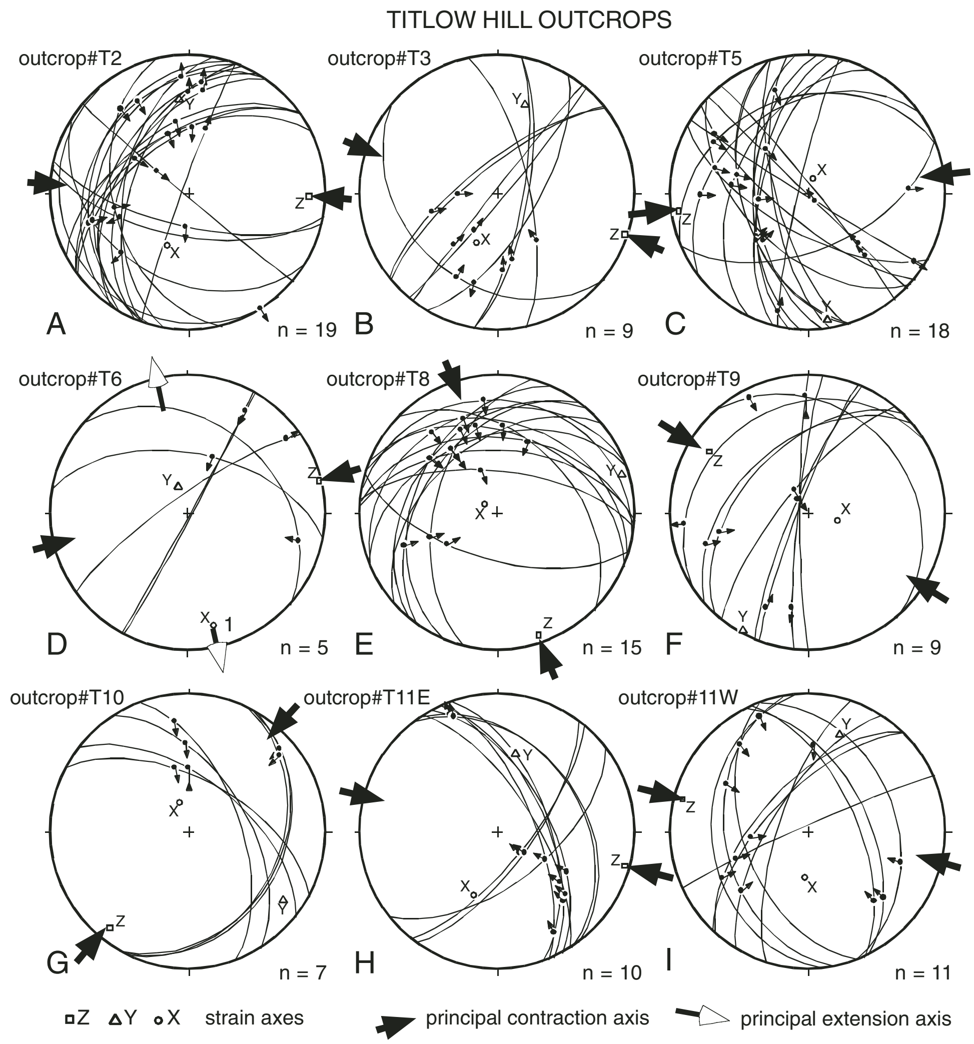

Figure A16. Stereograms showing fault data for present coordinates from nine outcrops at Titlow Hill south of Willow Creek east of Eureka (see Fig. A3 for locations); all data were from ~1 km^2 of severely imbricated portion of South Fork Mountain Schist directly above moderately E-dipping Redwood Mountain fault. Each fault is illustrated by great circle marking attitude of fault, and arrow indicating sense of slip; average orientation of principal shortening axes shown by solid arrows; arrows with hollow arrowheads indicate fault population with subhorizontal extension direction; deduced shortening axes for all outcrops scatter around E-W direction; note dextral NE-striking strike-slip faults, which dominate outcrop T6 (D).

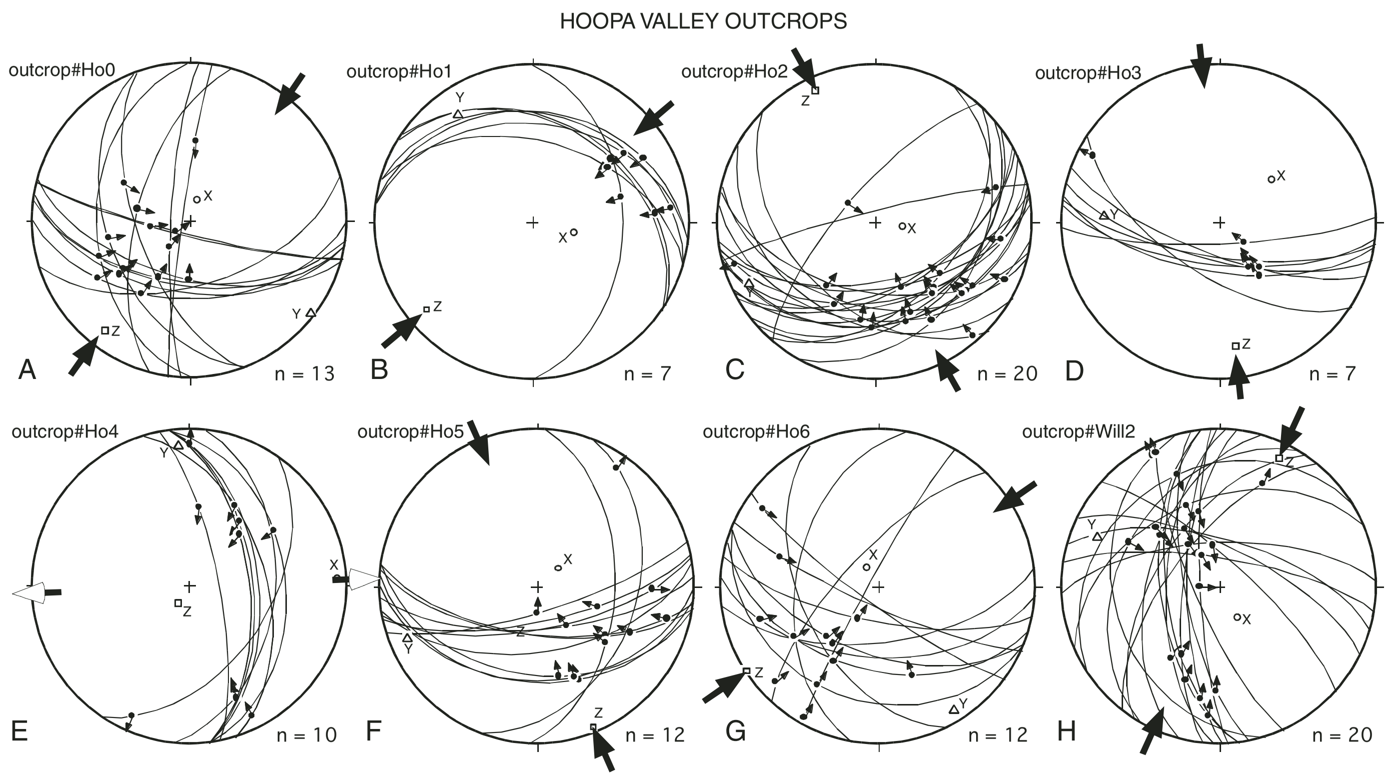

Figure A17. Stereograms showing fault data for 7 outcrops in Hoopa Valley and 1 outcrop in Willows Creek ~10–20 km along strike to north of Titlow Hill (see Fig. A3 for locations); all data were from imbricated sequence of Eastern Belt rocks between moderately E-dipping Redwood Mountain fault and Coast Range fault zone; each fault is illustrated by great circle marking attitude of fault, and arrow indicating sense of slip; average orientation of principal shortening axes shown by solid arrows; shortening axes in studied outcrops show larger scatter than at Titlow Hill but in general still cluster around E-W direction.

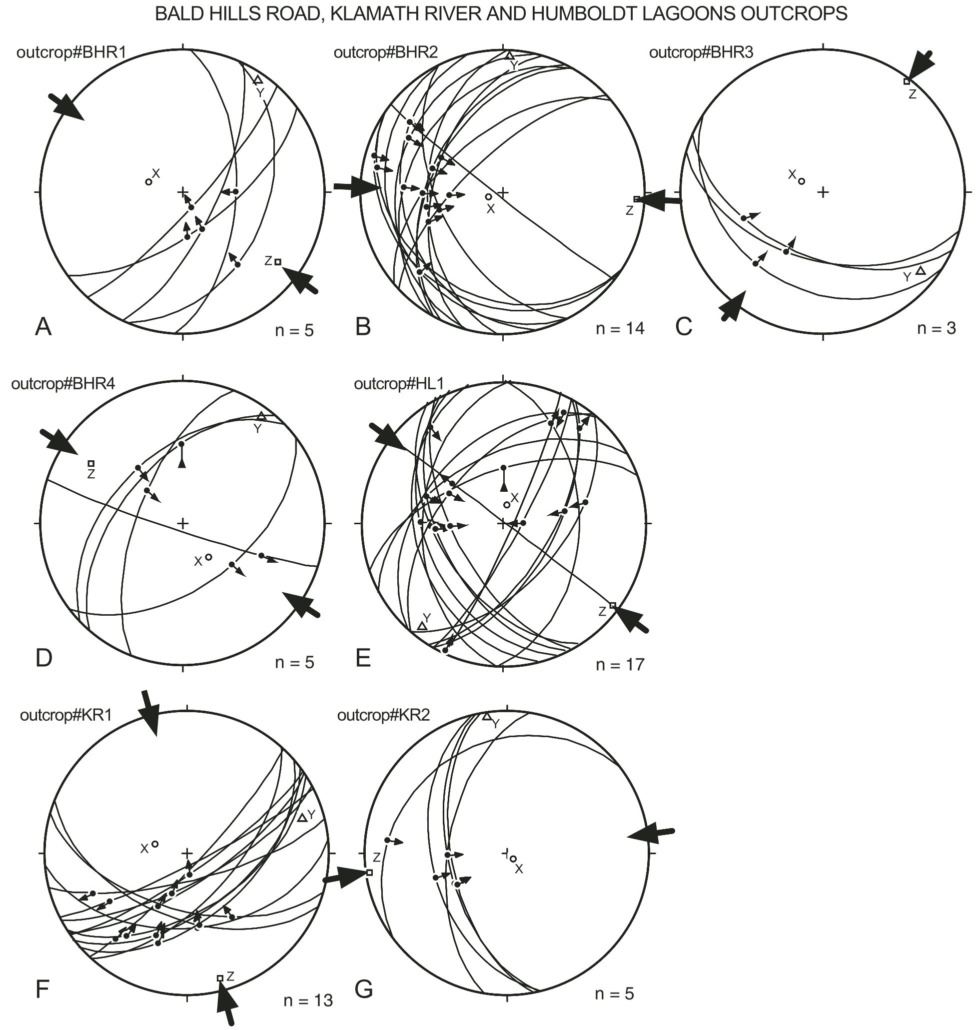

Figure A18. Stereograms showing fault data for 4 outcrops at Bald Hills Road, 1 outcrop at Humboldt Lagoons below Bald Mountain fault, and 2 outcrops in Klamath River Valley near Redwood Mountain fault (see Fig. A3 for locations); all data were from imbricated sequence of Eastern and Central Belt rocks between E-dipping Bald Mountain, Grogan, and Redwood Mountain faults; each fault illustrated by great circle, marking attitude of fault and an arrow indicating sense of slip; average orientation of principal shortening axes shown by solid arrows; shortening axes in studied outcrops again scatter around E-W direction.

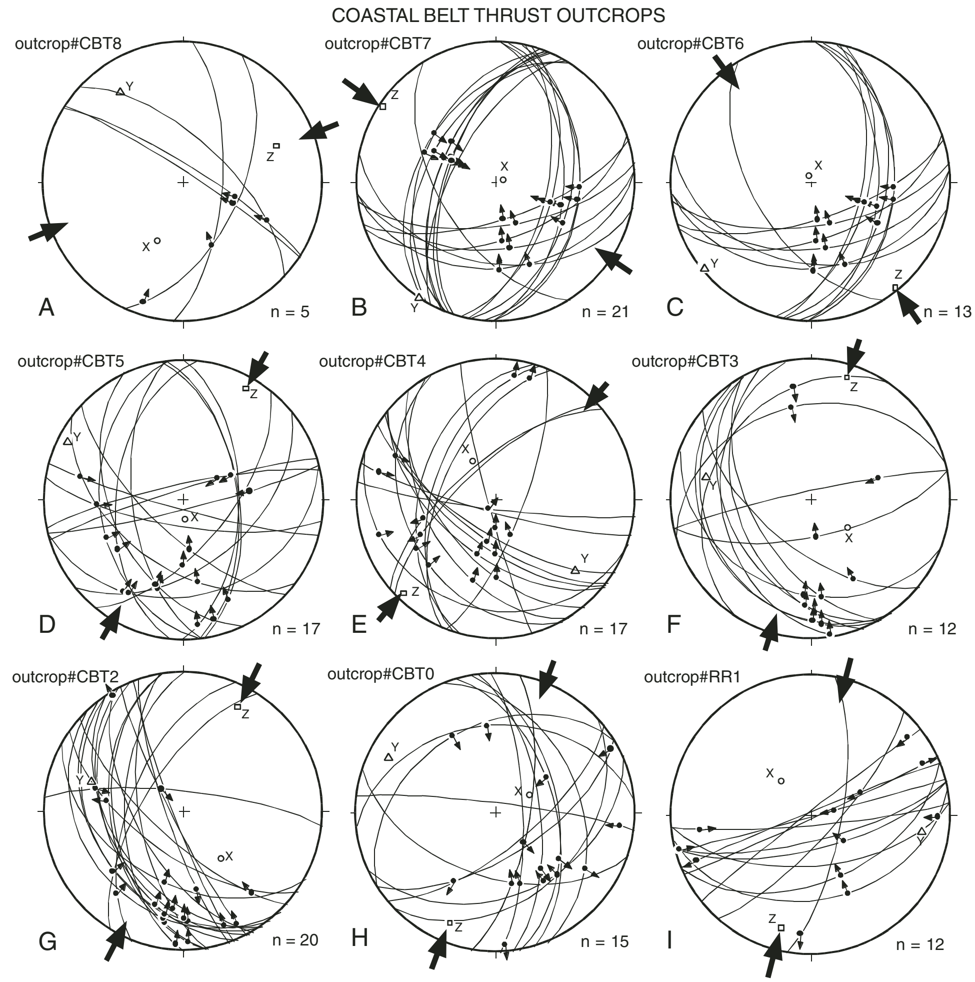

Figure A19. Stereograms showing fault data for 7 outcrops along Coastal Belt thrust between Cloverdale and Garberville and 1 outcrop in Russian River Valley (see Fig. A3 for locations); all data were from imbricated sequence in vicinity of Coastal Belt thrust; each fault illustrated by great circle, marking attitude of fault, and arrow indicating sense of slip; average orientation of principal shortening axes shown by solid arrows; shortening axes show some scatter but on average cluster around NE-SW direction.

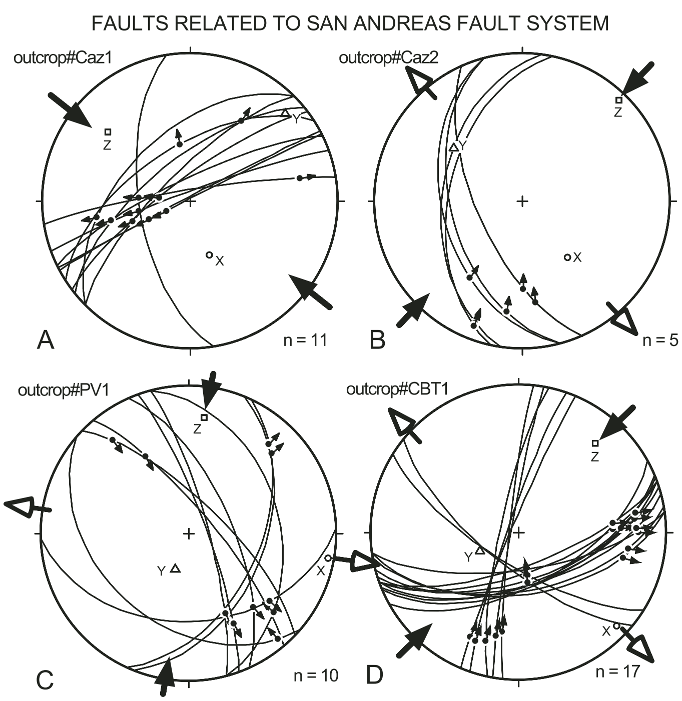

Figure A20. Stereograms showing fault data for 2 outcrops near Cazadero, 1 outcrop in Potter Valley, and 1 outcrop at Coastal Belt thrust north of Cloverdale (see Fig. A3 for locations); each fault illustrated by great circle, marking attitude of fault, and arrow indicating sense of slip; average orientation of principal shortening axes shown by solid arrows, and average orientation of principal extension axes by hollow arrowheads.

REFERENCES CITED

Almgren, A.A., 1984, Timing of Tertiary submarine canyons and marine cycles of deposition in the southern Sacramento Valley, *in* Almgren, A., and Hacker, P.D., eds., Paleogene Submarine Canyons of the Sacramento Valley, California: American Association of Petroleum Geologists, Pacific Section, Los Angeles, p. 1–16.

Alvarez, W., Kent, D.V., Silva, I.P., Schweickert, R.A., and Larson, R.A., 1980, Franciscan Complex limestone deposited at 17° South paleolatitude: Geological Society of America Bulletin, v. 91, p. 476–484, doi: 10.1130/0016-7606(1980)91<476:FCLDAS>2.0.CO;2.

Anczkiewicz, R., Platt, J.P., Thirlwall, M.F., and Wakabayashi, J., 2004, Franciscan subduction off to a slow start: Evidence from high-precision Lu-Hf garnet ages on high-grade blocks: Earth and Planetary Science Letters, v. 225, p. 147–161, doi: 10.1016/j.epsl.2004.06.003.

Anderson, L.W., Anders, M.A., and Ostenaa, D.A., 1982, Late Quaternary faulting and seismic hazard potential, eastern Diablo Range, California, *in* Hart, E.W., et al., eds., Proceedings, Conference on Earthquake Hazards in the Eastern San Francisco Bay Area: California Division of Mines and Geology Special Publications, v. 62, p. 197–206.

Argus, D.F., and Gordon, R.G., 2001, Present tectonic motion across the Coast Ranges and San Andreas fault system in central California: Geological Society of America Bulletin, v. 113, p. 1580–1592, doi: 10.1130/0016-7606(2001)113<1580:PTMATC>2.0.CO;2.

Armstrong, R.L., 1972, Low-angle (denudation) faults, hinterland of the Sevier Orogenic Belt, eastern Nevada and western Utah: Geological Society of America Bulletin, v. 83, p. 1729–1754, doi: 10.1130/0016-7606(1972)83[1729:LDFHOT]2.0.CO;2.

Atwater, T., 1970, Implications of plate tectonics for the Cenozoic tectonic evolution of western North America: Geological Society of America Bulletin, v. 81, p. 3513–3536, doi: 10.1130/0016-7606(1970)81[3513:IOPTFT]2.0.CO;2.

Bailey, E.H., Irwin, W.P., and Jones, D.L., 1964, Franciscan and Related Rocks, and Their Significance in the Geology of Western California: California Division of Mines and Geology Bulletin, v. 183, 177 p.

Bailey, E.H., Blake, M.C., Jr., and Jones, D.L., 1970, On-land Mesozoic oceanic crust in California Coast Ranges, *in* Geological Survey Research, 1970: U.S. Geological Survey Professional Paper 770-C, p. C70–C81.

Bauder, J.M., and Liou, J.G., 1979, Tectonic outlier of Great Valley Group in Franciscan terrane, Diablo Range, California: Geological Society of America Bulletin, v. 90, p. 561–568, doi: 10.1130/0016-7606(1979)90<561:TOOGVS>2.0.CO;2.

Berkland, J.O., Raymond, L.A., Kramer, J.C., Moores, E.M., and O'Day, M., 1972, What is Franciscan?: American Association of Petroleum Geologists Bulletin, v. 56, p. 2295–2302.

Berthé, D., Choukroune, P., and Jeguzo, P., 1979, Orthogneiss, mylonite and non-coaxial deformation of granites: Journal of Structural Geology, v. 1, p. 31–42, doi: 10.1016/0191-8141(79)90019-1.

Blake, M.C., Jr., 1965, Structure and petrology of low grade metamorphic rocks, blueschist facies: Yolla Bolly area, northern California [Ph.D. thesis]: Stanford, California, Stanford University, 91 p.

Blake, M.C., Jr., ed., 1984, Franciscan geology of northern California: Society of Economic Paleontologists and Mineralogists, Pacific Section, 254 p.

Blake, M.C., Jr., and Jones, D.L., 1981, The Franciscan assemblage and related rocks in northern California: A reinterpretation, *in* Ernst, W.G., ed., The Geotectonic Development of California: Rubey Volume I: Englewood Cliffs, New Jersey, Prentice Hall, p. 306–328.

Blake, M.C., Jr., Engebretson, D.C., Jayko, A.S., and Jones, D.L., 1985, Tectonostratigraphic terranes in southwest Oregon, *in* Howell, D.G., ed., Tectonostratigraphic Domains of the Circum-Pacific Region: Houston, Circum-Pacific Council for Energy and Mineral Resources, p. 147–157.

Blake, M.C., Jr., Jayko, A.S., McLaughlin, R.J., and Underwood, M.B., 1988, Metamorphic and tectonic evolution of the Franciscan Complex, northern California, *in* Ernst, W.G., ed., Metamorphism and Crustal Evolution of the Western United States: Englewood Cliffs, New Jersey, Prentice Hall, p. 1036–1059.

Bolhar, R., and Ring, U., 2001, Deformation history of the Yolla Bolly terrane at Leech Lake Mountain, Eastern Belt, Franciscan Subduction Complex, Californian Coast Ranges: Geological Society of America Bulletin, v. 113, p. 181–195, doi: 10.1130/0016-7606(2001)113<0181:DHOTYB>2.0.CO;2.

Brandon, M.T., 1995, Analysis of geologic strain data in strain-magnitude space: Journal of Structural Geology, v. 17, p. 1375–1385, doi: 10.1016/0191-8141(95)00032-9.

Brandon, M.T., and Calderwood, A.R., 1990, High-pressure metamorphism and uplift of the Olympic subduction complex: Geology, v. 18, p. 1252–1255, doi: 10.1130/0091-7613(1990)018<1252:HPMAUO>2.3.CO;2.

Brandon, M.T., and Vance, J.A., 1992, Tectonic evolution of the Cenozoic Olympic subduction complex, Washington State, as deduced from fission track ages for detrital zircons: American Journal of Science, v. 292, p. 565–636.

Brandon, M.T., Cowan, D.S., and Feehan, J.G., 1994, Fault-zone structures and solution-mass-transfer cleavage in Late Cretaceous nappes, San Juan Islands, Washington, *in* Swanson, D.A., and Haugerud, R.A., eds., Geologic Field Trips in the Pacific Northwest: 1994 Geological Society of America Annual Meeting, Seattle, Washington, 2L, p. 1–19.

Brandon, M.T., Roden-Tice, M.K., and Garver, J.I., 1998, Late Cenozoic exhumation of the Cascadia accretionary wedge in the Olympic Mountains, northwest Washington State: Geological Society of America Bulletin, v. 110, p. 985–1009, doi: 10.1130/0016-7606(1998)110<0985:LCEOTC>2.3.CO;2.

Brown, E.H., and Ghent, E.D., 1983, Mineralogical and phase relations in the blueschist facies of the Black Butte and Ball Rock areas, northern California Coast Ranges: American Mineralogist, v. 68, p. 365–372.

Brown, R.D., Jr., and Rich, E.I., 1967, Implications of two Cretaceous mass transport deposits, Sacramento Valley, California: Comment on a paper by Gary L. Peterson: Journal of Sedimentary Petrology, v. 37, p. 240–248.

Buick, I.S., 1991, The late Alpine evolution of an extensional shear zone, Naxos, Greece: Journal of the Geological Society of London, v. 148, p. 93–103.

Chapple, W.M., 1978, Mechanics of thin-skinned fold-and-thrust belts: Geological Society of America Bulletin, v. 89, p. 1189–1198, doi: 10.1130/0016-7606(1978)89<1189:MOTFB>2.0.CO;2.

Christensen, N.I., 1978, Ophiolite, seismic velocities and oceanic crustal structure: Tectonophysics, v. 47, p. 131–157, doi: 10.1016/0040-1951(78)90155-5.

Cladouhos, T.T., and Allmendinger, R.W., 1993, Finite strain and rotation from fault-slip data: Journal of Structural Geology, v. 15, p. 771–784, doi: 10.1016/0191-8141(93)90061-E.

Cloos, M., and Shreve, R., 1988, Subduction-channel model of prism accretion, mélange formation, sediment subduction, and subduction erosion at convergent plate margins: 2. Implications and discussion: Pure and Applied Geophysics, v. 128, p. 501–545, doi: 10.1007/BF00874549.

Constenius, K.N., Johnson, R.A., Dickinson, W.R., and Williams, T.A., 2000, Tectonic evolution of the Jurassic–Cretaceous Great Valley forearc, California: Implications for the Franciscan thrust-wedge hypothesis: Geological Society of America Bulletin, v. 112, p. 1703–1723, doi: 10.1130/0016-7606(2000)112<1703:TEOTJC>2.0.CO;2.

Cowan, D.S., 1974, Deformation and metamorphism of the Franciscan subduction zone complex northwest of Pacheco Pass, California: Geological Society of America Bulletin, v. 85, p. 1623–1634, doi: 10.1130/0016-7606(1974)85<1623:DAMOTF>2.0.CO;2.

Cowan, D.S., 1978, Origin of blueschist-bearing chaotic rocks in the Franciscan Complex, San Simeon, California: Geological Society of America Bulletin, v. 89, p. 1415–1423, doi: 10.1130/0016-7606(1978)89<1415:OOBCRI>2.0.CO;2.

Cowan, D.S., and Brandon, M.T., 1994, A symmetry-based method for kinematic analysis of large-slip brittle fault zones: American Journal of Science, v. 294, p. 257–306.

Cowan, D.S., and Bruhn, R.L., 1992, Late Jurassic to early Late Cretaceous geology of the U.S. Cordillera, *in* Burchfiel, B.C., et al., eds., The Cordilleran Orogen: Conterminous U.S.: Boulder, Colorado, Geological Society of America, Geology of North America, v. G-3, p. 169–203.

Cowan, D.S., and Page, B.M., 1975, Recycled material in Franciscan mélange west of Paso Robles, California: Geological Society of America Bulletin, v. 86, p. 1089–1095, doi: 10.1130/0016-7606(1975)86<1089:RFMIFM>2.0.CO;2.

Cowan, D.S., Botros, M., and Johnson, H.P., 1986, Bookshelf tectonics; rotated crustal blocks within the Sovanco fracture zone: Geophysical Research Letters, v. 13, p. 995–998, doi: 10.1029/GL013i010p00995.

Davis, D., Suppe, J., and Dahlen, F.A., 1983, Mechanics of fold-and-thrust belts and accretionary wedges: Journal of Geophysical Research, v. 88, p. 1153–1172, doi: 10.1029/JB088iB02p01153.

Davis, G.A., 1988, Rapid upward transport of mid-crustal mylonitic gneisses in the footwall of a Miocene detachment fault, Whipple Mountains, southeastern California: Geologische Rundschau, v. 77, p. 191–209, doi: 10.1007/BF01848684.

Deckert, H., Ring, U., and Mortimer, N., 2002, Tectonic significance of Cretaceous bivergent extensional shear zones in the Torlesse accretionary wedge, central Otago Schist, New Zealand: New Zealand Journal of Geology and Geophysics, v. 45, p. 537–547.

DeGraaff-Surpless, K., Graham, S.A., Wooden, J.L., and McWilliams, M.O., 2002, Detrital zircon provenance analysis of the Great Valley Group, California: Evolution of an arc-forearc system: Geological Society of America Bulletin, v. 114, p. 1564–1580, doi: 10.1130/0016-7606(2002)114<1564:DZPAOT>2.0.CO;2.

Dickinson, W.R., 1970, Relations of andesites, granites, and derivative sandstones to arc-trench tectonics: Reviews in Geophysics and Space Physics, v. 8, p. 813–860, doi: 10.1029/RG008i004p00813.

Dickinson, W.R., 1971, Clastic sedimentary sequences deposited in shelf, slope and trough settings between magmatic arcs and associated trenches: Pacific Geology, v. 8, p. 15–30.

Dickinson, W.R., 1976, Sedimentary basins developed during evolution of Mesozoic-Cenozoic arc-trench systems in western North America: Canadian Journal of Earth Sciences, v. 13, no. 9, p. 1268–1287.

Dickinson, W.R., 2002, Reappraisal of hypothetical Franciscan thrust wedging at Coalinga: Implications for tectonic relations along the Great Valley flank of the California Coast Ranges: Tectonics, v. 21, p. 3–11, doi: 10.1029/2001TC001315.

Dickinson, W.R., Helmold, K.P., and Stein, J.A., 1979, Mesozoic lithic sandstones in central Oregon: Journal of Sedimentary Petrology, v. 49, no. 2, p. 501–506.

Dickinson, W.R., and Seely, D.R., 1979, Structure and stratigraphy of forearc regions: The American Association of Petroleum Geologists Bulletin, v. 63, p. 2–31.

Dickinson, W.R., Ojakangas, R.W., and Stewart, R.J., 1969, Burial metamorphism of the late Mesozoic Great Valley sequence, Cache Creek, California: Geological Society of America Bulletin, v. 80, p. 519–526, doi: 10.1130/0016-7606(1969)80[519:BMOTLM]2.0.CO;2.

Dickinson, W.R., Ingersoll, R.V., Cowan, D.S., Helmold, K.P., and Suczek, C.A., 1982, Provenance of Franciscan graywackes in coastal California: Geological Society of America Bulletin, v. 93, p. 95–107, doi: 10.1130/0016-7606(1982)93<95:POFGIC>2.0.CO;2.

Dickinson, W.R., Hopson, C.A., and Saleeby, J.B., 1996, Alternate origins of the Coast Range ophiolite (California): Introduction and implications: GSA Today, v. 6, no. 2, p. 1–10.

Dumitru, T.A., 1988, Subnormal geothermal gradients in the Great Valley forearc basin, California, during Franciscan subduction: A fission-track study: Tectonics, v. 7, p. 1201–1222, doi: 10.1029/TC007i006p01201.

Dumitru, T.A., 1989, Constraints on uplift in the Franciscan subduction complex from apatite fission track analysis: Tectonics, v. 8, p. 197–220, doi: 10.1029/TC008i002p00197.

Durney, D.W., and Ramsay, J.G., 1973, Incremental strains measured by syntectonic crystal growths, *in* DeJong, K.A., and Scholten, R., eds., Gravity and Tectonics: New York, Wiley, p. 67–96.

Elder, W.P., and Miller, J.W., 1993, Map and Checklists of Jurassic and Cretaceous Macrofossil Localities within the San Jose 1:100,000 Quadrangle, California, and Discussion of Paleontological Results: U.S. Geological Survey Open-File Report 93-503.

Elliott, D., 1972, Deformation paths in structural geology: Geological Society of America Bulletin, v. 83, p. 2621–2638, doi: 10.1130/0016-7606(1972)83[2621:DPISG]2.0.CO;2.

Elliott, D., 1976, The motion of thrust sheets: Journal of Geophysical Research, v. 81, p. 949–963, doi: 10.1029/JB081i005p00949.

Engebretson, D.G., Cox, A., and Gordon, R.C., 1985, Relative Motions between Oceanic and Continental Plates in the Pacific Basin: Geological Society of America Special Paper 206, 59 p.

England, P., 1981, Metamorphic pressure estimates and sediment volumes for the Alpine orogeny: An independent control on geobarometers?: Earth and Planetary Science Letters, v. 56, p. 387–397, doi: 10.1016/0012-821X(81)90142-4.

England, P.C., and Richardson, S.W., 1977, The influence of erosion upon the mineral facies of rock from different metamorphic environments: Geological Society of London Journal, v. 134, p. 201–213, doi: 10.1144/gsjgs.134.2.0201.

Ernst, W.G., 1965, Mineral parageneses in Franciscan metamorphic rocks, Panoche Pass, California: Geological Society of America Bulletin, v. 76, p. 879–914, doi: 10.1130/0016-7606(1965)76[879:MPIFMR]2.0.CO;2.

Ernst, W.G., 1970, Tectonic contact between the Franciscan mélange and the Great Valley sequence—Crustal expression of a late Mesozoic Benioff zone: Journal of Geophysical Research, v. 75, p. 886–901, doi: 10.1029/JB075i005p00886.

Ernst, W.G., 1971, Metamorphic zonations on presumably subducted lithospheric plates from Japan, California and the Alps: Contributions to Mineralogy and Petrology, v. 34, p. 43–59, doi: 10.1007/BF00376030.

Ernst, W.G., 1972, CO_2-poor composition of fluid attending Franciscan and Sanbagawa low-grade metamorphism: Geochimica et Cosmochimica Acta, v. 36, p. 497–504, doi: 10.1016/0016-7037(72)90038-5.

Ernst, W.G., 1987, Jadeitized Franciscan metamorphic rocks of the Pacheco Pass–San Luis Reservoir area, central California Coast Ranges: Geological Society of America Centennial Field Guide—Cordilleran Section, v. 57, p. 245–250.

Ernst, W.G., 1993, Metamorphism of Franciscan tectonostratigraphic assemblage, Pacheco Pass area, east-central Diablo Range, California Coast Ranges: Geological Society of America Bulletin, v. 105, p. 618–636, doi: 10.1130/0016-7606(1993)105<0618:MOFTAP>2.3.CO;2.

Ernst, W.G., and Banno, S., 1991, Neoblastic jadeite pyroxene in Franciscan metagraywackes from Pacheco Pass, central Diablo Range, California, and implications for the inferred metamorphic P-T trajectory: New Zealand Journal of Geology and Geophysics, v. 34, p. 285–292.

Ernst, W.G., and Liou, J.G., 1995, Contrasting plate-tectonic styles of the Qinling-Dabie-Sulu and Franciscan metamorphic belts: Geology, v. 23, p. 353–356, doi: 10.1130/0091-7613(1995)023<0353:CPTSOT>2.3.CO;2.

Essene, E.J., and Fyfe, W.S., 1967, Omphacite in Californian metamorphic rocks: Contributions to Mineralogy and Petrography, v. 15, p. 1–23, doi: 10.1007/BF01167213.

Feehan, J.G., and Brandon, M.T., 1999, Contribution of ductile flow to exhumation of low T–high P metamorphic rocks: San Juan–Cascade Nappes, NW Washington State: Journal of Geophysical Research, v. 104, p. 10,883–10,901, doi: 10.1029/1998JB900054.

Fisher, D.M., and Byrne, T., 1992, Strain variations in an ancient accretionary complex: Implications for forearc evolution: Tectonics, v. 11, p. 330–347, doi: 10.1029/91TC01490.

Foster, D.A., and John, B.E., 1999, Quantifying tectonic exhumation in an extensional orogen with thermochronology: Examples from the southern Basin and Range province, *in* Ring, U., et al., eds., Exhumation Processes: Normal Faulting, Ductile Flow and Erosion: Geological Society of London Special Publication 154, p. 343–364.

Glen, R.A., 1990, Formation and thrusting in some Great Valley rocks near the Franciscan Complex, California, and implications for the tectonic wedging hypothesis: Tectonics, v. 9, p. 1451–1477, doi: 10.1029/TC009i006p01451.

Glodny, J., Ring, U., and Kühn, A., 2008, High-pressure metamorphism, thrusting, strike-slip and extensional shearing in the Tauern Window, Eastern Alps: All starting at the same time?: Tectonics, v. 27, TC4004, doi: 10.1029/2007TC002193.

Godfrey, N.J., Beaudoin, B.C., Klemperer, S.L., and Mendocino Working Group, 1997, Ophiolitic basement to the Great Valley forearc basin, California, from seismic and gravity data: Implications for crustal growth at the North American continental margin: Geological Society of America Bulletin, v. 109, p. 1536–1562, doi: 10.1130/0016-7606(1997)109<1536:OBTTGV>2.3.CO;2.

Hamilton, W., 1969, Mesozoic California and the underflow of the Pacific mantle: Geological Society of America Bulletin, v. 80, p. 2409–2430, doi: 10.1130/0016-7606(1969)80[2409:MCATUO]2.0.CO;2.

Hancock, P.L., 1985, Brittle microtectonics: Principles and practice: Journal of Structural Geology, v. 7, p. 437–457, doi: 10.1016/0191-8141(85)90048-3.

Hansen, E., 1971, Strain Facies: Berlin, Springer, 207 p.

Harms, T., Jayko, A.S., and Blake, M.C., 1992, Kinematic evidence for extensional unroofing of the Franciscan Complex along the Coast Range fault zone, northern Diablo Range, California: Tectonics, v. 11, p. 228–241, doi: 10.1029/91TC01880.

Ingersoll, R.V., 1978, Paleogeography and paleotectonics of the late Mesozoic forearc basin of northern and central California, *in* Howell, D.G., and McDougall, K.A., eds., Mesozoic Paleogeography of the Western United States, Pacific Coast Paleogeography Symposium 2: Society of Economic Paleontologists and Mineralogists, Pacific Section, p. 471–482.

Ingersoll, R.V., 1979, Evolution of the Late Cretaceous forearc basin, northern and central California: Geological Society of America Bulletin, v. 90, p. 813–826, doi: 10.1130/0016-7606(1979)90<813:EOTLCF>2.0.CO;2.

Ingersoll, R.V., and Dickinson, W.R., 1981, Great Valley Group (sequence), Sacramento Valley, California, *in* Frizell, V., ed., Upper Mesozoic Franciscan Rocks and Great Valley Sequence, Central Coast Ranges, California: Los Angeles, Society of Economic Paleontologists and Mineralogists, Pacific Section, Annual Meeting, Field Trips 1 and 4, p. 1–33.

Ingersoll, R.V., Rich, E.I., and Dickinson, W.R., 1977, Field Guide: Great Valley Sequence, Sacramento Valley, California: Fresno, Geological Society of America, Cordilleran Section, 72 p.

Jacobson, J.B., 1981, Reflection seismic expression of the cross sectional stratigraphy and structure of the southern Sacramento Valley, *in* Graham, S.A., ed., Field Guide of the Mesozoic Convergent Margin of Northern California, 50: Los Angeles, American Association of Petroleum Geologists, Pacific Section, p. 81.

Jayko, A.S., 1984, Structure and deformation in the Eastern Franciscan belt, California [Ph.D. thesis]: University of California, Santa Cruz, 204 p.

Jayko, A.S., Blake, M.C., Jr., and Brothers, R.N., 1986, Blueschist metamorphism of the Eastern Franciscan belt, northern California, *in* Evans, B.W., and Brown, E.H., eds., Blueschists and Eclogites: Geological Society of America Memoir 164, p. 107–124.

Jayko, A.S., Blake, M.C., Jr., and Harms, T., 1987, Attenuation of the Coast Range ophiolite by extensional faulting, and nature of the Coast Range "thrust," California: Tectonics, v. 6, p. 475–488, doi: 10.1029/TC006i004p00475.

Joesten, R., Wooden, J.L., Silver, L.T., Ernst, W.G., and McWilliams, M.O., 2004, Depositional age and provenance of jadeite-grade metagraywacke from the accretionary prism, Diablo Range, central California—SHRIMP Pb-isotope dating of detrital zircon: Geological Society of America Abstracts with Programs, v. 36, no. 5, p. 120.

Jones, D.L., Graymer, R., Wang, C., McEvilly, T.V., and Lomax, A., 1994, Neogene transpressive evolution of the California Coast Ranges: Tectonics, v. 13, p. 561–574, doi: 10.1029/93TC03323.

Kamb, W.B., 1959, Ice petrofabric observations from Blue Glacier, Washington, in relation to theory and experiment: Journal of Geophysical Research, v. 64, p. 1891–1909, doi: 10.1029/JZ064i011p01891.

Kamp, P.J.J., Green, P.F., and White, S.H., 1989, Fission track analysis reveals character of collisional tectonics in New Zealand: Tectonics, v. 8, p. 169–195.

Kassem, O.K., and Ring, U., 2004, Underplating-related finite-strain patterns in the Gran Paradiso massif, Italian Western Alps: Heterogeneous ductile strain superimposed on a nappe stack: Geological Society of London Journal, v. 161, p. 875–884, doi: 10.1144/0016-764903-159.

Kirby, J.M., 1943, Upper Cretaceous stratigraphy of the west side of Sacramento Valley south of Willows, Glenn County, California: American Association of Petroleum Geologists Bulletin, v. 27, p. 279–305.

Lanphere, M.B., Blake, M.C., and Irwin, W.P., 1978, Early Cretaceous metamorphic age of the South Fork Mountain schist in the northern Coast Ranges of California: American Journal of Science, v. 278, p. 798–815.

Lister, G.S., Banga, G., and Feenstra, A., 1984, Metamorphic core complexes of Cordilleran type in the Cyclades, Aegean Sea, Greece: Geology, v. 12, p. 221–225, doi: 10.1130/0091-7613(1984)12<221:MCCOCT>2.0.CO;2.

Malavieille, J., 1984, Modélisation expérimentale des chevauchements imbriqués: Application aux chaînes des montagnes: Société Géologique de France Bulletin, v. 26, p. 129–138.

Mancktelow, N., 1985, The Simplon Line—A major displacement zone in the western Lepontine Alps: Eclogae Geologicae Helvetiae, v. 78, p. 73–88.

Marrett, R., and Allmendinger, R.W., 1990, Kinematic analysis of fault-slip data: Journal of Structural Geology, v. 12, p. 973–986, doi: 10.1016/0191-8141(90)90093-E.

Maruyama, S., Liou, J.G., and Sasakura, Y., 1985, Low-temperature recrystallization of Franciscan graywackes from Pacheco Pass, California: Mineralogical Magazine, v. 49, p. 345–355, doi: 10.1180/minmag.1985.049.352.05.

Maruyama, S., Liou, J.G., and Terabayashi, M., 1996, Blueschists and eclogites of the world and their exhumation: International Geology Review, v. 39, p. 485–594.

Mattauer, M., Faure, M., and Malavieille, J., 1981, Transverse lineation and large-scale structures related to alpine obduction in Corsica: Journal of Structural Geology, v. 3, p. 401–409, doi: 10.1016/0191-8141(81)90040-7.

Mattinson, J.M., 1988, Constraints on the timing of Franciscan metamorphism: Geochronological approaches and their limitations, *in* Ernst, W.G., ed., Metamorphism and Crustal Evolution of the Western United States, Rubey Volume VII: Englewood Cliffs, New Jersey, Prentice Hall, p. 1023–1034.

Mattinson, J.M., and Echeverria, L.M., 1980, Ortigalita Peak gabbro, Franciscan complex–U-Pb ages of intrusion and high-pressure–low-temperature metamorphism: Geology, v. 8, p. 589–593, doi: 10.1130/0091-7613(1980)8<589:OPGFCU>2.0.CO;2.

Maxwell, J.C., 1974, Early western margin of the United States, *in* Burk, C.A., and Drake, C.L., eds., The Geology of Continental Margins: Berlin, Springer, p. 831–852.

McDowell, F., Lehmann, D.H., Gucwa, P.R., Fritz, D., and Maxwell, J.C., 1984, Glaucophane schists and ophiolites of the northern California Coast Ranges: Isotopic ages and their tectonic implications: Geological Society of America Bulletin, v. 95, p. 1373–1382, doi: 10.1130/0016-7606(1984)95<1373:GSAOOT>2.0.CO;2.

McKee, E.B., 1962, Widespread occurrence of jadeite, lawsonite, and glaucophane in central California: American Journal of Science, v. 260, p. 596–610.

Molnar, P., 1983, Average regional strain due to slip on numerous faults of different orientations: Journal of Geophysical Research, v. 88, p. 6430–6432, doi: 10.1029/JB088iB08p06430.

Moxon, I.W., 1988, Sequence stratigraphy of the Great Valley basin in the context of convergent margin tectonics, *in* Graham, S.A., ed., Studies of the Geology of the San Joaquin Basin: Society of Economic Paleontologists and Mineralogists, Pacific Section, v. 60, p. 3–28.

Moxon, I.W., and Graham, S.A., 1987, History and controls of subsidence in the Late Cretaceous–Tertiary Great Valley forearc basin, California: Geology, v. 15, p. 626–629, doi: 10.1130/0091-7613(1987)15<626:HACOSI>2.0.CO;2.

Murchey, B., 1984, Biostratigraphy and lithostratigraphy of chert in the Franciscan complex, Marin Headlands terrane, California, *in* Blake, M.C., ed., Franciscan Geology of Northern California: Society of Economic Paleontologists and Mineralogists, Pacific Section, p. 51–70.

Nadai, A., 1950, Theory of Flow and Fracture of Solids, Volume I: New York, McGraw-Hill, 572 p.

Nadai, A., 1963, Theory of Flow and Fracture of Solids, Volume II: New York, McGraw-Hill, 705 p.

Namson, J.S., and Davis, T.L., 1988, Seismically active fold and thrust belt in the San Joaquin valley, California: Geological Society of America Bulletin, v. 100, p. 257–273, doi: 10.1130/0016-7606(1988)100<0257:SAFATB>2.3.CO;2.

Norris, R.J., and Bishop, D.G., 1990, Deformed conglomerates and textural zones in the Otago Schists, South Island, New Zealand: Tectonophysics, v. 174, p. 331–349, doi: 10.1016/0040-1951(90)90330-B.

Page, B.M., 1981, The southern Coast Ranges, *in* Ernst, W.G., ed., The Geotectonic Development of California: Englewood Cliffs, New Jersey, Prentice Hall, p. 329–417.

Page, B.M., and Tabor, C.M., 1967, Chaotic structure and décollement in Cenozoic rocks near Stanford University, California: Geological Society of America Bulletin, v. 78, p. 1–12, doi: 10.1130/0016-7606(1967)78[1:CSADIC]2.0.CO;2.

Passchier, C.W., and Trouw, R.A.J., 1996, Microtectonics: Berlin, Springer, 289 p.

Paterson, M.S., and Weiss, L.E., 1961, Symmetry concepts in the structural analysis of deformed rocks: Geological Society of America Bulletin, v. 72, p. 841–882, doi: 10.1130/0016-7606(1961)72[841:SCITSA]2.0.CO;2.

Patrick, B.E., and Day, H.W., 1989, Controls on the first appearance of jadeitic pyroxene, northern Diablo Range, California: Journal of Metamorphic Geology, v. 7, p. 629–639, doi: 10.1111/j.1525-1314.1989.tb00623.x.

Phipps, S.P., 1984, Mesozoic ophiolitic olistostromes and Cenozoic imbricate thrust faulting in the northern California Coast Ranges [Ph.D. thesis]: Princeton, New Jersey, Princeton University, 352 p.

Platt, J.P., 1975, Metamorphic and deformational processes in the Franciscan Complex, California: Some insights from the Catalina schist terrane: Geological Society of America Bulletin, v. 86, p. 1337–1347, doi: 10.1130/0016-7606(1975)86<1337:MADPIT>2.0.CO;2.

Platt, J.P., 1986, Dynamics of orogenic wedges and the uplift of high-pressure metamorphic rocks: Geological Society of America Bulletin, v. 97, p. 1037–1053, doi: 10.1130/0016-7606(1986)97<1037:DOOWAT>2.0.CO;2.

Platt, J.P., 1987, The uplift of high-pressure–low-temperature metamorphic rocks: Philosophical Transactions of the Royal Society of London, ser. A, v. 321, p. 87–103, doi: 10.1098/rsta.1987.0006.

Platt, J.P., 1993, Exhumation of high-pressure rocks: A review of concepts and processes: Terra Nova, v. 5, p. 119–133, doi: 10.1111/j.1365-3121.1993.tb00237.x.

Platt, J.P., 2007, From orogenic hinterlands to Mediterranean-style back-arc basins: A comparative analysis: Geological Society of London Journal, v. 164, p. 297–311, doi: 10.1144/0016-76492006-093.

Platt, J.P., and Vissers, R.L.M., 1980, Extensional structures in anisotropic rocks: Journal of Structural Geology, v. 2, p. 397–410, doi: 10.1016/0191-8141(80)90002-4.

Quinquis, H., Audren, C., Brun, J.P., and Cobbold, R.R., 1978, Intense progressive shear in Ile de Groix blueschists and compatibility with subduction or obduction: Nature, v. 273, p. 43–45, doi: 10.1038/273043a0.

Ramirez, V.R., 1992, Geology and deep structure of the Rumsey Hills area, Sacramento Valley, California, *in* Erskine, M., et al., eds., Field Guide to the Tectonics of the Boundary between the Coast Ranges and the Great Valley of California: American Association of Petroleum Geologists, Pacific Section, Guidebook 70, p. 85–94.

Ramsay, J.G., and Huber, M.I., 1983, The Techniques of Modern Structural Geology, Volume 1: Strain Analysis: London, Academic Press, 307 p.

Ramsay, J.G., Casey, M., and Kligfield, R., 1983, Role of shear in development of the Helvetic fold-thrust belt of Switzerland: Geology, v. 11, v. 439–442.

Reches, Z., 1987, Determination of the tectonic stress tensor from slip along faults that obey the Coulomb yield condition: Tectonics, v. 6, p. 849–861.

Reddy, S.M., Wheeler, J., and Cliff, R.A., 1999, The geometry and timing of orogenic extension: An example from the western Italian Alps: Journal of Metamorphic Geology, v. 17, p. 573–589, doi: 10.1046/j.1525-1314.1999.00220.x.

Rich, E.I., 1971, Geologic Map of the Wilbur Springs Quadrangle, Colusa and Lake Counties, California: U.S. Geological Survey Miscellaneous Geological Investigations Map I-538, scale 1:63,000.

Richter, P.P., Ring, U., Willner, A.P., and Leiss, B., 2007, Structural contacts in subduction complexes and their tectonic significance: The Late Palaeozoic coastal accretionary wedge of central Chile: Geological Society of London Journal, v. 164, p. 203–214, doi: 10.1144/0016-76492005-181.

Riedel, W., 1929, Zur Mechanik geologischer Brucherscheinungen: Zentral blatt für Mineralogie: Geologie und Paläontologie, v. 1929, p. 354–368.

Ring, U., 1992, An Alpine kinematical analysis of the Penninic nappes east of the Lepontine dome: Implications for the evolution of the Central Alps: Tectonics, v. 11, p. 1139–1158, doi: 10.1029/92TC00616.

Ring, U., 1995a, Horizontal contraction or horizontal extension: Heterogeneous Late Eocene and Early Oligocene general shearing during blueschist- and greenschist-facies metamorphism at the Pennine-Austroalpine boundary zone in the Western Alps: Geologische Rundschau, v. 84, p. 843–859.

Ring, U., 1995b, Lithological and kinematic constraints on the evolution of the Karoo rifts of northern Malawi (Africa): Geologische Rundschau, v. 84, p. 607–625, doi: 10.1007/s005310050028.

Ring, U., and Brandon, M.T., 1994, Kinematic data for the Coast Range fault and implications for exhumation of the Franciscan subduction complex: Geology, v. 22, p. 735–738, doi: 10.1130/0091-7613(1994)022<0735:KDFTCR>2.3.CO;2.

Ring, U., and Brandon, M.T., 1997, Kinematics of the Coast Range fault zone, California: Implications for the evolution of the Franciscan subduction complex: Geological Society of America Abstracts with Programs, v. 29, no. 4, p. 60.

Ring, U., and Brandon, M.T., 1999, Ductile deformation and mass loss in the Franciscan subduction complex: Implications for exhumation processes in accretionary wedges, *in* Ring, U., et al., eds., Exhumation Processes: Normal Faulting, Ductile Flow and Erosion: Geological Society of London Special Publication 154, p. 55–86.

Ring, U., and Brandon, M.T., 2008, Exhumation settings. Part I: Relatively simple cases: International Geology Review, v. 50, p. 97–120, doi: 10.2747/0020-6814.50.2.97.

Ring, U., and Kassem, O.K.K., 2007, The nappe rule: Why does it work?: Geological Society of London Journal, v. 164, p. 1109–1112, doi: 10.1144/0016-76492007-020.

Ring, U., and Merle, O., 1992, The relation between thrusting, lateral gravitational spreading and backfolding in the northern part of the Western Alps (Monte Rosa region): Geological Society of America Bulletin, v. 104, p. 901–914, doi: 10.1130/0016-7606(1992)104<0901:FBALGE>2.3.CO;2.

Ring, U., and Richter, P.P., 2004, Normal faulting at convergent plate boundaries: The Del Puerto Canyon shear zone in the Franciscan subduction complex revisited: Tectonics, v. 23, TC2006, doi: 10.1029/2002TC001476.

Ring, U., Ratschbacher, L., and Frisch, W., 1988, Plate boundary kinematics in the Alps: Motion in the Arosa suture zone: Geology, v. 16, p. 696–698, doi: 10.1130/0091-7613(1988).

Ring, U., Ratschbacher, L., Frisch, W., Biehler, D., and Kralik, M., 1989, Kinematics of the Alpine plate margin: Structural styles, strain and motion along the Penninic–Austroalpine boundary in the Swiss-Austrian Alps: Geological Society of London Journal, v. 146, p. 835–849, doi: 10.1144/gsjgs.146.5.0835.

Ring, U., Brandon, M.T., Willett, S.D., and Lister, G.S., 1999, Exhumation processes, *in* Ring, U., et al., eds., Exhumation Processes: Normal Faulting, Ductile Flow and Erosion: Geological Society of London Special Publication 154, p. 1–27.

Ring, U., Layer, P.W., and Reischmann, T., 2001a, Miocene high-pressure metamorphism in the Cyclades and Crete, Aegean Sea, Greece: Evidence for large-magnitude displacement on the Cretan detachment: Geology, v. 29, p. 395–398, doi: 10.1130/0091-7613(2001)029<0395:MHPMIT>2.0.CO;2.

Ring, U., Brandon, M.T., and Ramthun, A., 2001b, Solution-mass-transfer deformation adjacent to the Glarus thrust, with implications for the tectonic evolution of the Alpine wedge in eastern Switzerland: Journal of Structural Geology, v. 23, p. 1491–1505, doi: 10.1016/S0191-8141(01)00015-3.

Ring, U., Thomson, S.N., and Bröcker, M., 2003, Fast extension but little exhumation: The Vari detachment in the Cyclades, Greece: Geological Magazine, v. 140, p. 245–252, doi: 10.1017/S0016756803007799.

Ring, U., Will, T., Glodny, J., Kumerics, C., Gessner, K., Thomson, S.N., Güngür, T., Monie, P., Okrusch, M., and Drüppel, K., 2007, Early exhumation of high-pressure rocks in extrusion wedges: The Cycladic blueschist unit in the eastern Aegean, Greece and Turkey: Tectonics, v. 26, TC2001, doi: 10.1029/2005TC001872.

Ross, J.A., and Sharp, W.D., 1986, ^{40}Ar/^{39}Ar and Sm/Nd dating of garnet amphibolite in the Coast Ranges, California: Eos (Transactions, American Geophysical Union), v. 67, p. 1249.

Ross, J.A., and Sharp, W.D., 1988, The effects of sub-blocking temperature metamorphism on the K/Ar systematics of hornblendes: ^{40}Ar/^{39}Ar dating of polymetamorphic garnet amphibolite from the Franciscan Complex, California: Contributions to Mineralogy and Petrology, v. 100, p. 213–221, doi: 10.1007/BF00373587.

Rubie, D.C., 1984, A thermal-tectonic model for high-pressure metamorphism and deformation in the Sesia zone, western Alps: Journal of Geology, v. 92, p. 21–36.

Rutter, E.H., 1983, Pressure solution in nature, theory and experiment: Geological Society of London Journal, v. 140, p. 725–740, doi: 10.1144/gsjgs.140.5.0725.

Scholz, C.H., 1987, Wear and gouge formation in brittle faulting: Geology, v. 15, p. 493–495, doi: 10.1130/0091-7613(1987)15<493:WAGFIB>2.0.CO;2.

Scholz, C.H., and Cowie, P.A., 1990, Determination of total strain from faulting using slip measurements: Nature, v. 346, p. 837–839, doi: 10.1038/346837a0.

Sclater, J.G., Anderson, R.N., and Bell, M.L., 1971, Elevation of ridges and evolution of the Central Eastern Pacific: Journal of Geophysical Research, v. 76, p. 7888–7915, doi: 10.1029/JB076i032p07888.

Seiders, V.M., 1983, Correlation and provenance of upper Mesozoic chert-rich conglomerate of California: Geological Society of America Bulletin, v. 94, p. 875–888, doi: 10.1130/0016-7606(1983)94<875:CAPOUM>2.0.CO;2.

Seiders, V.M., 1988, Origin of conglomerate stratigraphy in the Franciscan assemblage and the Great Valley Sequence, northern California: Geology, v. 16, p. 783–787, doi: 10.1130/0091-7613(1988)016<0783:OOCSIT>2.3.CO;2.

Seki, Y., Ernst, W.G., and Onuki, H., 1969, Phase Proportions and Physical Properties of Minerals and Rocks from the Franciscan and Sanbagawa Metamorphic Terranes: Geological Society of America Memoir 124, 85 p.

Selverstone, J., 1985, Petrologic constraints on imbrication, metamorphism, and uplift in the SW Tauern window, Eastern Alps: Tectonics, v. 4, p. 687–704, doi: 10.1029/TC004i007p00687.

Selverstone, J., 2005, Are the Alps collapsing?: Annual Review of Earth and Planetary Sciences, v. 33, p. 113–132, doi: 10.1146/annurev.earth.33.092203.122535.

Smith, G.W., Howell, D.G., and Ingersoll, R.V., 1979, Late Cretaceous trench-slope basins of central California: Geology, v. 7, p. 303–306, doi: 10.1130/0091-7613(1979)7<303:LCTBOC>2.0.CO;2.

Suchecki, R.K., 1984, Facies history of the upper Jurassic–lower Cretaceous Great Valley sequence: Response to structural development of an outer-arc basin: Journal of Sedimentary Petrology, v. 54, p. 170–191.

Suppe, J., 1973, Geology of the Leech Lake Mountain–Ball Mountain region, California: A cross-section of the northeastern Franciscan belt and its tectonic implications: University of California Publications in Geological Sciences, v. 107, 82 p.

Suppe, J., 1978, Cross-section of southern part of Northern Coast Ranges and Sacramento Valley, California: Geological Society of America Map and Chart Series MC-28B, scale 1:250,000, 1 sheet.

Suppe, J., 1979, Structural interpretation of the southern part of the northern Coast Ranges and Sacramento Valley, California: Summary: Geological Society of America Bulletin, v. 90, p. 327–330, doi: 10.1130/0016-7606(1979)90<327:SIOTSP>2.0.CO;2.

Suppe, J., 1980, A retrodeformable cross section of northern Taiwan: Proceedings of the Geological Society of China, v. 23, p. 46–55.

Suppe, J., 1981, Mechanics of mountain-building and metamorphism in Taiwan: Memoir of the Geological Society of China, v. 4, p. 67–89.

Suppe, J., and Armstrong, R.L., 1972, Potassium-argon dating of Franciscan metamorphic rocks: American Journal of Science, v. 272, p. 217–233.

Surpless, K.D., Graham, S.A., Covault, J.A., and Wooden, J.L., 2006, Does the Great Valley Group contain Jurassic strata? Reevaluation of the age and early evolution of a classic forearc basin: Geology, v. 34, p. 21–24, doi: 10.1130/G21940.1.

Swe, W., and Dickinson, W.R., 1970, Sedimentation and thrusting of Mesozoic rocks in the Coast Ranges near Clear Lake, California: Geological Society of America Bulletin, v. 81, p. 165–188, doi: 10.1130/0016-7606(1970)81[165:SATOLM]2.0.CO;2.

Tagami, T., and Dumitru, T.A., 1996, Provenance and thermal history of the Franciscan accretionary complex: Constraints from zircon fission track thermochronology: Journal of Geophysical Research, v. 101, p. 11,353–11,364, doi: 10.1029/96JB00407.

Terabayashi, M., and Maruyama, S., 1998, Large pressure gap between the coastal and central Franciscan belts, northern and central California: Tectonophysics, v. 285, p. 87–101, doi: 10.1016/S0040-1951(97)00194-7.

Thomson, S.N., Stöckhert, B., and Brix, M.A., 1999, Miocene high-pressure metamorphic rocks of Crete, Greece: Rapid exhumation by buoyant escape, *in* Ring, U., et al., eds., Exhumation Processes: Normal Faulting, Ductile Flow and Erosion: Geological Society of London Special Publication 154, p. 87–108.

Tripathy, A., Housh, T.B., Morisani, A.M., and Cloos, M., 2005, Detrital zircon geochronology of coherent jadeitic pyroxene-bearing rocks of the Franciscan Complex, Pacheco Pass, California: Implications for unroofing: Geological Society of America Abstracts with Programs, v. 37, no. 7, p. 18.

Twiss, R.J., and Gefell, M.J., 1990, Curved slickenfibres: A new brittle shear sense indicator with application to a sheared serpentinite: Journal of Structural Geology, v. 12, p. 471–481, doi: 10.1016/0191-8141(90)90035-W.

Twiss, R.J., Souter, B.J., and Unruh, J.R., 1993, The effect of block rotation on the global seismic moment tensor and patterns of seismic P and T axes: Journal of Geophysical Research, v. 98, p. 645–674, doi: 10.1029/92JB01678.

Underwood, M.B., and Bachman, S.B., 1986, Sandstone petrofacies of the Yager Complex and the Franciscan coastal belt, Paleogene of northern California: Geological Society of America Bulletin, v. 97, p. 809–817, doi: 10.1130/0016-7606(1986)97<809:SPOTYC>2.0.CO;2.

Underwood, M.B., O'Leary, J.D., and Strong, R.H., 1988, Contrasts in thermal maturity within terranes and across terrane boundaries of the Franciscan Complex, northern California: Journal of Geology, v. 96, p. 399–415.

Unruh, J.R., and Moores, E.M., 1992, Quaternary blind thrusting in the southwestern Sacramento Valley, California: Tectonics, v. 11, p. 192–203, doi: 10.1029/91TC02494.

Unruh, J.R., Loewen, B.A., and Moores, E.M., 1995, Progressive arcward contraction of a Mesozoic–Tertiary forearc basin, southwestern Sacramento Valley, California: Geological Society of America Bulletin, v. 107, p. 38–53, doi: 10.1130/0016-7606(1995)107<0038:PACOAM>2.3.CO;2.

Unruh, J.R., Dumitru, T.A., and Sawyer, T.L., 2007, Coupling of early Tertiary extension in the Great Valley forearc basin with blueschist exhumation in the underlying Franciscan accretionary wedge at Mount Diablo, California: Geological Society of America Bulletin, v. 119, p. 1347–1367, doi: 10.1130/B26057.1.

Vermeesch, P., Miller, D.D., Graham, S.A., and McWilliams, M.O., 2006, Multimethod detrital thermochronology of the Great Valley Group near New Idria, California: Geological Society of America Bulletin, v. 118, p. 210–218.

Wakabayashi, J., 1990, Counterclockwise P-T-t paths from amphibolites, Franciscan Complex, California: Relicts from the early stages of subduction zone metamorphism: Journal of Geology, v. 98, p. 657–680.

Wakabayashi, J., 1992, Nappes, tectonics of oblique plate convergence, and metamorphic evolution related to 140 Ma of continuous subduction, Franciscan Complex, California: Journal of Geology, v. 100, p. 19–40.

Wakabayashi, J., and Dumitru, T.A., 2007, ^{40}Ar/^{39}Ar ages from coherent high-pressure metamorphic rocks of the Franciscan Complex, California: Revisiting the timing of metamorphism of the world's type subduction complex: International Geology Review, v. 49, p. 873–906, doi: 10.2747/0020-6814.49.10.873.

Wakabayashi, J., and Unruh, J.R., 1995, Tectonic wedging, blueschist metamorphism, and exposure of blueschists: Are they compatible?: Geology, v. 23, p. 85–88, doi: 10.1130/0091-7613(1995)023<0085:TWBMAE>2.3.CO;2.

Wallis, S.R., 1992, Vorticity analysis in a metachert from the Sanbagawa Belt, SW Japan: Journal of Structural Geology, v. 14, p. 271–280, doi: 10.1016/0191-8141(92)90085-B.

Wallis, S.R., Platt, J.P., and Knott, S.D., 1993, Recognition of syn-convergence extension in accretionary wedges with examples from the Calabrian arc and the Eastern Alps: American Journal of Science, v. 293, p. 463–495.

Wentworth, C.W., and Zoback, M.D., 1989, The style of Late Cenozoic deformation at the eastern front of the California Coast Ranges: Tectonics, v. 8, p. 237–246, doi: 10.1029/TC008i002p00237.

Wentworth, C.W., Blake, M.C., Jones, D.L., Walter, A.W., and Zoback, M.D., 1984, Tectonic wedging associated with emplacement of the Franciscan assemblage, California Coast Ranges, *in* Blake, M.C., ed., Franciscan Geology of Northern California: Society of Economic Paleontologists and Mineralogists, Pacific Section, p. 163–173.

Wernicke, B., and Burchfiel, B.C., 1982, Modes of extensional tectonics: Journal of Structural Geology, v. 4, p. 105–115, doi: 10.1016/0191-8141(82)90021-9.

Wheeler, J., and Butler, R.W.H., 1994, Criteria for identifying structures related to true crustal extension in orogens: Journal of Structural Geology, v. 16, p. 1023–1027, doi: 10.1016/0191-8141(94)90083-3.

White, S.H., Burrows, S.E., Carreras, J., Shaw, N.D., and Humphreys, F.J., 1980, On mylonites in ductile shear zones: Journal of Structural Geology, v. 2, p. 175–187, doi: 10.1016/0191-8141(80)90048-6.

Willett, S., Beaumont, C., and Fullsack, P., 1993, Mechanical model for the tectonics of doubly vergent compressional orogens: Geology, v. 21, p. 371–374, doi: 10.1130/0091-7613(1993)021<0371:MMFTTO>2.3.CO;2.

Wintsch, R.P., Byrne, T., and Toriumi, M., 1999, Exhumation of the Sanbagawa blueschist belt, SW Japan, by lateral flow and extrusion: Evidence from structural kinematics and retrograde P-T-t paths, *in* Ring, U., et al., eds., Exhumation Processes: Normal Faulting, Ductile Flow and Erosion: Geological Society of London Special Publication 154, p. 129–155.

Wojtal, S.F., 1989, Measuring displacement gradients and strains in faulted rocks: Journal of Structural Geology, v. 11, p. 669–678, doi: 10.1016/0191-8141(89)90003-5.

Worrall, D.M., 1981, Imbricate low-angle faulting in uppermost Franciscan rocks, South Yolla Bolly area, northern California: Geological Society of America Bulletin, v. 92, p. 703–729, doi: 10.1130/0016-7606(1981)92<703:ILFIUF>2.0.CO;2.

Manuscript Accepted by the Society 21 April 2008

Printed in the USA

Contents

THE GEOLOGICAL SOCIETY OF AMERICA®

3300 Penrose Place ▪ P.O. Box 9140
Boulder, CO 80301-9140, USA

ISBN 978-0-8137-2445-4